NASA Contractor Report 182108

A Survey of Oscillating Flow in Stirling Engine Heat Exchangers

Terrence W. Simon and Jorge R. Seume

University of Minnesota
Minneapolis, Minnesota

March 1988

NNSN

National Aeronautics and
Space Administration

Table of Contents

APPENDICES

Nomenclature

symbol	units	explanation
a	m/sec	speed of sound
$A_R = x_{max}/\ell$		relative amplitude of fluid displacement
Au		augmentation coefficient
c_p	J/(kgK)	specific heat at constant pressure
d	m	diameter
$d_h = \dfrac{\text{void volume}}{\text{surface area}}$	m	hydraulic diameter
D	m	pipe diameter
$De = Re\sqrt{\dfrac{d}{2\,R_c}}$		Dean number
$Ec = \dfrac{u_{m,max}^2}{c_p\,(T_H - T_L)}$		Eckert number
f	sec^{-1}	frequency
$f = \dfrac{(-dp/dx)\,\sqrt{k}}{\rho\,V^2}$		friction factor
h	$\dfrac{W}{m^2 sec}$	heat transfer coefficient
I_ϕ	W	integrated dissipation function
k	W/(mK)	thermal conductivity
k	m^2	permeability
l	m	length
ℓ	m	heat exchanger length
ℓ	m	connecting rod length
ℓ_h	m	heated length of heat exchanger
L	m	characteristic length
L	m	engine flow length
m	kg	mass
$M = u/a$		Mach number
$M_{max} = u_{m,max}/a$		Mach number based on the velocity amplitude
$Nu = hl/k$		Nusselt number
p	Pa	pressure
$Pr = c_p\mu/k$		Prandtl number
$\dot{q}$	W	heat transfer rate
r	m	radius
R_c	m	pipe radius of curvature
$Re = \dfrac{u\,L}{\nu}$		Reynolds number based on length L

iii

Re_{max}		Reynolds number based on the amplitude of the cross-sectional mean velocity
Re_ω		dimensionless frquency, Valensi number, kinetic Reynolds number
$Str = \dfrac{\omega\, d}{u_{m,max}}$		Strouhal number
t	sec	time
t_o	sec	characteristic time
T_{ij}	Pa	stress tensor
$\vec{u}$	m/sec	velocity
u	m/sec	streamwise velocity
U	m/sec	characteristic velocity
V	m/sec	superficial velocity
V_T		dimensionless tidal volume
$\vec{x}$	m	distance, location
x	m	streamwise coordinate
x_{max}	m	amplitude of fluid displacement
y	m	cross-stream coordinate

Greek

α		augmentation factor
α		symbol of proportionality
γ		ratio of specific heats
ϵ		coefficient of excess work
λ	°, rad	lead angle
λ	m	wave length
μ	$\dfrac{N\ sec}{m^2}$	dynamic viscosity
ν	m^2/sec	kinematic viscosity
ρ	kg/m^3	density
τ	Pa	shear stress
ϕ		porosity
Φ	W/m^3	dissipation function
ψ		axial augmentation function
$\omega = 2\pi f$	rad/sec	angular velocity

Superscripts

| * | | normalized quantity |
| # | | at shock formation |

Subscripts

c	cold end
h	hot end
H	high temperature
L	low temperature
lm	log-mean
m	average over cross-section
max	maximum during one cycle
o	reference state
p	of pressure
r	of the regenerator
w	at the wall
τ	of wall shear stress

1. INTRODUCTION

1.1 Purpose of this Report

Two design objectives for Stirling engines are to keep mechanical losses low and to achieve good heat transfer from and to the working fluid. These objectives conflict because heat exchangers with higher heat transfer effectiveness generally have higher flow losses. It is therefore valuable for the designer to know the trade-off between pressure drop and heat transfer. This is particularly important when high performance is required as ir the Automotive Stirling Engine and the Space Power Demonstrator Engine.

Computer modelling is used to evaluate options in Stirling engine design. Measured Stirling engine efficiencies and power output are often lower than predictions would indicate, however. Transient pressure variations in the Stirling engine working spaces are also often not predicted correctly (Rix 1984). Inadequate modelling of fluid mechanics and heat transfer in the heat exchangers (usually by using steady-state correlations for pressure drop and heat transfer) may partially account for this discrepancy. Improving this model will require more physically correct expressions for the effect of oscillation. It is hoped that this report will make a step in that direction by improving the understanding of fluid mechanics and heat transfer in Stirling engines. It summarizes, extends and discusses research found in the literature and draws tentative conclusions.

1.2 Outline

The oscillating flow effect is isolated as the focus of this report. Similarity parameters to characterize fluid mechanics and heat transfer in

Stirling engine heat exchangers are proposed. A literature review and some analyses address fluid mechanics and heat transfer in oscillating flow in pipes under conditions which are similar to conditions in heaters and coolers. Literature which deals with flow in porous media, similar to regenerators, is also reviewed. The operating characteristics of 11 Stirling engines are described in terms of similarity parameters and tentative conclusions are drawn about the fluid mechanics and heat transfer conditions in Stirling engine heat exchangers. Open questions to be answered by future research are identified. Some of the material covered in this report is summarized in Seume and Simon (1986).

2. SIMILARITY PARAMETERS

Similarity parameters are required to concisely and generally describe fluid mechanics and heat transfer in physically similar systems. Their proper choice is crucial for the development of an experimental program and the interpretation of experimental data.

Section 2.1 discusses some characteristics of the flow in Stirling engine heat exchangers that are not described by similarity parameters—in particular, simplifying assumptions to isolate the oscillating flow effect. Section 2.2 presents physical arguments for the chosen set of similarity parameters and Section 2.3 derives the similarity parameters by normalizing the governing equations.

2.1 Isolating the Oscillating Flow Effect

The effect of oscillation on fluid mechanics and heat transfer has been the subject of several studies related to Stirling engines (e.g., Kim 1970, Organ 1975, Miyabe et al. 1982, Chen and Griffin 1983, Hwang and Dybbs 1980 and 1983, Taylor and Aghili 1984, Dijkstra 1984, Jones 1985, Rice et al. 1985). In review of these studies, it became clear that the effect of oscillation on pressure drop, viscous dissipation and heat transfer must first be studied isolated from the remainder of the processes occurring in the engine, in particular isolated from:

- compression and expansion of the working fluid

- non-harmonic fluid motion

- high temperature gradients.

Some discussion about each of these effects in the Stirling engine follows.

3

Compression and expansion of the working fluid. The working fluid in Stirling engines moves from the compression space toward the expansion space and back during each cycle. Simultaneously, it undergoes compression and expansion (Figure 2-1). Therefore, the mass of fluid in the heater in Figure 2-1 varies with time and consequently the mass flow rates at the ends of the heater differ throughout the cycle (full and dashed line).

Appendix A provides a survey of the cycle variations of pressure and Reynolds numbers in Stirling engine heat exchangers using the isothermal and Schmidt analyses (c.f. Section 6.1). The engines and their operating points are described in Section 6.2. Figure 2-1 shows that the pressure change is fastest when the fluid velocity in the heater is near zero. In the cooler and in the regenerator, however, velocities are high when the pressure is changing most rapidly.

During compression, the gas temperature rises. This decreases the temperature difference between the bulk of the gas and the heater wall and thereby may reduce the heat transfer from the heater pipe to the gas. In the cooler, compression increases the temperature difference between the bulk fluid temperature and the wall temperature. The heat transfer may, however, be out of phase with the bulk-to-wall temperature difference. This was shown by Faulkner and Smith (1984) in a study related to heat transfer in the cylinders of reciprocating machinery. In the heater, fluid velocities are low during expansion and compression. Consequently, convective heat transfer is not expected to be as strong as in the cooler and regenerator during compression and expansion.

In the cooler and regenerator, temperature in the gas increases simultaneously with convective heat transfer during the cold blow, i.e., when gas moves from the compression space towards the expansion space.

4
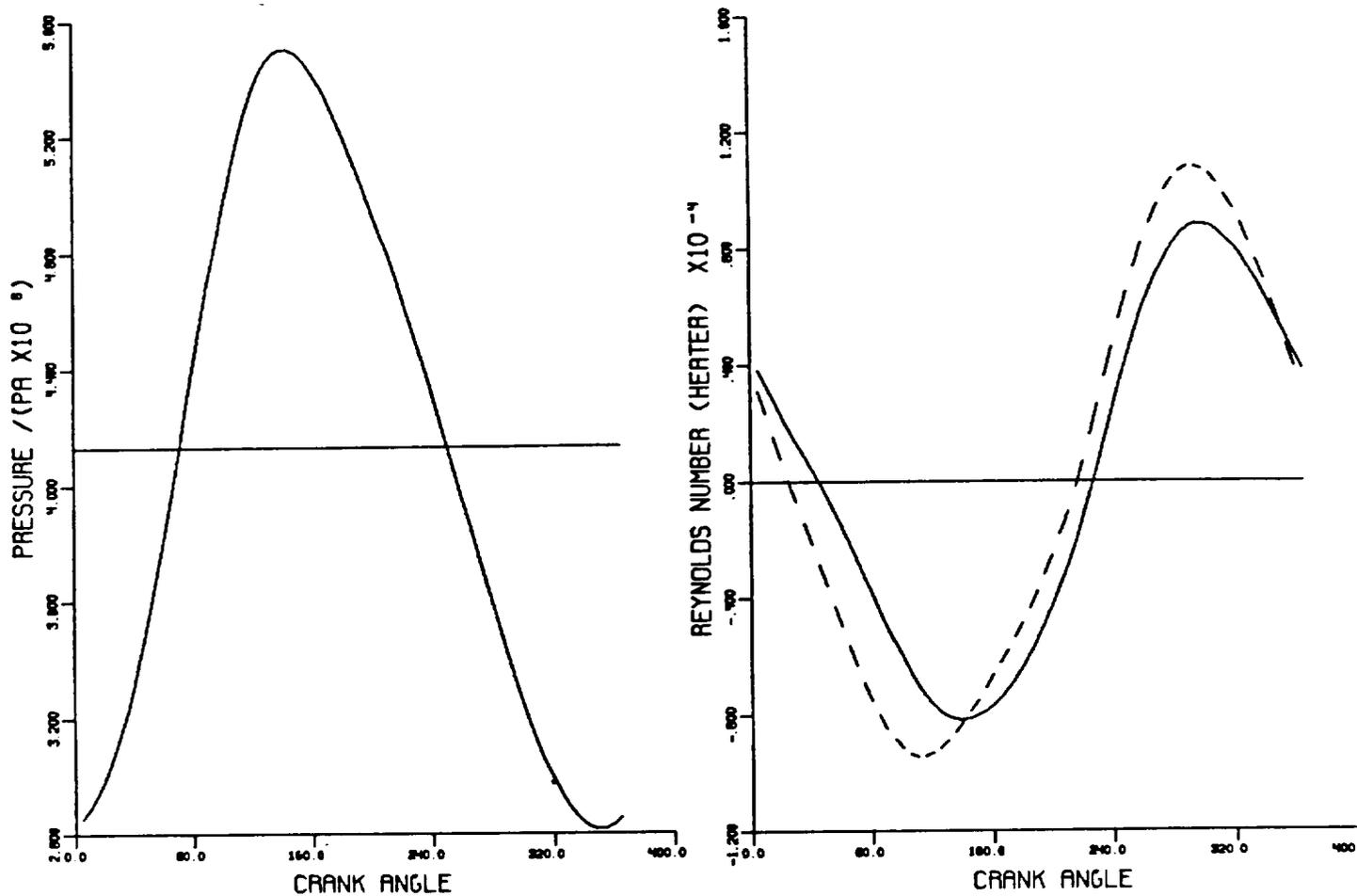
Figure 2-1: Variation of pressure and Reynolds number
in the heater of a GPU 3, isothermal analysis.
Flow toward the cold end is positive;
full line = hot end, dashed line = cold end.

5

During the hot blow, the gas expands as it flows through the cooler and regenerator.

Dijkstra (1984, p. 1886) proposed to model the compression of the working gas as bulk heating of a fluid flowing through heat exchangers. He pointed out that the convective heat transfer coefficient in the case of bulk heating is very different from that for specified wall temperature or specified heat flux. The differences are particularly big in the entrance region of tubes and in the turbulent flow regime. It is, however, not clear whether bulk heating can be used to model temperature changes in the working gas due to compression and expansion.

This report focuses on the effect of the oscillation of the working fluid on fluid mechanics and heat transfer in the heat exchangers. To isolate this effect, compression and expansion of the working fluid are neglected in most of the discussion below.

Mean velocity variation. In Figure 2-2, the mean velocity is normalized with the speed of sound to form a Mach number; according to the assumptions implicit in the isothermal analysis, the speed of sound is uniform and constant in each heat exchanger. Figure 2-2 shows that the mean velocity variation in a typical Stirling engine is roughly sinusoidal and very similar to the Reynolds number variation shown in Figure 2-1.

Velocity and Reynolds number variation deviate from a sine function in that:

(1) the hot blow period, during which the flow is positive (i.e., towards the compression space), is shorter than the cold blow period.

(2) The maximum velocity during the hot blow period is greater than during the cold blow period.

6
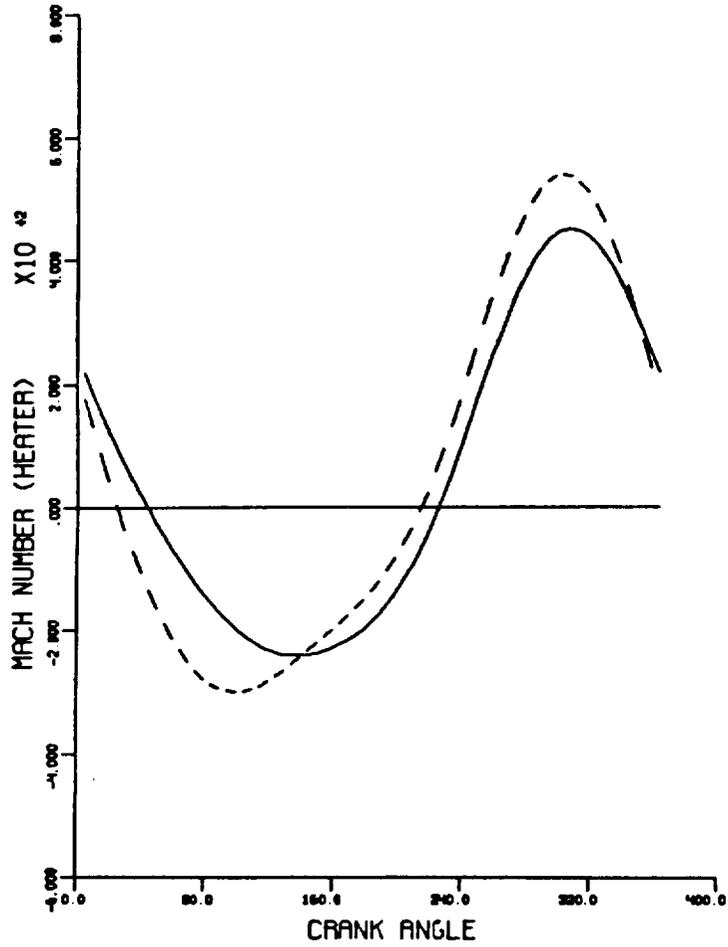
Figure 2-2:   Variation of Mach number in the heater
of a GPU 3, isothermal analysis.
Flow toward the cold end is positive;
full line = hot end, dashed line = cold end.

The differences of the mass flow variation (Figure 2-1) and the mean

velocity variation (Figure 2-2) from harmonic motion will be neglected in

the discussion below.

Temperature dependent properties. The molecular viscosity and thermal

conductivity of gases increase with temperature. Due to the temperature

gradients in the heat exchangers, the gas properties vary in the radial and

axial directions.

In particular, the viscosity near the heater wall is expected to be

higher than in the core; the viscosity of the gas is lower near the wall of

the cooler than in the core of the flow. Therefore calculations based on

the assumption of constant properties in this report should only be

considered approximate. Some authors consider density variations (buoyancy

effects) in turbulent forced convection with large density gradients

important. For a review of this subject, see Petukhov et al. (1982).

2.2 Physical Arguments for the Choice of Similarity Parameters

This section describes qualitatively some of the transient phenomena

expected in Stirling engine heat exchangers. Similarity parameters

characterizing each of these phenomena are proposed.

Velocity and acceleration. In steady flow, the friction factor (a

non-dimensional viscous pressure drop) is a function of Reynolds number (a

non-dimensional mass flux). Oscillating flow experiments, e.g. those by

Taylor and Aghili (1984) showed that the functional relationship between

friction factor and Reynolds number is different for oscillating flow than

for steady unidirectional flow.

In the limit of very slow oscillations, the oscillating flow

relationships should approach that of steady flow. This suggests that the

8

friction factor in oscillating flow is also a function of a dimensionless frequency or dimensionless acceleration. Following Chen and Griffin (1983), this dimensionless frequency is chosen as:

$$Re_\omega = \frac{\omega \, d^2}{4 \, \nu}$$

In this report, the Reynolds number is based on the maximum velocity in the cycle:

$$Re_{max} = \frac{u_{m,max} d}{\nu}$$

Fluid displacement. Walker (1962, 1963 and 1980, p. 130) shows that the fluid displacement in Stirling engines may be so small that some working fluid merely moves back and forth within the heat exchanger without exiting. If the gas moves as a plug and if there is no axial mixing, this gas contributes to the axial heating only by absorbing thermal energy from the wall or adjacent fluid at the high temperature end of the heat exchanger and releasing it at the low temperature end. Only the gas that enters and leaves the heat exchanger transfers heat directly to the volume in the cylinders. Organ (1975) argued that the gas that stays within the heat exchanger may be considered an undesirable addition to the dead space in the engine. The amplitude ratio, A_R, is used to describe fluid displacement in heat exchangers. It is the fluid displacement during half a cycle divided by the tube length, computed by assuming that the fluid moves as a plug at a mean velocity, u_m. This is the reciprocal of Λ introduced by Organ (1975). If $A_R \ll 1$, most fluid oscillates within the tube without exiting; if $A_R \gg 1$, the fluid traverses quickly through the tube, residing in the upstream and downstream spaces during most of the cycle.

9

Entrance and exit effects. The pressure drop at the entrance of a heat exchanger has two components. The reversible pressure drop is the result of an increase in kinetic energy by expending flow work (pressure drop) in the contraction upon entrance to a heat exchanger. In the case of a compressible working gas, density will decrease as the gas is expanded (approximately adiabatically) in this contraction. The irreversible part of the entrance pressure drop is due to viscous dissipation in the shear flow of the vena contracta. It is typically small in steady flows. At the exit, pressure may be recovered as the gas velocity decreases. The pressure rises and kinetic energy is lost irreversibly by viscous dissipation in the shear layers of the separated flow upon exit from the heat exchanger into the downstream chamber.

Since the magnitude of entrance and exit losses depends on the area ratios of the contraction and expansion of the duct, these area ratios (or the corresponding diameter ratios, (d/D)) are added to the Reynolds number as similarity parameters for capturing entrance and exit losses.

Pipe curvature. The pipes in Stirling engine heaters are often curved. It is known from steady unidirectional flow that secondary flows develop in curved pipes as centrifugal forces act on the fluid. The Dean number,

$$De = Re\sqrt{\frac{d}{2R_c}} ,$$

where R_c is the radius of curvature of the pipe centerline, is commonly used as a similarity parameter for this effect (Berger et al. 1983).

Developing flow. In steady flow, the velocity profile in a pipe changes in the flow direction until fully developed conditions are reached. The entrance length scales on the diameter of the pipe (or the hydraulic diameter of the duct). The friction factor in the entrance (developing)

10

region is higher than in the fully developed region. Therefore, the average friction factor for developing duct flow is a function of the length/diameter ratio, ℓ/d, as well as the Reynolds number.

Flow in regenerators. Flow in the complex geometries of Stirling engine regenerators is commonly described in terms of a Reynolds number based on the hydraulic diameter and the matrix porosity. Other choices of similarity parameters are discussed in Section 5.1.

Compressibility of the working gas. The compressibility of the working gas affects the entrance and exit losses of the heat exchangers as described above and the propagation of pressure changes throughout the engine. If the gas velocity in a heat exchanger is of the same order as the speed at which pressure changes propagate (approx. the speed of sound), pressure (and, therefore, density) variations in the engine due to compressibility will be significant. As the ratio of gas velocity to speed of sound (i.e. the Mach number) approaches unity, shock waves form and the flow becomes choked. The Mach number, based upon the highest velocity in the engine cycle, is therefore chosen as a measure of compressibility effects.

Temperature transients. The walls of the heater and cooler and the matrix of the regenerator undergo temperature transients as they are subjected to different gas temperatures during hot and cold blows. The transient response, particularly of the regenerator matrix, affects the engine performance (Walker 1980, p. 140). This response is described by dimensionless parameters from regenerator theory, e.g. dimensionless regenerator length and dimensionless blow period, as discussed in Section 5.3. Also, the transient response of the heater and cooler walls may contribute to enhanced axial heat transfer as discussed in Section 4.1.

11

2.3 Derivation of Similarity Parameters

Momentum equation. Similarity parameters, introduced in Section 2.1, can be derived by normalizing the momentum and the energy equations.

Neglecting gravity, the momentum (Navier-Stokes) equation is:

$$\frac{\partial \vec{u}}{\partial t} + \vec{u} \cdot \nabla \vec{u} = -\frac{\nabla p}{\rho} + \nu \nabla^2 \vec{u}$$

A normalized form suitable for pipe flow is derived in Appendix B:

$$Re_\omega \frac{\partial \vec{u}^*}{\partial t^*} + \frac{Re_{max}}{2} \vec{u}^* \cdot \nabla^* \vec{u}^* = -\frac{Re_{max}}{2} \frac{\nabla^* p^*}{\rho^*} + \nu^* \nabla^{*2} \vec{u}^*$$

Here the superscript * denotes a normalized quantity. The dimensionless frequency, Re_ω, is the coefficient of the temporal acceleration (or unsteady) term, whereas the maximum Reynolds number, Re_{max}, is the coefficient of the spatial acceleration and the pressure gradient term.

The viscous term has no coefficient. This does not imply, however, that Re_{max} is the ratio of the $\vec{u} \cdot \nabla \vec{u}$ (steady inertia) term to the $\nu \nabla^2 \vec{u}$ (viscous) term. That would only be true if both non-dimensional terms were of the same order, i.e., if

$$O(\vec{u}^* \cdot \nabla \vec{u}^*) = O(\nu^* \nabla^{*2} \vec{u}^*)$$

This is not necessarily the case. In a fully developed laminar pipe flow, for example, the $\vec{u} \cdot \nabla \vec{u}$ term vanishes but the Reynolds number is still non-zero.

The dimensionless frequency, Re_ω, has also been called the kinetic Reynolds number (White 1974, p. 144) or the Valensi number (Park and Baird

12

1970). It is a multiple of the Stokes number (Grassmann and Tuma 1979) and it is the square of the Womersley parameter.

A slightly rearranged version of the normalized momentum equation is:

$$\frac{Str}{2} \frac{\partial \vec{u}^*}{\partial t^*} + \vec{u}^* \cdot \nabla \vec{u}^* = -\frac{\nabla^* p^*}{\rho^*} + \frac{2}{Re_{max}} \nu^* \nabla^{*2} \vec{u}^*$$

where $Str = \omega d / u_{m,max}$ is the Strouhal number. Note that the definition of the Strouhal number may vary in the literature (Telionis 1981, p. 88), and that Str is a multiple of the Strouhal number used by Dijkstra (1984).

Geometric similarity. The choice of length scales for the normalization of the momentum equation is arbitrary. To maintain similarity, however, all dimensions must scale on the same length; in this case the pipe radius or the diameter d was chosen. Therefore, (ℓ/d) is the appropriate similarity variable describing the pipe length. The relative amplitude of fluid displacement is not an independent similarity parameter. For sinusoidal fluid motion, it is shown in Appendix B to be:

$$A_R = \frac{1}{2} \frac{\ell}{d} \frac{Re_{max}}{Re_\omega}$$

Description of geometries other than straight pipes, such as the various regenerator types, curved pipes, or ducts of rectangular cross-section, require additional descriptors to complement the similarity parameters described in this section, e.g. the Dean number.

Energy equation. Heat transfer is governed by the energy equation:

$$\rho c_p \left(\frac{\partial T}{\partial t} + \vec{u} \cdot \nabla T\right) = \frac{\partial p}{\partial t} + \vec{u} \cdot \nabla p + \nabla \cdot (k \nabla T) + \phi$$

13

where ϕ is the dissipation function (Appendix B). A normalized form for pipe flow is:

$$\rho^* c_p^* \left(2 \, Re_\omega \frac{\partial T^*}{\partial t^*} + Re_{max} \, \vec{u}^* \cdot \nabla^* T^*\right)$$

$$= 2 \, Re_\omega \, Ec \frac{\partial p^*}{\partial t^*} + Ec \, Re_{max} \, \vec{u}^* \cdot \nabla^* p^* + \frac{\nabla^* \cdot (k^* \nabla^* T^*)}{Pr} + Ec \, \phi^*$$

where $Pr = \dfrac{\mu_o \, c_{po}}{k_o}$

$$Ec = \frac{u_{m,max}^2}{c_{po} \, (T_h - T_c)}$$

Other choices of similarity variables. Other forms of the normalized governing equations are obtained if the variables are normalized differently. If the temperature is normalized as $T^* = T/T_o$ and we assume that the fluid is an ideal gas with constant specific heats, the Eckert number, Ec, can be replaced by $(\gamma - 1) \, M_{max}^2$.

The Mach number can also enter the normalized momentum equation through the equation of state if pressure is normalized with a reference pressure:

$$p^* = \frac{p}{p_o} \qquad p_o = \rho_o R T_o = \frac{\rho_o}{\gamma} \left(\frac{u_{m,max}}{M_{max}}\right)^2$$

Then the Mach number appears in the pressure term:

$$Re_\omega \frac{\partial \vec{u}^*}{\partial t^*} + \frac{Re_{max}}{2} \vec{u} \cdot \nabla^* \vec{u}^* = -\frac{Re_{max}}{2} \frac{1}{\gamma M_{max}^2} \frac{\nabla^* p^*}{\rho^*} + \nu^* \nabla^{*2} \vec{u}^*$$

These examples show that the choice of similarity parameters is somewhat arbitrary. The appearance of a dimensionless parameter in a normalized equation alone does not imply that it is a relevant similarity parameter. Meaningful similarity parameters are obtained when all normalized terms in an equation are of order 1, e.g. in the momentum equation:

$$O\left(\frac{\partial u^*}{\partial t^*}\right) = O\left(u^*\frac{\partial u^*}{\partial x^*}\right) = O\left(\frac{1}{\rho^*}\frac{dp^*}{dx^*}\right) = O\left(\nu^*\frac{\partial^2 u^*}{\partial y^{*2}}\right) = 1$$

Then the coefficients of those normalized terms, i.e., Re_ω, Re_{max}, Str in the momentum equation, represent the relative magnitude of the terms in the dimensional momentum equation, e.g. Re_ω is the ratio of the temporal acceleration term to the viscous term of the momentum equation in a laminar oscillating pipe flow or the Dean number is the ratio of the spatial acceleration term (due to centrifugal force) to the viscous term of the momentum equation in a laminar flow in a curved pipe.

In the energy equation, an Eckert number on the order of 1 would indicate that viscous heating is important and a Mach number of order 1 would indicate that density variations due to high fluid velocities are expected.

3. FLUID MECHANICS OF OSCILLATING PIPE FLOW

In unsteady flows, pressure and shear forces in the fluid are not in equilibrium; instead there is a local balance of inertia, pressure and shear forces. Therefore, the fluid mechanics of oscillating flows are different from those of steady flow.

Figure 3-1 presents an integral momentum balance on a cylindrical control volume in fully developed flow ($\vec{u} \cdot \nabla \vec{u} = 0$). The oscillating flow case shows the additional term associated with temporal acceleration ($\partial u / \partial t$, where u is the cross-sectional mean velocity).
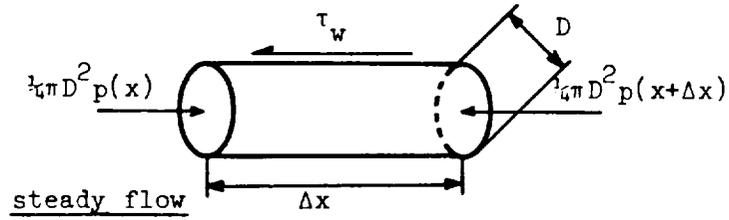
(a) pressure in balance with wall shear stress
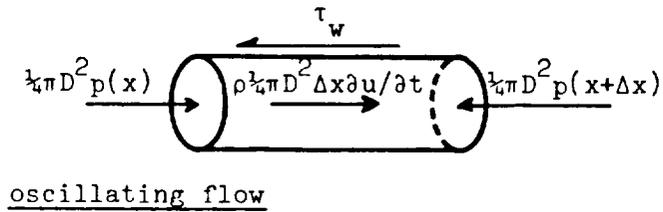
(b) pressure in balance with wall shear stress + fluid inertia

Figure 3-1: Force balance in fully developed pipe flow.

3.1 Analysis of Laminar Flow in a Straight Pipe

Measurements by Richardson and Tyler (1929) first indicated an oscillating flow effect. They found a maximum velocity near the wall for oscillating pipe flow. Sexl (1930), Womersley (1955) and Uchida (1956) have since shown this by analysis of both sinusoidal and non-sinusoidal oscillating flows. Similar analyses were performed by Drake (1965) for rectangular channels and by Gedeon (1986) for flow between parallel plates. Zielke (1968) and Trikha (1975) used Laplace transforms to calculate pressure drop in unsteady laminar flow.

Figure 3-2, based upon the Uchida (1956) analysis, shows velocity distributions for fully-developed flow at several times during the cycle and for several values of Re_ω. All profiles assume the same magnitude of pressure gradient oscillation, and the local velocities are normalized with the maximum mean velocity that would occur with steady laminar flow (responding to the cycle-maximum pressure gradient). Velocity distributions similar to these were measured by Shizgal et al. (1965, p. 99) and Edwards and Wilkenson (1971, p. 87). An analysis similar to Uchida's but for flow between parallel flat plates was made by Gedeon (1986). Figure 3-2 shows parabolic distributions for slowly oscillating pipe flow ($Re_\omega = 1$). With higher Re_ω, however, the velocity amplitude decreases and, during parts of the cycle, the near-wall flow direction is opposite to the mean flow direction ($Re_\omega = 30$). A velocity maximum develops near the wall. At the maximum frequency ($Re_\omega = 1000$), this free shear layer becomes narrower and moves closer to the wall. A uniform velocity core exists and velocity gradients become concentrated in a Stokes layer near the wall.
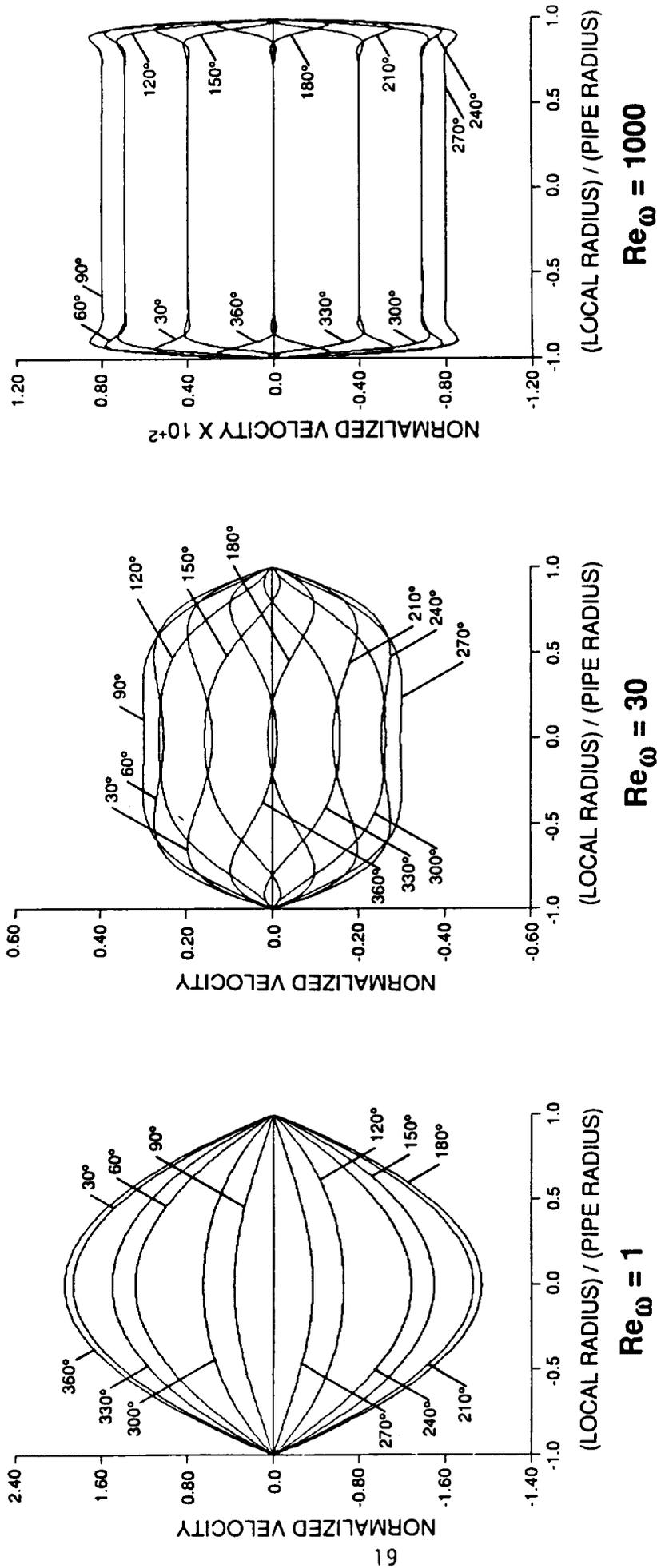
Figure 3-2: Velocity profiles in oscillating, laminar, fully developed pipe flow

19

The presence of a large velocity gradient between the maximum velocity and the core (the free shear layer) may play an important role in laminar-to-turbulent transition. Further velocity profiles are shown in Appendix C.

To discuss the effect of flow oscillation on shear stress and pressure drop, augmentation factors, α_τ and α_p, and lead angles, λ_τ and λ_p, are introduced as:

$$u_m = u_{m,max} \cos(\omega t)$$

$$\tau_w = \alpha_\tau\, 8\mu/d\; u_{m,max} \cos(\omega t + \lambda_\tau)$$

$$\Delta p = \alpha_p\, 32\mu l/d^2\; u_{m,max} \cos(\omega t + \lambda_p)$$

Note that for steady flow, α_τ and α_p are unity and λ_τ and λ_p are zero. These quantities, taken from the Uchida (1956) analysis, are plotted versus Re_ω on Figures 3-3 and 3-4. Note (Fig. 3-3) that for the Re_ω range chosen, the wall shear stress is enhanced by a factor of 8 over that of unidirectional flow, and that the pressure change is enhanced by a factor of 130.

The phase relationships given in Figure 3-4 indicate that, in the limit of high Re_ω, the shear stress leads the mean velocity by 45° and the pressure change leads the mean velocity by 90°. The near-wall fluid responds more quickly to the imposed pressure gradient than does the higher inertia core flow. Clearly, neither the shear stress nor the pressure drop should be computed from the pressure gradient by assuming quasi-steady flow.

In oscillating flow, loss of engine work due to viscous dissipation cannot be calculated by multiplying mean velocity and wall shear stress as is done in steady flow. Instead, the viscous power dissipation in a pipe section of length l must be computed as:
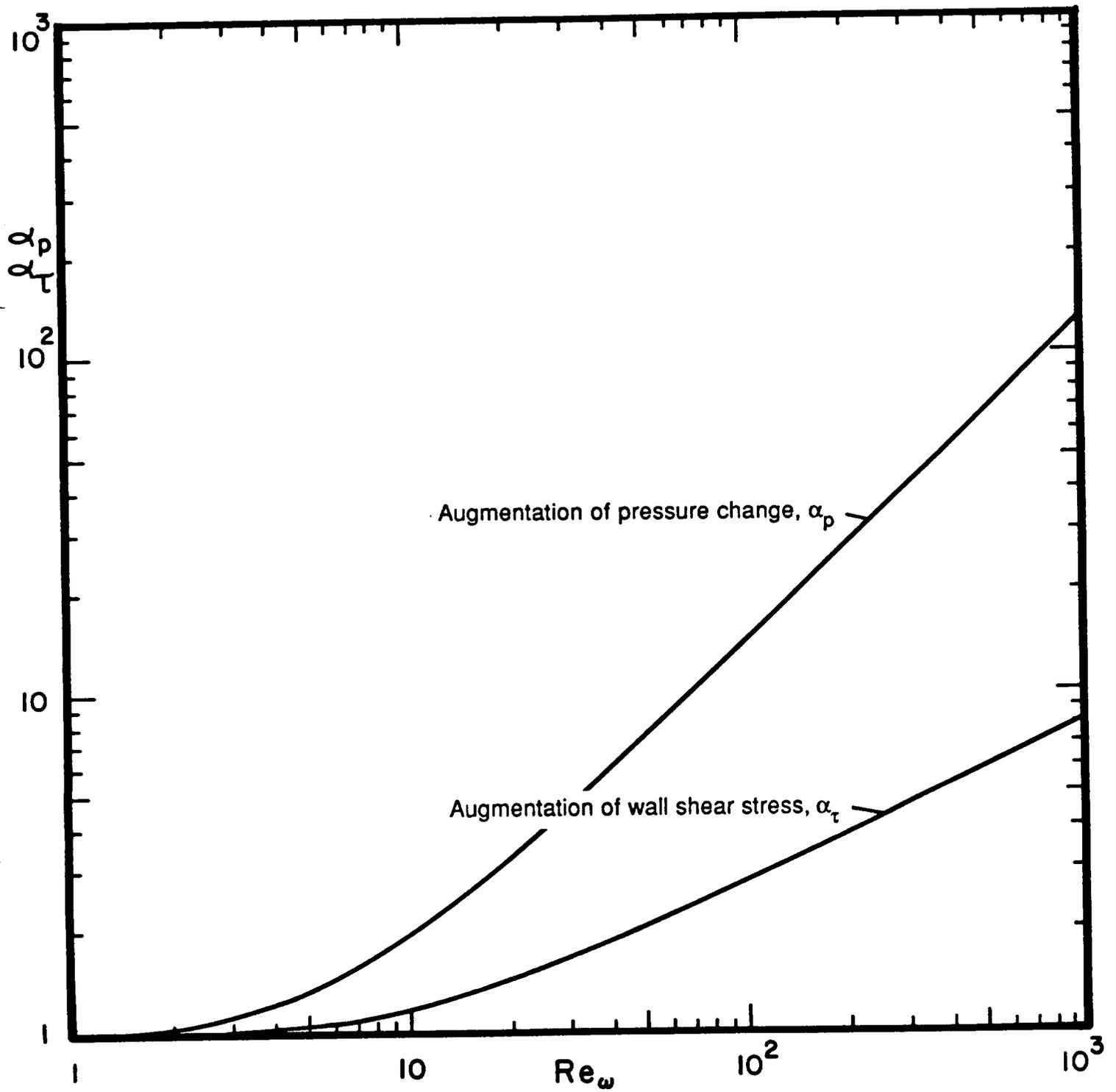
Figure 3-3:   Coefficients of amplitude of pressure drop
and wall shear stress

21
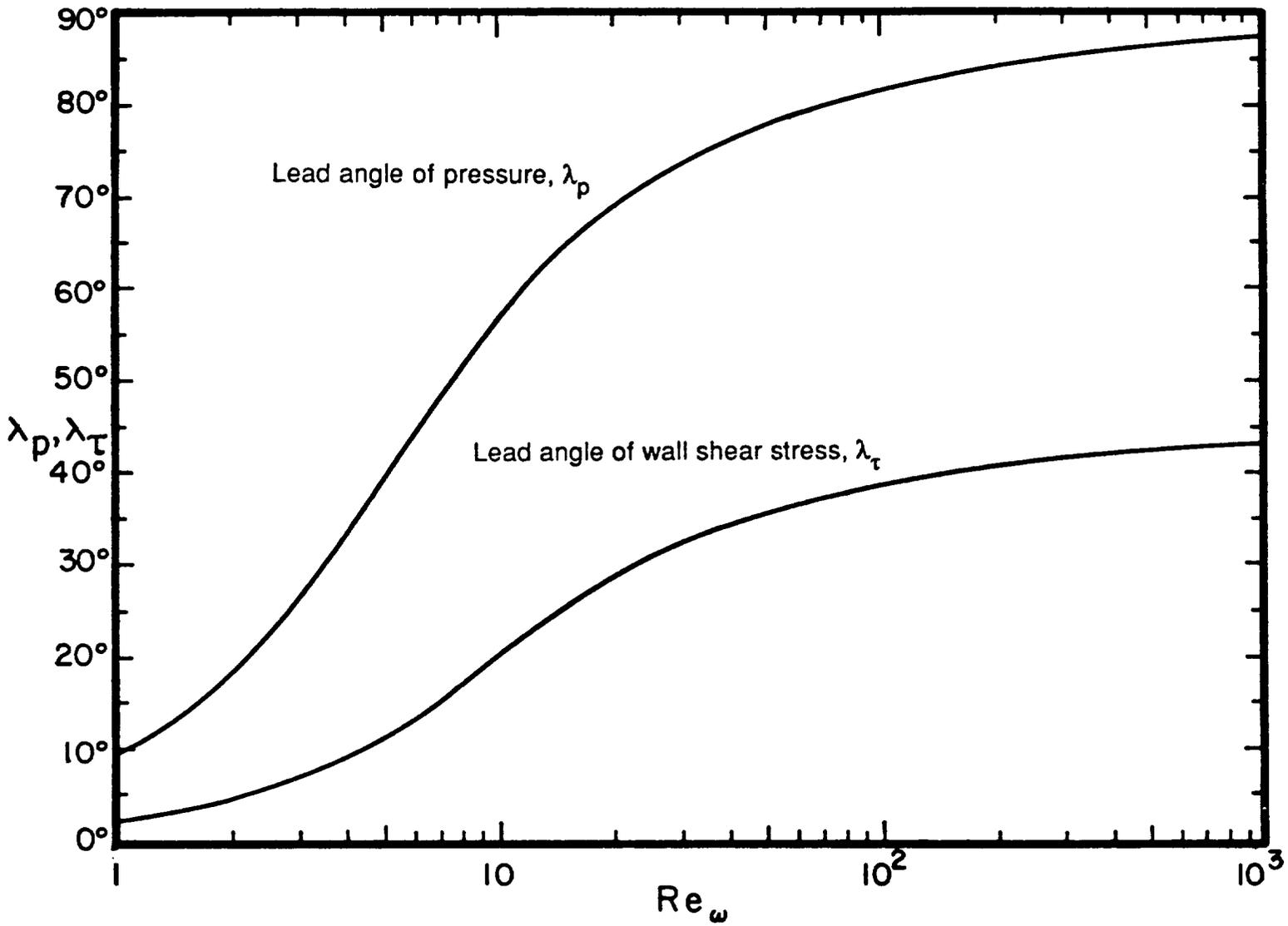
Figure 3-4:   Lead angles of pressure drop and wall shear stress

$$I_\phi = 2\pi \, \ell \int_0^{d/2} \mu(\frac{\partial u}{\partial r})^2 \, r \, dr$$

The relative increases (due to flow oscillation) of shear (irreversible) work and total pumping work (reversible and irreversible) over those for steady flow can be expressed by the coefficients of excess work, ϵ_i and ϵ_p, respectively.

$$\epsilon_i = \frac{[\int_0^{2\pi} I_\phi(\omega t) \, d(\omega t)]}{[\int_0^{2\pi} I_\phi(\omega t) \, d(\omega t)]_{Re_\omega \to 0}}$$

$$\epsilon_p = \frac{[\int_0^{2\pi} \left| -(\frac{dp}{dx})u_m \right| \, d(\omega t)]}{[\int_0^{2\pi} \left| -(\frac{dp}{dx})u_m \right| \, d(\omega t)]_{Re_\omega \to 0}}$$

These quantities are plotted versus Re_ω on Figure 3-5. Note that over the Re_ω range shown, the irreversible work increases by a factor of six, whereas the pumping work increases by a factor of 125. The difference between the pumping and shear work values represents reversible work. In the Stirling engine most of this is eventually lost due to dissipation upon entry to or exit from the heat exchanger channels. Some of this reversible work may be recovered as gas exiting the channels impinges upon and does work on a piston surface.
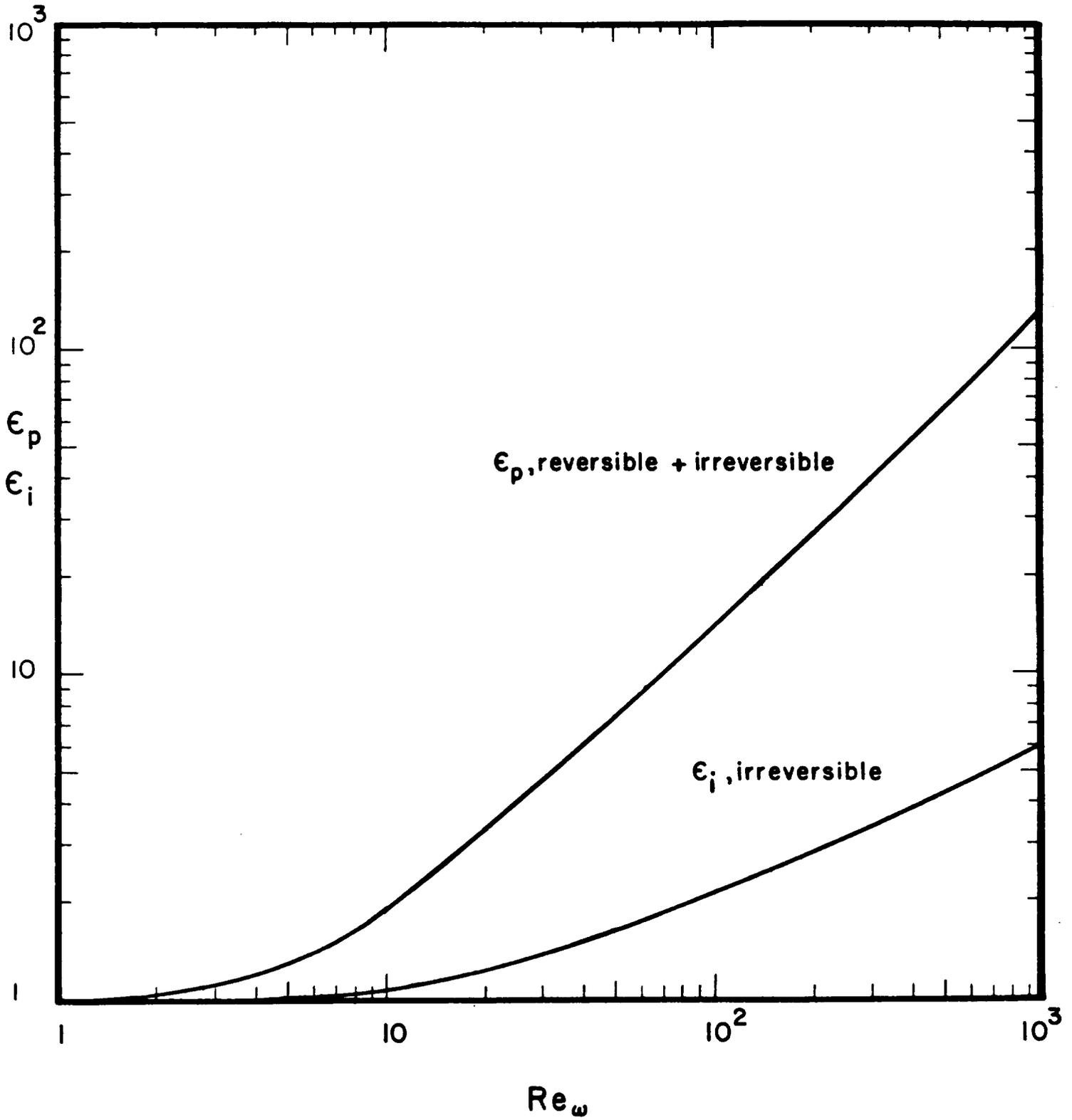
Figure 3-5:   Relative increase of pumping work due to flow oscillation

24

3.2 Laminar Oscillating Flow in Curved Pipes

The pipes in many Stirling engine heaters are bent. If the radius of curvature of a pipe is small, secondary flows are strong. This is true for steady and for oscillating flows. Due to the pipe curvature, centrifugal forces act on the fluid; therefore the spatial acceleration term $\vec{u} \cdot \vec{\nabla u}$ is non-zero while it is zero in fully developed laminar flow in a straight pipe.

In the normalized momentum equation, the Dean number replaces the Reynolds number. The unsteadiness is again characterized by Re_ω. Telionis (1981, p. 183) gives a different but equivalent set of similarity parameters. Figure 3-6 shows a schematic of oscillating flow in a curved pipe. In each half of the pipe there are two counter-rotating secondary flows: one in the potential core and one in the Stokes layer.

a = d/2 r_o = R_c
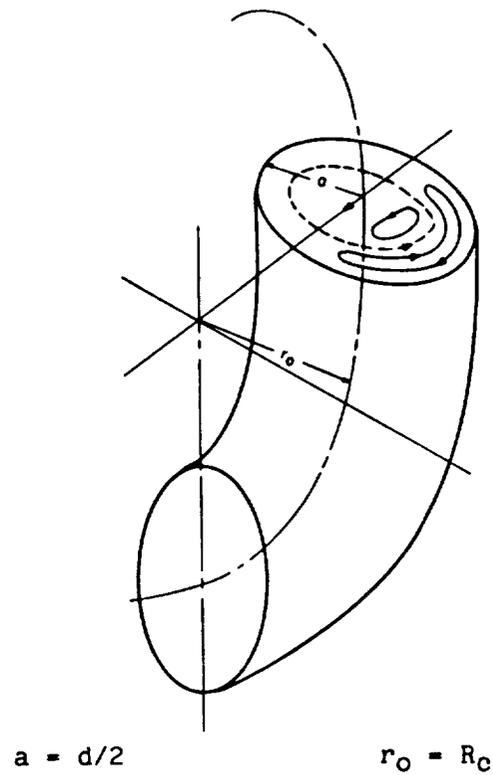
Figure 3-6:   Oscillating flow in a curved pipe

(from Telionis 1981, p. 182)

Yamane et al. (1985) calculated these streamlines and axial velocity profiles. The latter were confirmed experimentally by Sudou et al. (1985). Streamlines and velocity profiles for laminar, oscillating flow in rectangular curved ducts were calculated by Sumida and Sudou (1985).

Yamane et al. (1985) calculated and measured the increase of wall shear stress and pressure drop in a curved pipe over that in a straight pipe. They presented these ratios as a function of Dean number and Womersley parameter.

26

3.3 Non-sinusoidal and Free Oscillations

Section 3.1 discussed sinusoidal oscillations in a straight pipe. Uchida (1956) used a Fourier series representation to extend this analysis to general, non-sinusoidal periodic laminar flows. This analysis may be useful since oscillations in Stirling engines are generally not sinusoidal. Chan and Baird (1974) studied forced oscillations of liquid columns in a range that is of interest for the design of liquid piston engines (West 1983, pp. 54-59, 131). Free (damped) oscillations of liquid columns in U-tubes were studied by Valensi (1947), Park and Baird (1970), and Iguchi et al. (1982). It is not clear to what extent their results regarding fluid friction and the transition from laminar to turbulent flow (see Section 3.4) can be applied to the forced oscillations of liquid columns occurring in liquid piston engines.

The effect of pipe curvature on the flow was neglected in the studies referred to above and in the transition studies discussed in the next section. The authors assumed that the curvature effect is negligible because the pipe radius of curvature is small compared to the pipe radius.

3.4 Transition from Laminar to Turbulent Flow

The transition process. Transition in unidirectional steady flow is known to be sensitive to bulk mean velocity and acceleration. Lower velocities and acceleration stabilize, whereas higher velocities and deceleration destabilize. Since in oscillating flows both velocity and acceleration vary, it is expected that flow patterns may change from laminar-like to turbulent-like throughout the cycle under near-critical conditions. Hino et al. (1976) probed an oscillating pipe flow with a single hot-wire and presented the traces of absolute value of the velocity shown in Figure 3-7. The parameter η is the radial location with $\eta = 0$ being the center of the pipe. The traces show a laminar-like flow during acceleration and a turbulent-like flow during deceleration. With increased Re_{max} (5830, Fig. 3-7b), the turbulence persists into the acceleration portion of the cycle. From these traces, one would expect transition to extend over a broad range of Re_{max}. This supposition is consistent with measurements taken by Ohmi et al. (1982) where a wide range in Re_{max} was observed between laminar-like and turbulent-like oscillating flows. The signal in the first part of the cycle shows slightly stronger fluctuations than that in the second part, probably because of flow separation in the asymmetric apparatus. At the same dimensionless frequency ($Re_{\omega} = 7.30$) but a higher amplitude Reynolds number ($Re_{max} = 5830$) the turbulent fluctuations are stronger than at $Re_{max} = 2070$ (Figure 3-7(a); they start prior to deceleration during the high velocity part of the cycle.
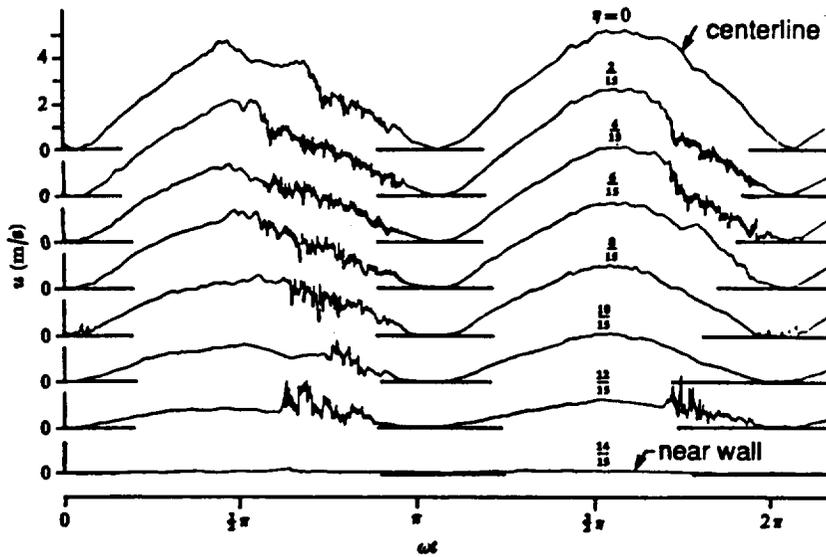
(a) $Re_\omega = 7.30$ $Re_{max} = 2070$
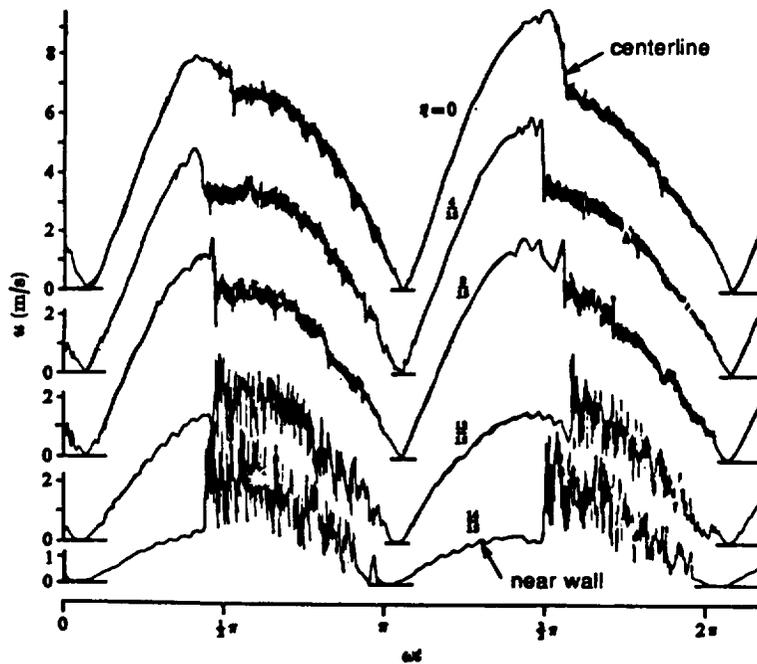
(b) $Re_\omega = 7.30$ $Re_{max} = 5830$

η = local radius / pipe radius

Figure 3-7:   Velocity measurements taken with a hot wire by Hino et al.(1976)

The ensemble-averaged velocity is lower than the laminar velocity at the center of the pipe and higher than the laminar velocity near the pipe wall. This indicates that the profile becomes flatter, which is characteristic of turbulent velocity profiles. This observation is consistent with the work of Ohmi et al. (1982) who found that the velocity profile during the laminar part of the cycle agrees well with the theoretical laminar solution (see Section 3.1) and that the velocity profile during the turbulent part agrees well with the 1/7 power law for steady turbulent pipe flow (see e.g. Schlichting 1979, p. 597-602).

Experimental observations of transition. Figure 3-8 shows observations of transition. Ohmi et al. (1982) studied forced oscillations of a gas in a straight pipe. They did not state their criterion for transition. Iguchi et al. (1982) observed free oscillations of a liquid column in a U-tube. They chose the laminar-to-transitional flow line to be where the amplitude of oscillation began to deviate from that of the laminar solution discussed earlier. The transitional-to-turbulent flow line is where measured amplitudes of oscillation began to agree with predictions based on 1/7th-power turbulent pipe flow profiles. Park and Baird (1970) observed the decay of free oscillations of liquid in a manometer. They calculated cycle maximum wall shear stress from the observed amplitudes of oscillation using two methods. The first was based on a laminar flow prediction, the second on the turbulent 1/7th-power profile. They assumed transition to occur at the amplitude where the maximum wall shear stress, calculated from the laminar prediction, exceeded that calculated from the 1/7th-power profile. They attribute their data scatter to column end effects in the liquid column which are a function of $L^2\omega/\nu$ where L is the length of the
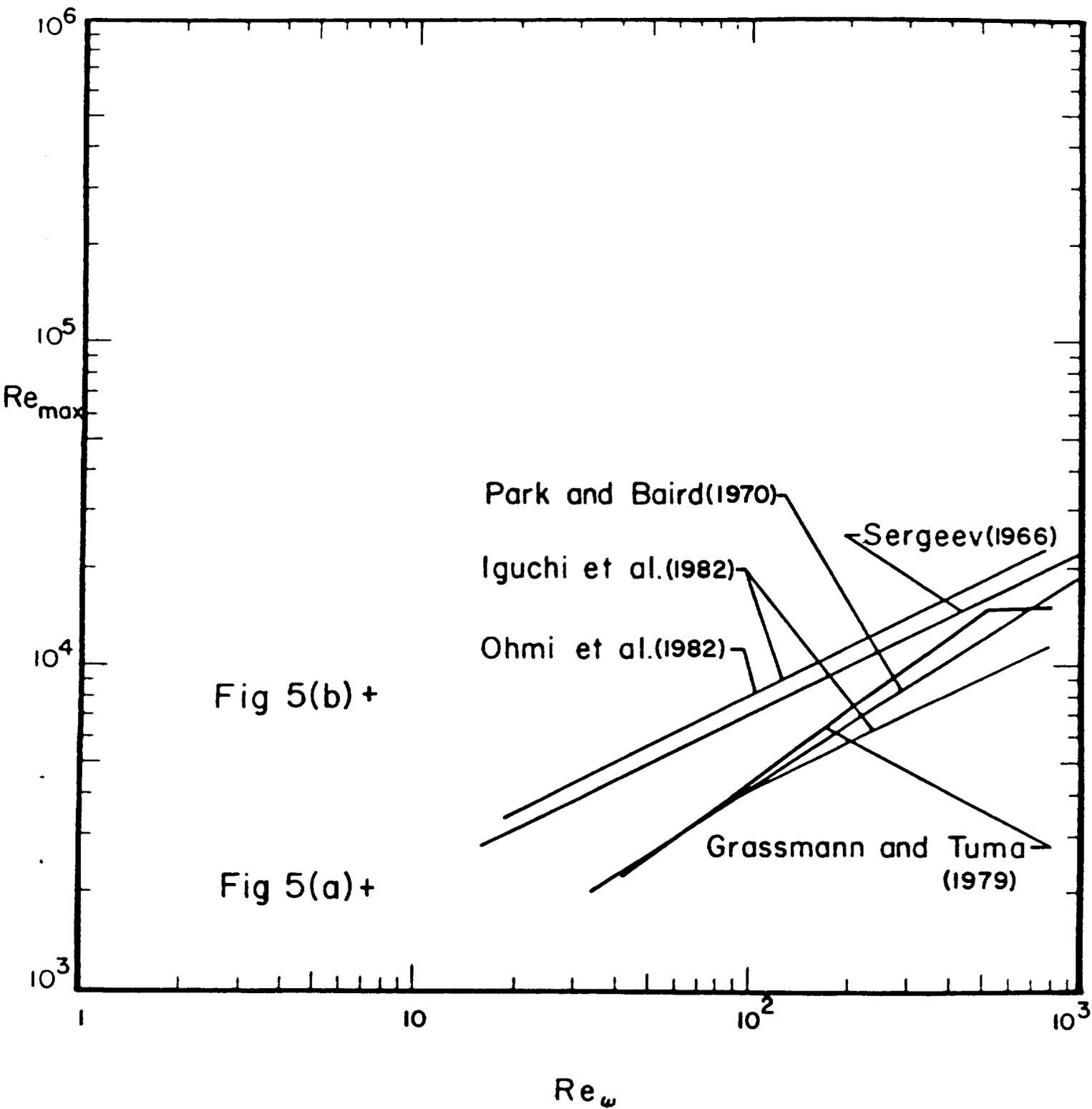
Figure 3-8:   Observations of transition in oscillating flow

31

liquid column. These end effects may be important in liquid piston Stirling engines. Sergeev (1966) did not state his criterion, but, since he used aluminum particle flow visualization, we surmise that transition was observed through the transparent walls as a change in the flow structure. His work was in straight-tube, forced-oscillation flow. Grassmann and Tuma (1979) used an electrolytic technique to observe turbulent fluctuations in wall mass transfer rate, thus locating transitional behavior.

Merkli and Thomann (1975) studied the transition from laminar to turbulent oscillating flow at dimensionless frequencies (Re_ω = 2500...4000) beyond the range presented in Figure 3-8. Their apparatus was a piston oscillating in a resonance tube. They noticed a secondary weak vortex motion outside the oscillating boundary layer. The tube was operated near resonance. The secondary vortex observed by Merkli and Thomann may be related to the vortex street that Sobey (1985) observed in steady and oscillating channel flow. Sobey also predicted the vortex street numerically and considered it a result of shear-layer instability.

Dijkstra (1984) observed, in the transitional regime, that water which was initially in the tube would remain laminar, while water entering the tube would flow in a turbulent pattern and would remain turbulent in the tube.

Though the transition predictions differ with criteria, the researchers agree that transition Re_{max} increases with Re_ω. The sequence of the transition predictions is consistent with the criteria used. Iguchi's et al. (1982) lower line is based on the first sign of deviation from laminar behavior. The Grassmann and Tuma (1979) criterion is based on fluctuations at the pipe surface. These fluctuations are likely to occur at about the same Re_ω as that established by Sergeev (1966) based on the onset of

32

turbulent motion of particles. Finally, the Iguchi et al. (1982) upper line
is based on agreement with the predictions from the 1/7th-power law. It
agrees with the observations by Ohmi (1982) in forced oscillation of gas in
a straight pipe. Equations for these observations of transition are listed
in Appendix D.

Theoretical prediction of transition. Von Kerczek and Davis (1972)
used the energy method to predict a lower bound for the instability of
Stokes layers on a flat plate. Figure 3-9 shows their results in the form
of the critical value of the Reynolds number Re_{max} below which the
oscillating flow cannot go unstable. This lower bound underpredicts the
transition Reynolds number by roughly one order of magnitude. The trends of
the two curves, however, agree well.

Cayzac et al. (1985) presented predictions for the lower bound of
stability in oscillating pipe flow. Like Von Kerczek and Davis, they found
good qualitative agreement in the trends but a quantitative discrepancy of
one order of magnitude. For steady pipe flows, they predicted the lower
bound for instabilities to be Re_D = 750 while Re_D ≈ 2000 is the well-known
experimental value.

The theoretical prediction of the lower bound of instability by the
energy method apparently does not yield results that are practically useful.
For other theoretical approaches to the stability of oscillating flows see
Davis (1976).

EXPERIMENTAL OBSERVATIONS

Von Kerczek & Davis (1972)
by the energy method

Re_{max}

Re_ω
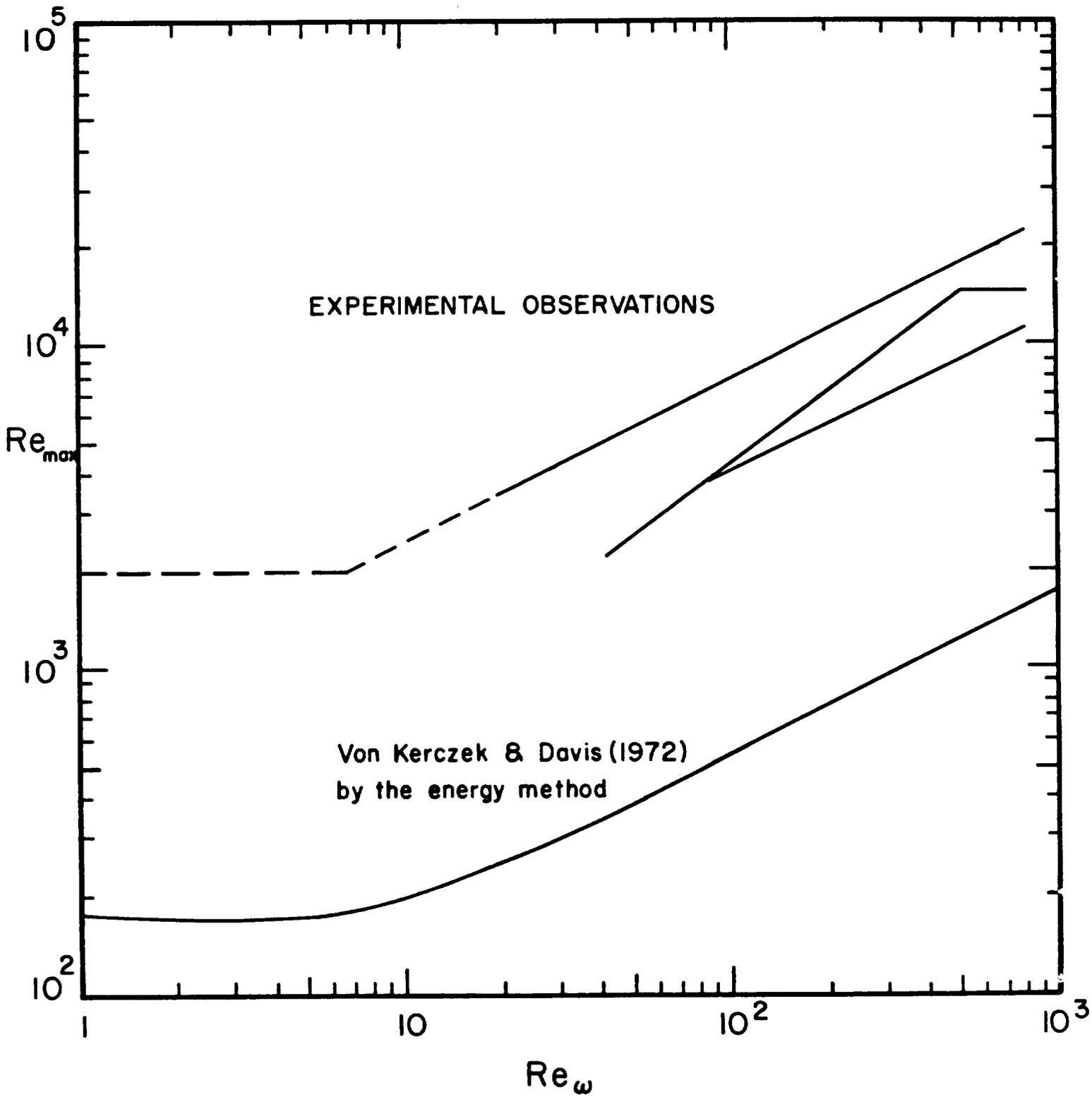
Figure 3-9:   Theoretical prediction of transition
and experimental observations

3.5 Turbulent Flow

Though much remains to be learned about the effect of oscillation on turbulent flows, significant findings have been documented.

Quasi-steady approach. Dijkstra (1984) and Vasiliev and Kvon (1971) applied turbulence models taken from steady flow to oscillating and pulsating pipe flow, respectively. Kirmse (1979) compared Vasiliev and Kvon's model to his experimental data and concluded that their quasi-steady prediction was not adequate.

The concept of an oscillation-sensitive and a quasi-steady turbulent regime was introduced by Ohmi et al. (1982, p. 536). In their experiment, the crank radius of the slider-crank mechanism driving the flow was increased thereby increasing Re_{max} at constant Re_ω. This increased the crank radius to connecting rod length ratio (r/ℓ). Figure 3-10 shows plots of the displacement (x), the velocity $(\dot{x})$ and the acceleration $(\ddot{x})$ of a slider-crank mechanism. For $r/\ell = 1/3$ the acceleration, $\dot{x}$, shows large deviations from a sine function though the displacement, x, is nearly sinusoidal. The turbulence structure is known to be sensitive to acceleration and deceleration. It is, therefore, not possible to decide whether deviations from sinusoidal, quasi-steady flow are due to changing the drive geometry or due to the increase in the ratio of Re_{max} / Re_ω. Ohmi et al. (1982) claimed the latter when they determined the line Re_{max} = 2800 $\sqrt{Re_\omega}$ above which they predict turbulent flow to be quasi-steady. They applied a quasi-steady 1/7-power law velocity profile and observed that it agreed well with their measured velocity profiled above this line.
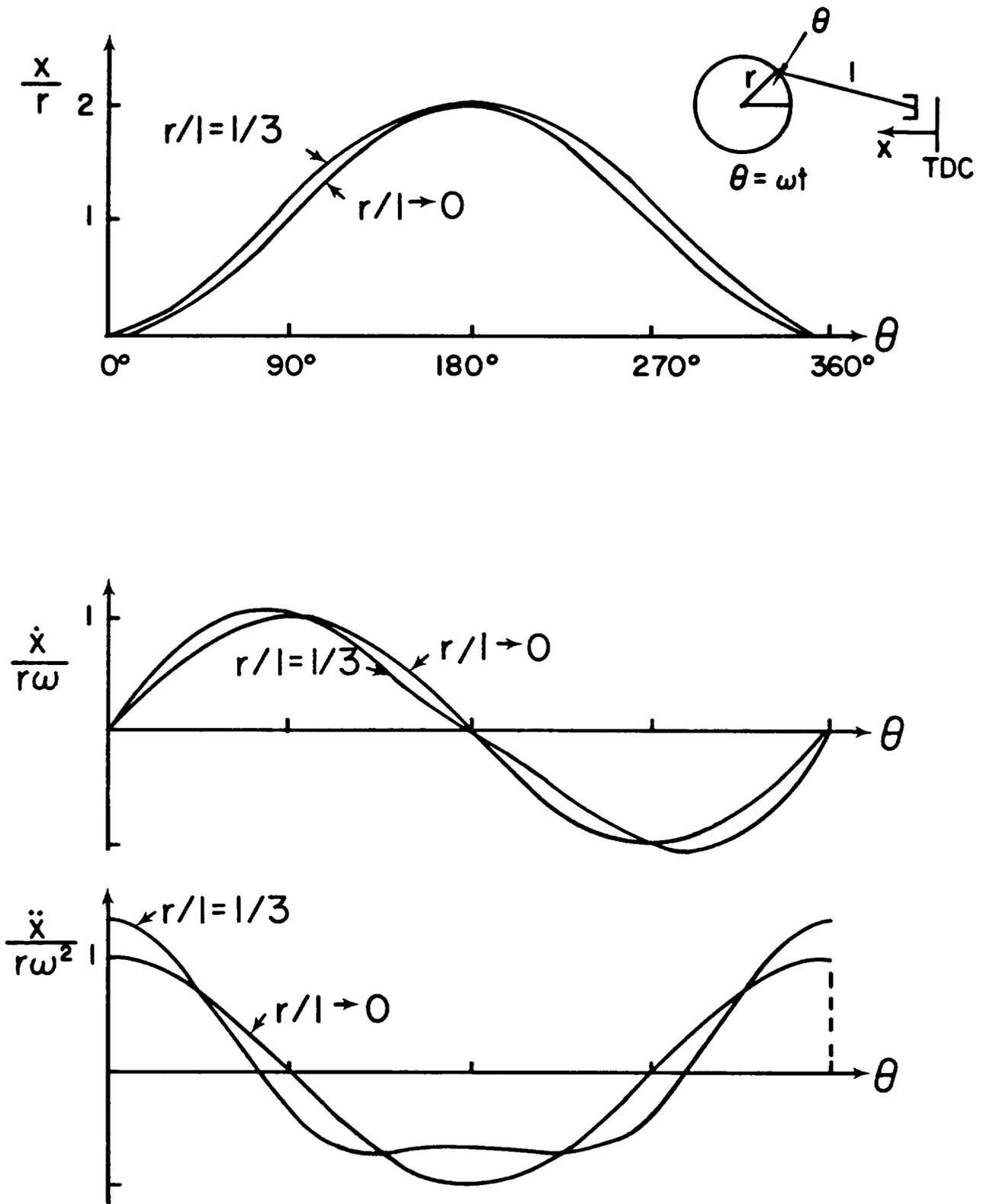
Figure 3-10:   Kinematics of the slider-crank mechanism

Fluctuating eddy viscosity model. Kita et al. (1980) found that the Reynolds stresses in pulsating flow could not be adequately described using a constant eddy viscosity. Therefore, they proposed a fluctuating eddy viscosity model. Their five-layer model shows good agreement with experimental results for pulsating flows; it was not tested for oscillating flows.

Empirical pressure drop correlations. Taylor and Aghili (1984) took data of pressure drop in oscillating flow through pipes of finite length ℓ. They plotted their data as a function of time-averaged Reynolds number for various values of ℓ/d. Their "friction factor" is based on a time-averaged pressure drop and a time-averaged absolute value of the mean velocity. The data indicate an increase of the friction factor by a factor of four over the steady, unidirectional case.

From the previous discussion of pressure drop in laminar oscillating pipe flow, it is clear that the acceleration and deceleration of the working fluid influence the pressure drop in oscillating flow. Only if the results were correlated in terms of a dimensionless frequency such as Re_ω, could they be applied appropriately. Taylor and Aghili's (1984) paper does not give sufficient data to calculate Re_ω.

3.6 Entrance and Exit Losses

Thus far, the discussion of pipe flow was restricted to fully developed flow or, equivalently, infinitely long pipes. For finite pipes, entrance effects may be important. The viscous losses are higher in the entrance length of a pipe. Because of the spatial acceleration of the fluid,

$\vec{u} \cdot \nabla \vec{u}$ term in the momentum equation is not zero.

37

Goldberg (1958) showed that the hydrodynamic and the thermal entrance length in hydraulically and thermally developing steady laminar flow is a function of Reynolds number. Based on this observation, Charreyron (1984) suggested that the entrance length varies over the cycle. Peacock and Stairmand (1983) hypothesized that the entrance length in laminar oscillating flow will be shorter than in unidirectional, steady flow. Since the velocity profiles tend to be flatter in oscillating flow, the velocity profile of the oncoming flow may not have to change much in the entrance region. Their hypothesis so far was not supported by experiments.

Disselhorst and van Wijngaarden (1980) studied separation near the entrance of a tube under conditions of acoustic resonance. They found that separation did not occur for high Strouhal numbers. During the inflow, a boundary layer forms on the pipe walls; during the outflow, a jet emerges from the pipe. They observed and predicted that vortices that were shed during the outflow would interfere with the formation of the boundary layer during inflow.

3.7 Compressibility Effects

Compressibility effects in Stirling engine heat exchangers may be due to

(1) pressure recovery when the working fluid exits from a duct or a heat exchanger tube into a large volume such as the cylinders,

(2) high Mach numbers in heat exchangers,

(3) travelling shock waves caused by the interaction of pressure waves generated by the motion of the pistons,

(4) finite speed of pressure propagation.

38

Pressure recovery. The effect of the increase in pressure on the gas
density can be approximated by an adiabatic expansion. This is commonly
done by a compressibility correction factor ("expansion factor") for flow
through nozzles or sudden expansions (e.g., Perry et al. 1973, p. 5-11).

High Mach numbers. If the Mach number of the fluid exiting from a heat
exchanger is one, a shock will form at the exit and the flow will be choked,
thereby limiting the mass flow rate. It will be shown later that these high
Mach numbers are not expected for Stirling engines discussed in this report.

Travelling shocks. Research on non-linear acoustics in a resonance
tube shows that travelling shocks can form near resonance conditions at Mach
numbers less than one ($M_{max} \approx 0.2$) (Merkli and Thomann 1975 a and b). This
was predicted theoretically by Jeminez (1973). Resonance conditions,
however, are unlikely in Stirling engines because the flow length is
typically much less than half the acoustic wavelength (see Appendix E).
Travelling shocks can develop without resonance, however, by the following
mechanism.

When a piston moves towards top dead center, it causes a compression
wave to travel from the piston face. This wave travels through the
cylinder, ducts and heat exchangers. The high-pressure part of a wave
travels faster than the low-pressure part of the wave. Therefore, the
pressure wave steepens and may form a shock (Shapiro 1954, p. 949-950).
This process is affected by friction and heat transfer only through the
change in the local velocity of sound due to change in local fluid
temperature. A simple analysis of this type of shock formation is carried
out in Appendix E. This worst case estimate assumes that the working fluid
motion is driven by a piston with a velocity amplitude of $M_{max} \approx 0.15$ (the
maximum value found in the data base, see Section 7). The fluid temperature

is assumed to vary linearly from $T_c = 350K$ to $T_h = 1050K$ throughout the engine and the frequency is the highest one found in the data base (SPDE-D), $f = 105$ Hz. Appendix E explains why this may be considered a worst case.

The results of this worst case show that formation of shocks in the Stirling engines in this data base is not expected. The analysis is limited in that it only includes right-travelling waves and does not take into account the interference of right- and left-travelling pressure waves from the opposing pistons of an engine, which would distort the Mach lines used to predict shock incipience.

A more complete analysis of compressible flow in Stirling engines was carried out by Organ (1982b) and modifications were proposed by Taylor and Aghili (1984). Organ's analysis predicts that there is no incipient shock for the special case of the air-charged engine discussed in his paper. This section shows that incipient shock formation is unlikely in the engines in the data base.

Finite speed of pressure propagation. Pressure changes propagate with finite speed, i.e., the sum of the velocity of the piston causing the pressure change and the velocity of sound. Therefore, a phase lag is expected between the pressures at both ends of a heat exchanger. If this phase lag is a small part of the cycle, pressure propagation throughout the heat exchangers may be considered instantaneous.

4. HEAT TRANSFER IN OSCILLATING PIPE FLOW

Since convective heat transfer depends on the velocity distribution, the similarity parameters for fluid mechanics affect the heat transfer: Re_{max}, Re_ω, A_R or ℓ/d. In addition, similarity parameters from the energy equation are important: the Prandtl number, Pr, and for high speed flows, the Eckert number, Ec, the Mach number, M, and ℓ_h/d as a measure of the thermal entrance length. The wall temperature, T_w, the bulk fluid temperature at the hot end, T_h, and at the cold end, T_c, also control heat transfer.

4.1 Qualitative Considerations

Limited fluid displacement. The limited streamwise displacement of fluid in Stirling engines may limit heat transfer from the heat exchanger wall or matrix as discussed in Section 2.1. Figure 4-1 shows fluid trajectories based on the plug flow assumption. While ℓ_h is the characteristic streamwise length for the heat transfer problem, the flow length ℓ is used in this study because $\ell \approx \ell_h$ in most Stirling engines and in many cases ℓ_h is not documented.
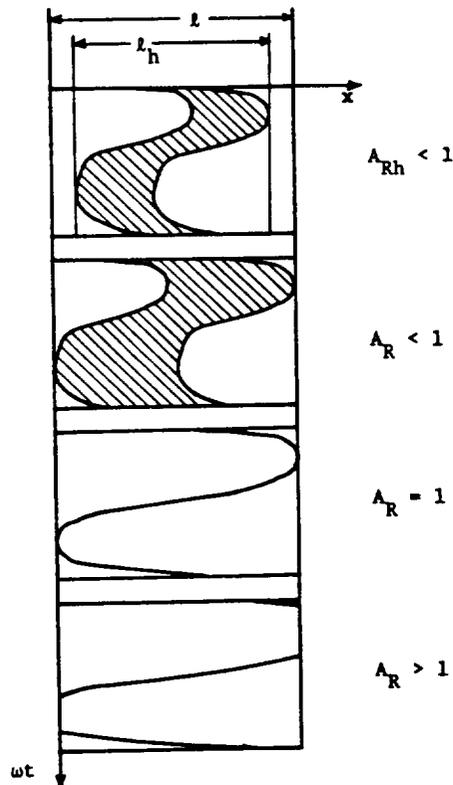
Figure 4-1: Fluid displacement in heat exchangers.

Under the plug flow assumption, the A_R values indicate:

$A_R < 1$	Some fluid does not leave the heat exchanger.
$A_R = 1$	All fluid moves into and out of the heat exchanger.
$A_R > 1$	Some fluid moves through, some fluid moves in and out of the heat exchanger.

Assessing plug flow, Organ (1975, p. 1016) argued that, in the absence of axial mixing, the fluid that never leaves the heat exchanger in the case of $A_R < 1$ could be considered additional dead volume. In turbulent flow, the presence of axial mixing may invalidate Organ's model.

The velocity profiles for laminar flow in Figure 3-2 and in Appendix C show that plug flow is not a good assumption unless Re_ω is very high. In turbulent flow, plug flow may be a good assumption but axial mixing will become important. The velocity profiles show that, in fully developed oscillating pipe flow, the fluid displacement varies with radial distance. Therefore, Organ's (1975) concept of moving temperature wavefronts is only a rough approximation for turbulent flows. In fact, the radial variation in fluid displacement leads to enhanced axial heat transfer as discussed in Section 4.2.

Two temperature driving potentials. Typical boundary conditions for a tubular heat exchanger in a Stirling engine are sketched in Figure 4-2.
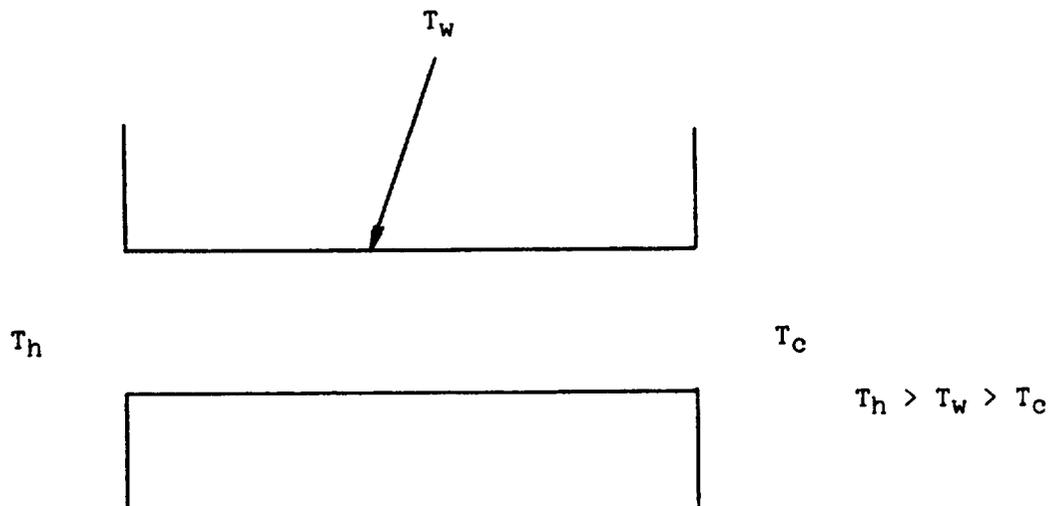
Figure 4-2:   Boundary conditions for heat transfer in a heater.

During the hot blow, gas from the expansion space (at temperature T_h) will stream through the tube into the regenerator. The laminar velocity profiles in Figure 3-2 show that, at higher values of Re_ω, the fluid near the tube wall may flow in one direction while the core moves into the opposite direction ($Re_\omega = 30$, crank angles 150° and 180°). For those parts of a cycle where counterflow occurs, an unusual heat transfer situation exists: the wall gives off heat to the fluid near the wall which enters the tube at T_c from the regenerator. The fluid coming from the expansion space receives heat from the near-wall-fluid in a counter-flow heat exchange process.

In this case, the heat transfer has two driving potentials, $(T_w - T_c)$ and $(T_h - T_c)$ where $(T_w - T_c) > (T_h - T_c)$. It appears that backflow near the wall may have a significant effect on heat transfer. Its influence would depend on the degree of mixing within the near wall shear layer. The concept of two driving potentials for heat transfer in oscillating flow is

44

also important because of the augmentation of heat transfer in the axial direction discussed in the next section.

A situation of two temperature driving potentials also exists in film cooling of gas turbine blades, where the temperature differences between the hot gas in the free stream and the injected cooling air determines the heat transfer in addition to the temperature difference between the free stream and the blade surface. A concept like the film cooling effectiveness may prove useful for the interpretation of experimental results on heat transfer in oscillating flow.

4.2 Axial Heat Transfer in Laminar Oscillating Flow

This section discusses how energy transport due to an axial temperature gradient is enhanced by flow oscillation. Note that this augmentation does not depend on turbulent cross-stream mixing and that the analysis only holds for laminar pipe flow.

Physical interpretation. When fluid oscillates in a duct in the presence of an axial temperature gradient, large oscillating temperature gradients normal to the flow direction are generated. During half of the cycle, cold fluid at the core of the duct extracts thermal energy from the hot fluid in the boundary layer. During the other half of the cycle, hot core fluid heats up cold fluid near the pipe wall. Thus heat is transferred from the hot end to the cold end of the duct. For further physical interpretation, see Kurzweg (1985b, p. 298).

Note that this physical interpretation, as well as the analyses discussed below, hold for laminar flow. In turbulent flow, convective eddy-transport in the cross-stream direction may reduce the oscillating cross-stream temperature gradients that are necessary for the augmentation of axial heat transfer.

Analysis. Watson (1983) analyzed diffusion in laminar, oscillating, fully developed flow in impermeable ducts of arbitrary, uniform cross-section. The analogous heat transfer situation is sketched in Figure 4-2 except that the walls are adiabatic. The pipe connects a high temperature reservoir (T_H) and a low temperature reservoir (T_L). Assume that end effects are negligible and that $A_R \ll 1$. In a stagnant fluid, assuming that there is no convection, the axial heat flow rate is due to conduction:

$$\dot{q} = \frac{\pi d^2}{4} k_f \frac{T_H - T_L}{\ell}$$

Watson (1983) showed that the flux through a duct in which an incompressible fluid oscillates in laminar flow can be expressed similarly as

$$\dot{q} = \frac{\pi d^2}{4} k_{eff} \frac{T_H - T_L}{\ell}$$

where the apparent thermal conductivity

$$k_{eff} = k_f (1 + Au)$$

depends on the augmentation coefficient Au, which is a function of Re_ω, Pr and the dimensionless tidal volume

$$V_T = A_R \frac{2\pi\ell}{d} = \pi \frac{Re_{max}}{Re_\omega}$$

The augmentation coefficient is

$$Au = Au (Re_\omega, Pr, V_T) = V_T^2 \Psi (Re_\omega, Pr)$$

Ψ is given in Appendix F for values of Pr and Re_ω that are relevant for Stirling engine heat exchangers. Kurzweg (1985a, p. 461) provides a plot of Au vs. $\sqrt{Re_\omega}$ for $Pr = 0.1$, 1., 10. He develops an asymptotic solution for $Re_\omega Pr < \pi$. Watson's (1983) exact solution was confirmed experimentally by Joshi et al. (1983) for the case of a circular pipe. Gedeon (1986) and Kurzweg (1985b) treat the case of flow between parallel plates. Kurzweg (1985b) calculates the augmentation of axial heat transfer in the case where the walls are diabatic, i.e. they undergo transient temperature fluctuations. The walls contribute to heat transfer by absorbing thermal energy from the hot fluid and giving off thermal energy to the cold fluid. Kurzweg's (1985b) analysis shows that the augmentation of axial transport is a function of Pr, Re_ω, V_T, and the ratios of fluid to wall conductivity and thermal diffusivity.

4.3 Experimental Data

Hwang and Dybbs (1980 and 1983) presented experimental heat transfer results for oscillating flow in a tube. Figure 4-3 shows a schematic of their experimental facility. Air was moved through a heater and cooler by an oscillating piston into an adiabatic cold space. The piston moved approximately sinusoidally. As it moved to the right, the air expanded in the cooler and into the heater. The heat transfer was calculated by measuring the temperature rise of the cooling water on the outside of the test section. Thermocouples measured the (apparently time averaged) gas temperatures at both ends of the cooler and the wall temperatures in the cooler pipe.
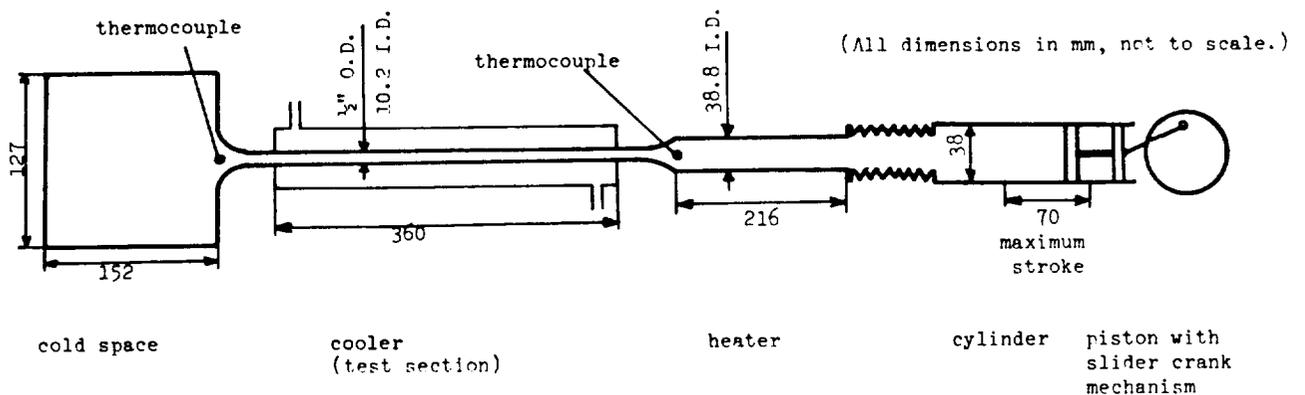
Figure 4-3: Schematic of Hwang and Dybbs' (1980) experiment

A Nusselt number was then formed by the use of the log-mean-temperature difference, the measured average heat flux, and the pipe diameter. The results are replotted in Figure 4-4 by the present authors.
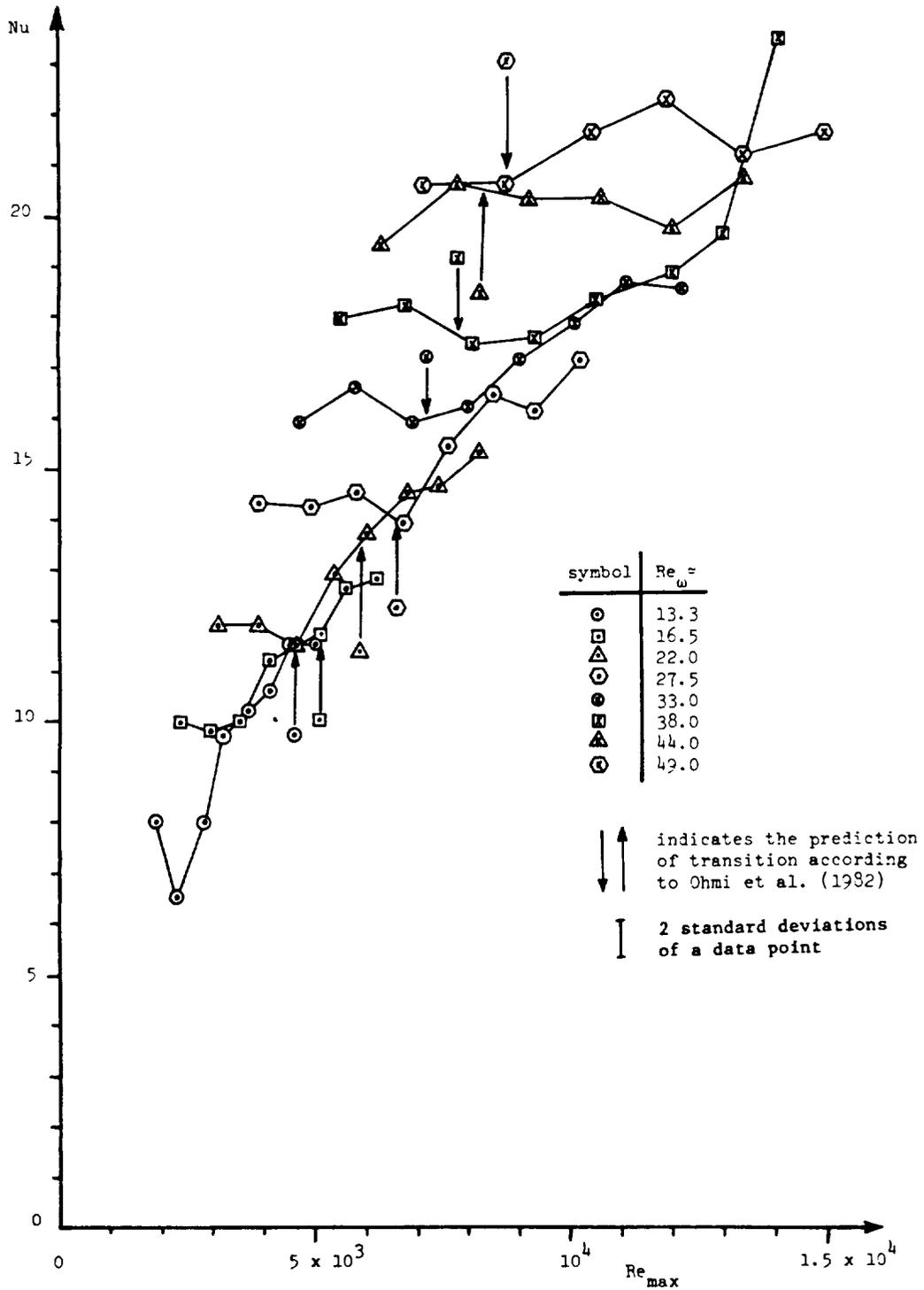
Figure 4-4:   Hwang and Dybbs' (1980) data

49

Hwang and Dybbs (1980 and 1983) plotted Nu vs. Re_{os} (Re_{os} = Re_{max} / (2π)) with A_m = $2/A_R$ as a parameter. In this experiment only two of the parameters A_R, Re_{max} and Re_ω could be specified independently. A_R is physically not significant since for most data points the gas will be blown completely through the heat exchanger ($A_R > 2$), thus Re_{max} and Re_ω remain as the only significant parameters.

The data in Figure 4-4 show certain trends:

(a) For most values of Re_ω, the data show a small slope for low values of Re_{max}, then the slope increases with increasing Re_ω.

(b) The data points with the higher slope tend to lie in one common band.

(c) The individual data points typically scatter within a band that is wider than two standard deviations of a single data point; i.e., the scatter of the data cannot be accounted for by the random error of single data points.

The lower Re_{max} data points of each curve may represent predominantly laminar flow patterns over a cycle while the parts of the curves with greater slope may represent turbulent flow during parts of the cycle. This is argued by Hwang and Dybbs analogous to unidirectional steady flow where $Nu \propto Re^{1/3}$ in laminar flow and $Nu \propto Re^{0.8}$ in turbulent flow. In view of statement (c) on the scatter of data no further conclusions are drawn.

The heat transfer in Hwang and Dybbs' experiment consists of two different processes:

(a) blow of hot air through the cooler pipe into the cold space. During this blow the heat transfer may be approximated by

$$\dot{q}'' = h \, \Delta_{T_{lm}}$$

where ΔT_{lm} is the log mean temperature difference

and $h = \dfrac{k_g Nu}{D}$ k_g = conductivity of the gas

This can be computed if the instantaneous heat flux and log-mean temperature difference (LMTD), or at least the time average values for this blow is known.

50

(b) blow of cool air through the cooler pipe into the heater.
Again, a value of Nu‾ based on the time-average heat flux and
LMTD for this part of the cycle could be calculated.

In Hwang and Dybbs' experiment, however, only the heat flux averaged
over the whole cycle and the LMTD based on temperatures averaged over the
whole cycle are known. Thus the Nusselt number calculated is neither
representative of the hot blow nor of the cold blow, but is an average of
the two. The heat flux that Hwang and Dybbs used to calculate a Nusselt
number may be due to heat transfer during the hot blow only. The LMTD which
is apparently based on time-averaged temperatures probably underestimates
the temperature differences during hot blow. Thus it is difficult to draw
further conclusions from this data set.

Apparently, none of the transition predictions fit Hwang and Dybbs'
data (Figure 4-5). Possible explanations for this discrepancy are:

(1) The tube was very short (ℓ/d = 28); therefore the transition
criteria which were presumably developed for fully developed
oscillating flow may not apply.

(2) The first data point on each curve may be taken from relative
amplitudes that are too small to measure the heat transfer
coefficient accurately (A_R = 1.8).

Neither criterion may be sufficient to explain the change in
time-averaged heat transfer for the Hwang and Dybbs experiment because the
heat transfer is a function of:

(a) the location where turbulence occurs (e.g., near the wall or
in the core).

(b) the relative time during which laminar and turbulent flow are
present during the same cycle.
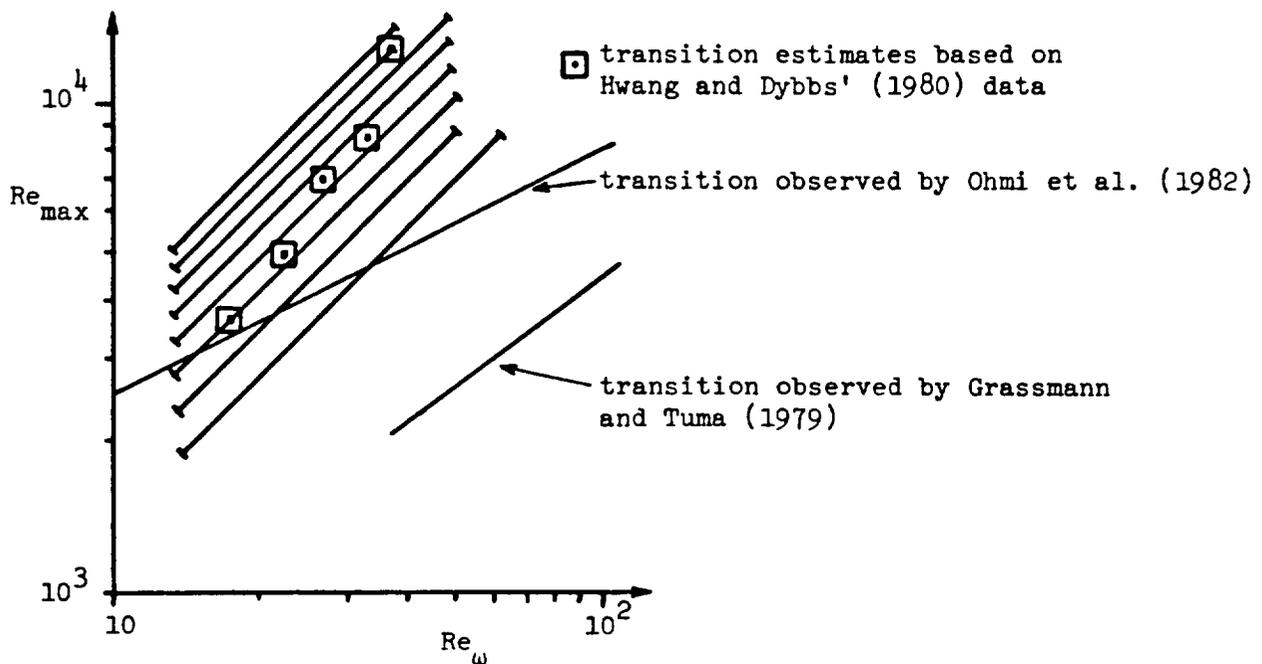
Figure 4-5: Comparison of prediction and observation of transition.

Iwabuchi and Kanzaka (1982) studied heat transfer in oscillating flow in a test facility that was designed to obtain results for the design of a specific prototype engine. A rough estimate indicates that they operated in the laminar regime (11 < Re_ω < 83, 145 < Re_{max} < 733). They did not correlate their results in terms of a Reynolds number and a dimensionless frequency but they studied the dependence of the heat transfer on parameters such as rpm, mean pressure and phase difference between the two opposing pistons. Their heat-transfer results are, therefore, not generally applicable. They made the observation, that the choice of the phase difference (90° or 180°) did not change the heat transfer provided that the

Schmidt analysis was used to calculate the mass flow of gas through the heat exchanger.

5. FLUID MECHANICS AND HEAT TRANSFER IN REGENERATORS

In the complex geometries of regenerators, flow separation is expected. Therefore, analytical methods are not applicable and experimental results are required.

5.1 Steady Flow

Stacked, woven wire screens, randomly stacked metal fibres, folded sheet metal, metal sponge and sintered metals are used as regenerator matrices. Steady flow through these matrices has been studied extensively in porous media research and in studies related to gas turbine and Stirling engine regenerators.

Flow Regimes in Porous Media Flow

Dybbs et al. (1984) classified the steady flow regimes in porous media according to a Reynolds number based on the average pore diameter.

Re < 1	Darcy flow regime
1 < Re < 10	Boundary layers begin to develop on the pore wall
10 < Re < 175	laminar flow
175 < Re < 250	separated laminar flow, vortex shedding
250 < Re < 300	separated flow with random wakes
Re > 300	turbulent flow

The Reynolds numbers separating these regimes are expected to hold for only small values of Re_ω and only for materials similar to those used by Dybbs et al. (1984), but they represent the only known work on transition that

would apply to regenerator matrices. The complex and irregular geometries
of porous media and the complex flow patterns in flows with Re > 175 make it
difficult to predict pressure drop and heat transfer with numerical methods.
Therefore experimental results are required for the prediction.

The Permeability Model

Beavers and Sparrow (1969) showed experimentally that the pressure drop
for steady flow of an incompressible fluid through a porous material can be
described by

$$-dp/dx = a\mu V + b\rho V^2$$

where:

a, b are constants to be determined;

V is the superficial velocity;

$$V = \frac{\dot{m}}{\rho A}$$

A is the frontal area of the porous material. In this equation, the
first term accounts for purely viscous pressure drop as it is described by
Darcy's law:

$$-dp/dx = \mu V/k$$

where the permeability, k, is a constant for each porous material.
Beavers and Sparrow were able to reduce pressure drop data for foamed nickel
(FOAMETAL by General Electric) of various geometries and porosities and for
wire screens by using the square-root of the permeability as the
characteristic length. The Reynolds number and friction factor were defined
as:

$$Re = \frac{V\sqrt{k}}{\nu}$$

$$f = \left(- \frac{dp}{dx}\right) \frac{\sqrt{k}}{\rho V^2}$$

Then the dimensionless pressure drop equation is:

$$f = 1/Re + C$$

The values for C were found to be close to C = 0.074 for FOAMETAL and wire screen, while a specimen of FELTMETAL (randomly stacked fibers, Huyck Mfg. Co.) had a higher value of C = 0.132. There are free fiber ends in FELTMETAL which are not found in the other materials. This structural difference may be the reason for the difference in C.

To see whether the results obtained by Beavers and Sparrow are relevant for Stirling engine flow conditions, the present authors calculated the Reynolds number for the wire screen specimen, which Beavers and Sparrow used. This Reynolds number, comparable to Re_{max}, ranged from about 64 to 10^4.

In order to use the friction factor correlation

$$f = 1/Re + 0.074 ,$$

the permeability must be known. This quantity is obtained experimentally. The pressure drop of creeping flow is measured and the permeability is calculated from the experimental data using Darcy's law as given above.

Dybbs et al. (1984) studied steady flow in porous media. They observed that at higher velocities than those characteristic of Darcy flow, the friction factor is a function of a Reynolds number based on the hydraulic diameter and on the ratio of length to diameter of a typical pore. Their explanation was that the flow must develop anew in every pore. For the prediction of pressure drop and heat transfer, this may mean that the length-to-diameter ratio of a typical pore should be included as an additional geometric parameter. The permeability cannot represent the effect of the pore shapes properly because it is measured in the

56

non-inertial Darcy regime. This is one reason why only geometrically similar materials have the same C-value as observed by Beavers and Sparrow (1969).

Macdonald et al. (1979) reviewed research on flow in porous media consisting of spherical beads, cylindrical fibers, sand, gravel, and many others. They obtained an equation that predicts pressure drop for a wide range of materials within ±50%.

Joseph et al. (1982) showed that the pressure drop in a bed of packed spheres can be related to the drag on a single sphere. They also lent theoretical support to the velocity-squared term proposed by Beavers and Sparrow (1969).

Beavers et al. (1973) studied the influence of the shroud bounding porous media. They found that the pressure drop in beds of packed spheres was influenced by the walls for shroud-diameters as small as 40 sphere diameters.

Friction Factor Correlations

Kays and London (1984, p. 149) provide widely used correlations for flow through stacked screens. Walker and Vasishta (1971) present experimental data for dense-mesh wire screens. Miyabe et al. (1982) provide additional experimental data for flow through stacked screens, Takahashi et al. (1984) present data for foamed-metal matrices. Chen and Griffin (1983) derived an empirical equation based on the Kays and London (1964) data that more accurately fits the data. A comprehensive review of regenerator pressure drop and heat transfer correlations for steady flow was prepared by Finegold and Sterrett (1978). The disadvantage of these correlations is that they do not collapse data as well as the correlation proposed by

Beavers and Sparrow (1969) because porosity remains as a parameter in addition to the Reynolds number. The advantage is that they were obtained for gas flows so that some compressibility effects such as reduced effective flow area, which is discussed below, are included.

Compressibility effects in flow through screens. Organ (1984) recommended that the Mach number be included as a correlating parameter for the prediction of pressure drop in regenerators. His suggestion is based on earlier work by Benson and Baruah (1965) and Pinker and Herbert (1967) where the flow of air through a single screen was investigated.

Benson and Baruah (1965) stated in their conclusions (p. 458) that "The resistance coefficient of a gauze is a function of Mach number, Reynolds number and solidity," as quoted by Organ, solidity = 1-porosity. In the same paper they plot the resistance coefficient of screens (with porosities of 0.47...0.67) versus downstream Mach numbers. For low Mach numbers (M < 0.1) Benson and Baruah's (1965) results show that the resistance coefficient is virtually independent of Mach number. Benson and Baruah (1965) also state in their conclusions (p. 458) that a "gauze behaves like a crude nozzle. There is a considerable entropy change in a flow across it." According to Pinker and Herbert (1967, p. 16 and p. 7) this "nozzle" develops at Mach numbers of the oncoming flow of M = 0.2 in the duct and of M = 0.38 for a porosity of 0.53. The duct Mach number required for choking increases with porosity.

Effective Flow Area in Compressible Flow

To calculate the mass flow rate through a nozzle, the flow area is multiplied by an expansion factor (see e.g., Perry et al. 1973, p. 5-11). It accounts for the reduction in effective flow area due to the adiabatic

expansion from the upstream to the downstream pressure. It is expected that

a similar effect can be observed when flow passes through a single screen.

It is not likely that this effect will be significant for flow through

stacked screens because the pressure differences across individual screens

will be small and heat transfer from the matrix to the gas will be possible.

Choking and Pressure Drop in Compressible Flow

Beavers and Sparrow (1971) calculated the conditions under which the

flow into a porous material would be choked based on isentropic flow.

According to Benson and Baruah (1965, p. 458), a considerable change in

entropy takes place when a gas passes through at higher Mach numbers. This

entropy change may not be significant for the low Mach numbers encountered

in Stirling engines, however.

Beavers and Sparrow (1971, p. 1856) also analyzed gas flow within a

porous matrix using $\sqrt{k}$ (the square-root of the permeability) as the length

scale. They calculated the maximum length ℓ_{max} of porous material before

the exit flow would be choked. A regenerator operated at high Mach number,

low Reynolds number and with a high $\ell/\sqrt{k}$ is most likely to choke. Even in

the extreme case of the cold blow through the 4L23 regenerator $\ell_{max}/\sqrt{k}$ >

$10\ell/\sqrt{k}$. Therefore choking is not expected in regenerators.

This analysis is tentative because:

(1) The permeabilities were calculated from the comparison of

permeability and hydraulic diameter for one specimen that Beavers and

Sparrow (1969) used; to calculate the permeabilities for other wire-mesh

regenerators a linear relationship between hydraulic diameter and the

square-root of the permeability was assumed.

59

(2) the graphs used to calculate $\ell_{max}/\sqrt{k}$ in Beavers and Sparrow (1971) were plotted...

(a) for air only.

(b) for discrete values of Reynolds number.

(c) for discrete values of porosity.

Heat transfer correlations. Kays and London (1984, p. 149), Walker and Vasishta (1971), Finegold and Sterrett (1978), and Miyabe et al. (1982) provide heat transfer correlations for packed woven wire screens. These correlations are derived from experimental data that were obtained by the single blow technique described in Kays and London (1984, pp. 154-155). Takahachi et al. (1984) calculated heat-transfer correlations from oscillating flow data. The use of $\sqrt{k}$ as the characteristic length instead of the hydraulic diameter may eliminate the porosity as the independent parameter in heat transfer correlations. This remains to be shown experimentally.

5.2 Unsteady Flow and Heat Transfer in Regenerators

Galitseiskii and Ushakov (1981) studied heat transfer augmentation due to reversing pulsatile flow in porous media. They observed a resonant phenomenon when the diameters of the stationary vortices (generated by the flow over the elements of the porous structure – e.g. the wires of the screen) are comparable to the dimensions of the secondary vortices generated by the flow oscillations. The experiments were performed for $0.6 < Re_{max} < 6$ and $6.5 < Re_{\omega} < 100$, a domain that does not seem applicable to regenerator flow conditions.

Kim (1970) studied oscillating flow through a regenerator consisting of packed spheres. The reduction of his experimental data was based on the

60

assumption that the momentum equation could be considered quasi-steady i.e., the pressure drop is in phase with the mass flow rate. He showed by order-of-magnitude estimates that this was justified (p. 130). He calculated friction factors for gas flow through a bed of packed spheres that were approximately 20% higher than the corresponding steady values. The range of frequencies covered less than a decade. Since the stroke of his apparatus was fixed, the dimensionless frequency of his experiments was proportional to the peak Reynolds number. Therefore, his data do not allow conclusions about the frequency dependence of the friction factor. His results do, however, suggest that fluid friction increases due to flow oscillation. Because the friction factor is higher in oscillating flows than in steady flow, it must depend on frequency (Re_ω). Whether the same is true for wire-screen regenerators must be answered by experiment.

5.3 Regenerator Theory

Stirling engine simulation typically uses a discretization of the engine volume. If the regenerator is subdivided in several control volumes it is not necessary to use regenerator effectiveness to predict heat transfer to and from the regenerator (Walker 1980, p. 140-149). Given an adequate regenerator theory, however, measured effectiveness values can be used to determine volume-averaged heat transfer coefficients of regenerators. This method has been used successfully for gas-turbine regenerators (Kays and London 1984, p. 154-155).

Rice et al. (1985) proposed a theory that takes into account the relatively short blow periods in Stirling engines. Willmot and Hinchcliffe (1976) and Harness and Neumann (1979) proposed methods to take "holdup" into account, i.e., the fact that some fluid may not leave the regenerator by

convection ($A_R < 1$). These approaches seem more promising than the application of standard regenerator theories (e.g. Shah 1981, p. 721-763 or Kays and London 1984, p. 79-89) to Stirling engine conditions, e.g. by Rice et al. (1983) and Miyabe et al. (1982).

6. STIRLING ENGINE DATA BASE

Representative values of the similarity parameters describing the operating conditions of the heat exchangers of 11 Stirling engines are obtained to form a Stirling engine heat exchanger data base.

6.1 Evaluation of Similarity Parameters

Schmidt analysis. The instantaneous mean mass velocity ρu_m is calculated using the Schmidt isothermal analysis (Urieli and Berchowitz 1984, Appendix A1, p. 152). The following assumptions are made for the analysis:

1. The engine consists of three isothermal volumes:
   The hot space (at T_h) consists of expansion space, connecting duct, heater, 1/2 heater-regenerator duct. The regenerator volume (at T_r) consists of 1/2 heater-regenerator duct, the regenerator and 1/2 regenerator-cooler duct. The cold space (at T_c) consists of compression space, connecting duct, cooler, 1/2 cooler-regenerator duct. T_r is the mean effective regenerator temperature (Urieli and Berchowitz 1984, Appendix A4, p. 158)

$$T_r = \frac{T_h - T_c}{\ln(T_h/T_c)}$$

2. The pressure is uniform throughout the engine.

3. The ideal gas law holds.

4. The variations of the compression and the expansion volume are sinusoidal.

5. There is no working gas leakage.

6. The engine operates at constant speed in a cyclic steady state.

7. The kinetic and potential energies of the gas are negligible.

Isothermal analysis. The isothermal analysis is based on the same assumptions as the Schmidt analysis except point 4. The variations of compression and expansion volumes are calculated from the kinematics of the drive mechanism. Appendix A shows Reynolds number variations calculated for

63

a rhombic drive engine (GM GPU-3) with Schmidt (Figure A-3) and isothermal

analysis (Figure A-1) (Youssef 1986). The two analyses differ in the shape

of the Reynolds number transients. The difference in amplitude of

approximately 20 percent is acceptable because this data base is only used

to establish approximate ranges of heat exchanger operating conditions.

Reynolds and Mach number. The thermodynamic analysis is used to

calculate the changes of mass in various control volumes of the engine.

From the mass changes in the control volumes, mass flow rates are

calculated, and from these Reynolds and Mach numbers. u_m, the mean

velocity, is the velocity averaged over the flow area, e.g. over the

cross-sectional area of a duct. Figure A-1 shows the variation of the

Reynolds numbers at the inlet and outlet of a GPU-3 heater calculated by the

isothermal analysis. The values at inlet and outlet differ because working

gas is stored in the heat exchanger during the compression and released

during the expansion part of the cycle. This changes the mass flux term ρu_m

in the Reynolds number. Therefore, the maximum Reynolds number at each

operating point is represented by a range of values. This range represents

the variation throughout the heat exchanger due to asymmetric volume

variations in storage and release of working gas during compression and

expansion (see Appendix A). The dynamic viscosity is evaluated at the

temperature of the corresponding control volume, the density is calculated

from the ideal gas law, and the speed of sound is evaluated assuming

constant specific heats, $a = \sqrt{\gamma RT}$. The hydraulic diameter used to calculate

Re_{max} for non-tubular geometries (rectangular ducts) is defined as the ratio

of volume to heat transfer area of the heat exchanger.

Dimensionless frequency Re_ω and relative amplitude A_R. The

dimensionless frequency is evaluated at the mean pressure and the

temperature of the respective heat exchanger. For regenerators, the hydraulic diameter is used as a length scale. The relative amplitude of fluid motion, A_R, is evaluated by integrating the mass flow at the heat exchanger inlet or outlet between two flow reversals. For the evaluation of the displacement of a fluid element between flow reversals the fluid is assumed to move into and out of the heat exchangers as a plug.

6.2 Documented Engines

The choice of documented flow conditions was restricted by the data available. Table 6-1 lists (alphabetically by abbreviation) the name of the engines included in the data base, a brief description of the operating conditions and the reference used. The amplitudes of the pistons and displacers of the free piston engines were not obtained from the analysis but experimental values were taken from the references.

The SPDE "design" point (SPDE-D) was calculated from phase angle and amplitudes, measured in the trial run represented by "SPDE-T" but using design pressure and frequency. A more realistic approximation to the intended operating conditions was calculated from data provided by Tew (1986) and is labeled "SPDE-O."

<center>Table 6-1: Documented Engines</center>

Engine Type	Operating Conditions: Speed or frequency Mean pressure Working fluid	Reference	Abbreviation

<center>Kinematic Engines</center>

General Motors GPU3	2500 rpm 41 bar He	Urieli and Berchowitz (1984), pp. 37 and 39	GPU3
Mechanical Technologies, Inc. MODI (upgraded)	4000 rpm 150 bar H_2	Richey (1986)	MODI
United Stirling AB P40	4000 rpm 150 bar H_2	Tew (1983) pp. 80-86	P40
Technical University of Denmark, Stirling Total Energy System	1500 rpm 100 bar He	Andersen (1979) pp. 50-52	STES
UK Consortium Stirling Engine (α-configuration)	3000 rpm 150 bar He	Dunn et al. (1982) p. 68	UK
Ford Phillips 4-215	4000 rpm 200 bar H_2	Urieli and Berchowitz (1984), p. 30	4-215
General Motors 4L23	2000 rpm 103 bar H_2	Martini (1982) p. 32	4L23

Table 6-1: Documented Engines (continued)

Engine Type	Operating Conditions: Speed or frequency Mean pressure Working fluid	Reference	Abbreviation
	Free Piston Engines		
Mechanical Technologies, Inc. Engineering Model	58 Hz 60 bar He	Dochat (1985)	EM
Sunpower, Inc. 3 kW Generator Set	60 Hz 25 bar air	Berchowitz (1985)	Genset
Sunpower, Inc. RE-1000	30 Hz 70 bar He	Schreiber (1983)	RE1000
Mechanical Technologies, Inc. Space Power Demonstrator Engine	trial parameters: 73 Hz 75 bar He	Dochat (1985)	SPDE-T
	extrapolated to design conditions: 105 Hz 150 bar He	Dochat (1985)	SPDE-D
	intended operation: 105Hz 150 bar He	Tew (1986)	SPDE-O

7. RESULTS AND DISCUSSION

The operating conditions of the heat exchangers in the Stirling engine data base are presented in terms of similarity parameters and conclusions are drawn about the conditions of fluid mechanics and heat transfer in heaters and coolers and in regenerators. The significance of various similarity parameters is discussed. Plots of heat exchanger operating conditions in terms of Re_{max}, Re_ω and A_R are used.

7.1 Heaters and Coolers

Entrance and exit losses. Table 7-1 gives a list of rough estimates of the points of the total heat exchanger pressure drop occurring at the heat exchanger entrance, in the duct of the heat exchanger, and at the exit. The estimates are based on the assumption of steady, unidirectional, turbulent flow in a rough pipe. Between 15% and 50% of the heat exchanger pressure drop occur at the pipe entrance and exit. Therefore entrance and exit effects are important. They could be estimated from an experiment such as the one by Taylor and Aghili (1984) and should be correlated in terms of the area ratios of contraction and expansion and Re_{max} and Re_ω.

Engine Abbreviation		Portion of the Pressure Drop (in percent) occurring...		
H = heater C = cooler		at the entrance	in the pipe	at the exit
GPU3	H	15	68	17
	C	22	53	25
MODI	H	14	71	15
	C	14	71	15
P40	H	15	70	15
	C	16	67	17
STES	H	22	56	22
	C	24	50	26
UK	H	7	85	8
	C	24	47	29
4-215	H	12	75	13
	C	14	71	15
4L23	H	14	70	16
	C	13	74	13
EM	H	16	67	17
	C	16	67	17
Genset	H	18	62	20
	C	16	62	22
RE1000	H	15	68	17
	C	13	72	15
SPDE	H	17	65	18
	C	18	62	20

Table 7-1: Estimated pressure drop distribution
in heaters and coolers.

Estimated area ratios for the heater-regenerator and cooler-regenerator
flow are listed in Table 7-2 to provide the similarity parameters for
experiments on entrance and exit losses in oscillating flow.

Engine Abbreviation	Heater-Regenerator	Cooler-regenerator
GPU3	11.	11.
MODI	21.	13.
P40	40.	17.
STES	32.	16.
UK	29.	5.9
4-125	30.	18.
4L23	9.2	18.
EM	13.	9.4
Genset	7.6	3.0
RE1000	7.8	4.5
SPDE	13.	9.0

Table 7-2: Ratios of regenerator housing area to heater/cooler flow area.

Developing profiles. Table 7-3 lists ℓ/d values. For heaters and coolers with rectangular cross-section, the hydraulic diameter is used. In steady turbulent flow, the hydrodynamic entrance length is independent of Reynolds number and between 10 and 60 pipe diameters long (Incropera and DeWitt 1981, p. 377). Therefore, developing velocity profiles may be expected throughout many heaters and coolers.

| Engine | (ℓ/d) | |
Abbreviation	Heater	Cooler
GPU3	81.1	42.7
MODI	96.9	92.0
P40	93.7	80.0
STES	51.0	38.9
UK	219.0	30.8
4-215	115.0	96.7
4L23	88.6	112.0
EM	81.4	75.9
Genset	59.1	50.9
RE1000	88.5	77.6
SPDE	71.0	62.5

Table 7-3:   Length to diameter ratios of heaters
and coolers.

Flow patterns and axial heat transfer. Figure 7-1 shows that the

operating conditions of heaters and coolers fall within two decades of

dimensionless frequency. The amplitude Reynolds numbers are all above the

Reynolds number at which transition occurs in steady unidirectional flow.

Most heaters and coolers operate in the turbulent flow regime but many are

near transition. Therefore, it is important to understand the transition

process and the characteristics of fluid mechanics and heat transfer in

turbulent oscillating flow. Three heat exchangers operated under

transitional conditions: the RE1000 cooler and the SPDE heater and cooler.

The SPDE cooler is shifted from turbulent to transitional operation as the

engine frequency is reduced. The same is expected if the Genset cooler or

heater is operated at frequencies below the design point. Based on the

discussion above, higher power dissipation and pressure drop than predicted

by quasi-steady analysis are expected in the laminar and transitional

regimes. Due to fluid inertia, there will be a phase shift between pressure

and mean velocity. Therefore, the instantaneous pressure drop cannot be
determined from the instantaneous velocity and acceleration alone.

The trial and design operating conditions of the SPDE fall on a
straight line of slope 1 in the double logarithmic coordinates of Figures
7-1 and 7-3. The ratio of the two similarity parameters is

$$\frac{Re_{max}}{Re_\omega} = \frac{\dfrac{u_{max}d}{\nu}}{\dfrac{\omega d^2}{4\nu}} = \frac{4\ u_{max}}{\omega d}$$

Since d is constant and u_{max} is proportional to ω for any one engine, the
ratio is constant. Therefore Re_{max} is proportional to Re_ω if operating
conditions are extrapolated assuming that only ω changes.
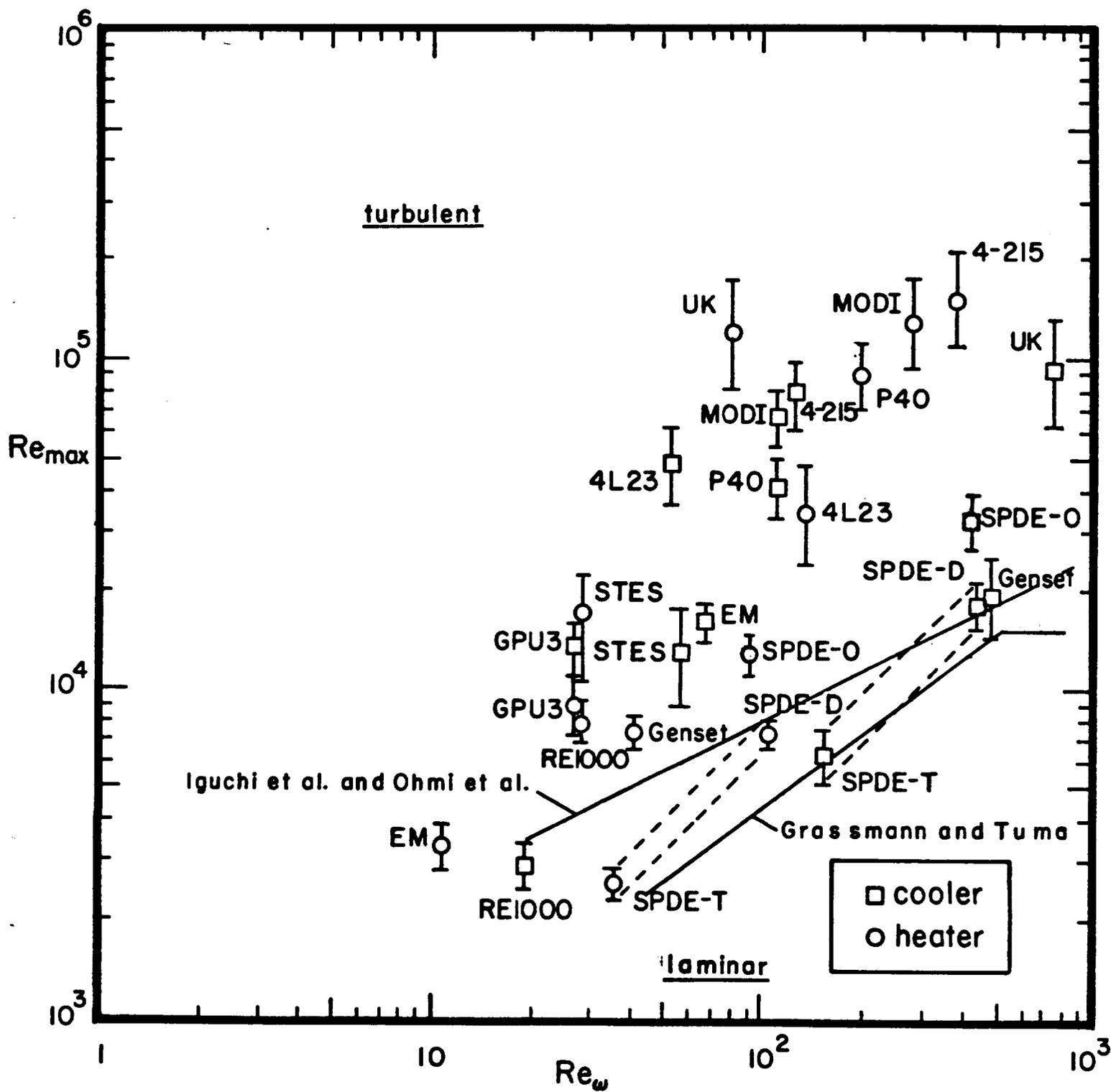
Figure 7-1: Re_{max} vs. Re_ω for heaters and coolers

73

Figure 7-2 shows that the four heat exchangers in the transitional regime are operating with $A_R < 1$; therefore, one might think that axial augmentation would be important. Estimates of this heat transfer augmentation for the SPDE heater and cooler indicate that the axial heat transfer is only about 0.1 - 1.0% of the heat transferred by the heat exchanger, however. This estimate was made using Watson's (1983) analysis and is based on the assumtion that the pipe walls are adiabatic. Further work is required to extend this analysis to non-adiabatic wall conditions as in the Stirling engine.

Figures 7-2 and 7-4 show that the relative amplitude of fluid displacement A_R is the same for the trial and the design conditions, while the dimensionless frequency Re_ω is different. The trial and design conditions differ in the operating frequency and in the fluid density because of the different mean pressures. Therefore

$$Re_\omega = \frac{\omega d^2}{4\nu}$$

is affected while A_R is not affected.

Figure 7-2: A_R vs. Re_ω for heaters and coolers

75
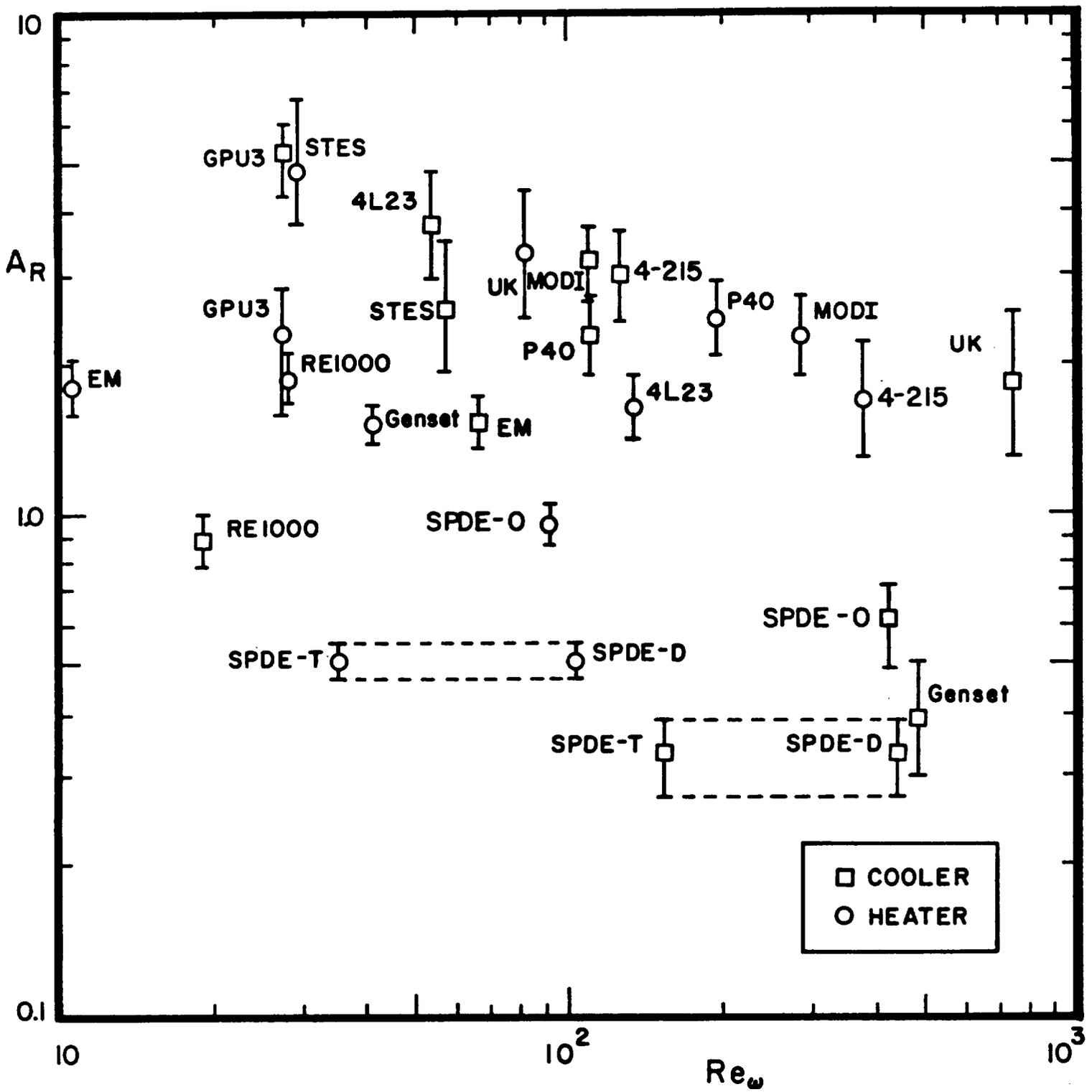
Compressibility effects. Table 7-4 shows that the Mach numbers are small in heaters and coolers, $M_{max} < 0.075$, with the exception of the UK heater ($M_{max} = 0.15$). The density variation due to high velocity in the latter case is (Schlichting 1979, p. 10):

$$\frac{\Delta\rho}{\rho} = \frac{1}{2} M_{max}^2 = 0.012$$

Therefore, high density variations due to high fluid velocity are not expected in the coolers and heaters of these Stirling engines.

Engine Abbreviation	Highest Mach Number in the	
	Heater	Cooler
GPU3	0.042	0.034
MODI	0.067	0.046
P40	0.064	0.030
STES	0.035	0.015
UK	0.153	0.031
4-215	0.072	0.043
4L23	0.027	0.040
EM	0.020	0.029
Genset	0.038	0.026
RE1000	0.007	0.020
SPDE-T	0.008	0.008
SPDE-D	0.011	0.009

Table 7-4: Mach numbers in heaters and coolers.

7.2 Regenerators

Figure 7-3 shows that the flow pattern in most regenerators may be expected to be complex. According to the observations by Dybbs et al. (1984), the flow would be turbulent or transitional for 8 of the 12 regenerator operating points. Since their observations were made in steady-state experiments, they may not hold in oscillating flow or may hold only for low Re_ω and will probably only apply to matrices similar to those studied by Dybbs et al.(1984).

Six of the 11 engines shown in Figure 7-4 have $A_R < 1$ which may limit the heat transfer from the matrix to the adjacent heater and cooler ("holdup").

Mach numbers in the regenerators are $M_{max} < 0.01$ (Table 7-5). Choking of the regenerators is therefore not expected. At these low Mach numbers, the pressure drop in the regenerator matrices is expected to be independent of Mach number, according to the results of Beavers and Sparrow (1971) and Benson and Baruah (1965) discussed in section 5.1. Since porosities of regenerators typically exceed 0.5 and Mach numbers are less than 0.2, choking in regenerator screens is not expected according to experimental results by Pinker and Herbert (1967, p. 16 and 17) which were discussed in Section 5.1.
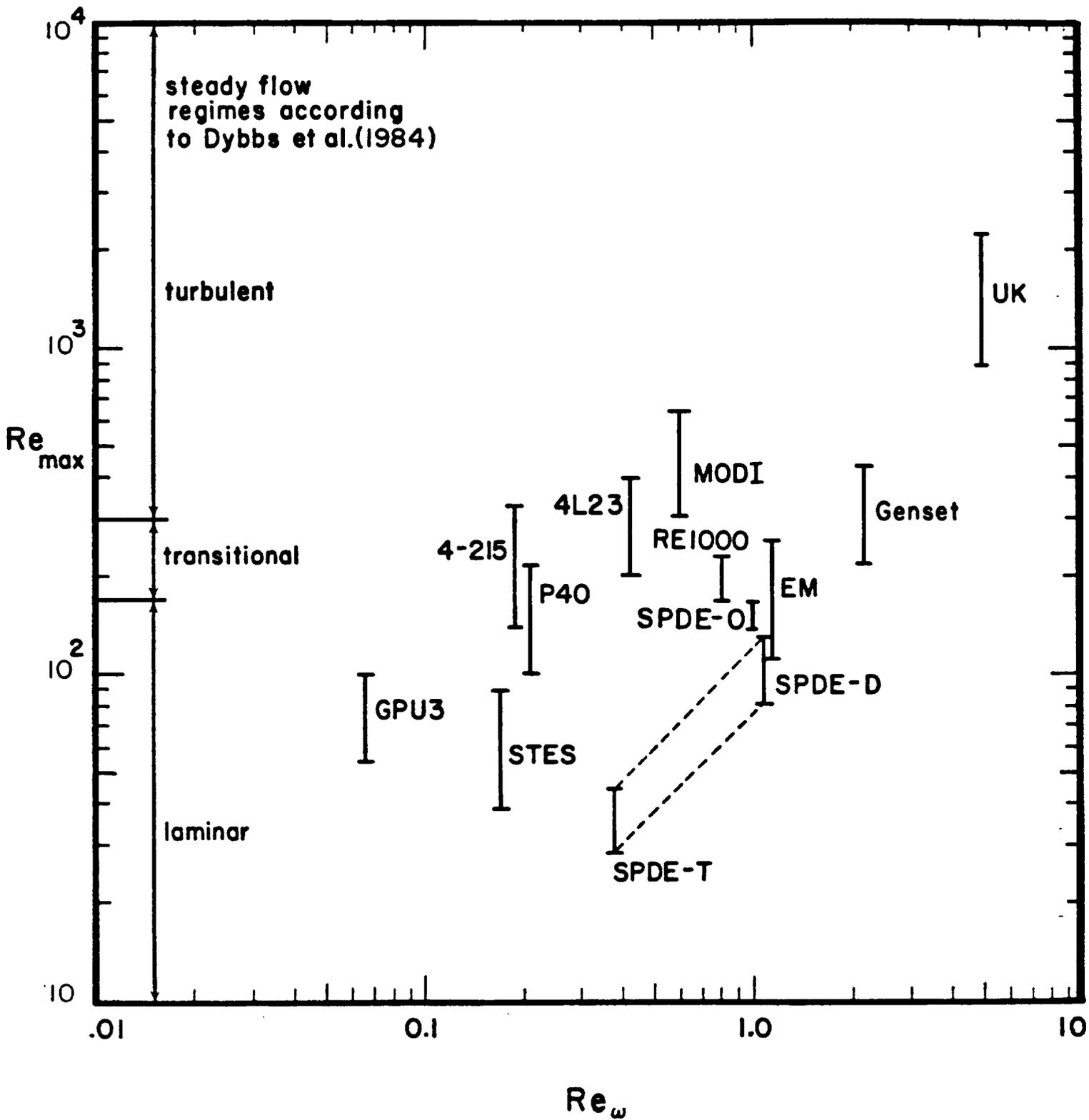
Figure 7-3: Re_{max} vs. Re_{ω} for regenerators

78
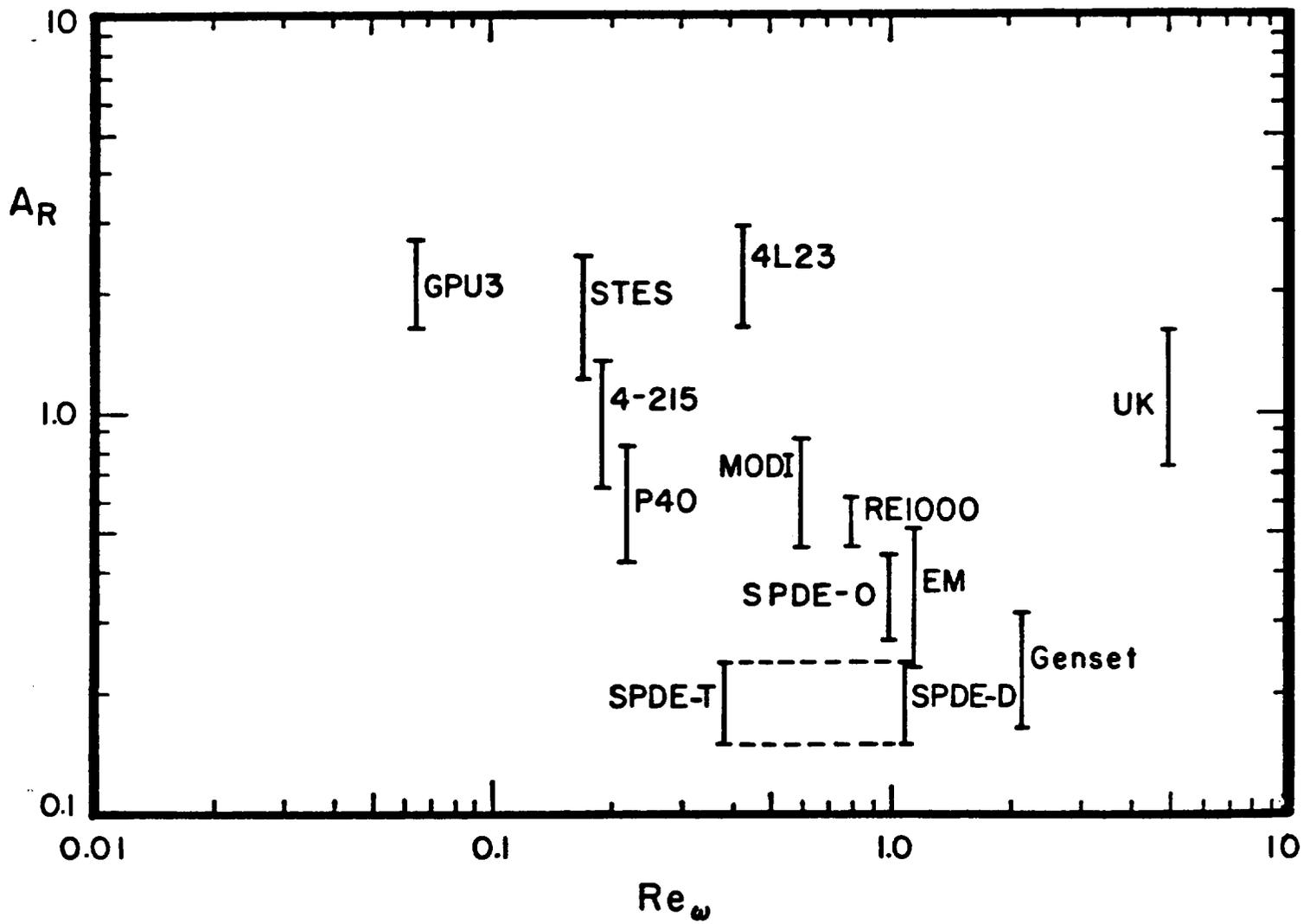
Figure 7-4: A_R vs. Re_ω for regenerators

Engine Abbreviation	Highest Mach Number in the Regenerator
GPU3	0.0078
MODI	0.0093
P40	0.0061
STES	0.0031
UK	0.0103
4-215	0.0055
4L23	0.0047
EM	0.0056
Genset	0.0096
RE1000	0.0038
SPDE-T	0.0017
SPDE-D	0.0024

Table 7-5: Mach numbers in regenerators.

7.3 Similarity Parameters

After a review of the operating conditions of Stirling engine heat exchangers, several similarity parameters can be eliminated. Eckert numbers were calculated from

$$Ec = (\gamma - 1) \frac{T}{\Delta T} M_{max}^2$$

They range from 0.0066 (SPDE-D, heater) over 0.025 (MODI, heater) to 0.13 (UK heater). Therefore, viscous dissipation is not considered to contribute significantly to the heat transfer, with the exception of the UK heater. The exact numerical value of the Eckert number is not important, provided that it is less than ~ 0.1.

A similar argument can be made for the Mach number, because Tables 7-4 and 7-5 show that they are small, with the possible exception of the UK heater. Thus similarity with respect to Mach number is not required as long as $M_{max} < 0.1$. Organ (1982a) challenged this argument with experimental

80

pressure drop results, but his data seem to support a strong frequency -
(rpm-) dependence of pumping power.

Pressure propagates through the heat exchangers fast compared to the
cycle time. Table 7-6 provides estimates of the time required for
propagation of pressure through the heat exchangers. It is assumed that
pressure waves travel with the speed of sound which underestimates the
propagation speed slightly. The data are given in degrees of crank angle.
In all heat exchangers but the UK and 4-215 heater, pressure propagates
through the individual heat exchangers within 1/100 of the cycle time.
Therefore, effects due to the finite propagation speed of pressure are not
expected to be significant.

Engine	Heater	Cooler	Regen.
GPU-3	2.0	0.69	0.24
MODI	3.3	1.5	0.83
P40	2.9	1.3	0.51
STES	0.76	0.58	0.094
UK	5.2	1.6	0.64
4-215	4.5	1.5	0.43
4L23	2.0	1.1	0.16
EM	1.2	2.0	0.86
Genset	2.8	6.2	3.1
RE1000	1.2	0.82	0.52
SPDE-T	1.7	2.4	0.54
SPDE-D	2.4	3.5	0.78

Table 7-6: Time estimates for pressure wave propagation
through heat exchangers in degrees of crank angle.

8. CONCLUSIONS AND RECOMMENDATIONS

In this report, important similarity parameters are introduced:

Re_{max} like Reynolds number in steady flow

Re_ω measure of unsteadiness

A_R, A_{Rh} relative amplitude, important for heat transfer

ℓ/d, ℓ_h/d developing length effects

Length ratios maintain geometric similarity.

De   like Re_{max} for curved pipes

Area ratios maintain similarity for entrance and exit losses.

For porous media, the square-root of the permeability, $\sqrt{K}$, may be the appropriate length scale to be used in Re_{max} and Re_ω.

Previous research results are discussed and 11 Stirling engine operating points are plotted in terms of the parameters.

Due to the acceleration and deceleration of the fluid, velocity profiles and stability of laminar oscillating flow differ from steady laminar flow. Transition occurs at higher Re_{max} as Re_ω is increased. Adequate turbulence models or correlations for turbulent oscillating flow do not exist. Results of past research on heat transfer are not generally applicable except the results for enhanced axial transport in oscillating laminar flow. It was shown that the heat exchangers of several engines are operating in or near the laminar-to-turbulent transition region while most heat exchangers operate in the turbulent regime. Several heat exchangers are long relative to the fluid displacement, $A_R < 1$. This means that some heat exchangers may add to the engine dead volume.

The effect of compressibility of the working gas on pressure recovery can be accounted for by assuming an adiabatic expansion at the heat

exchanger and duct outlets. Choking is not expected due to the low Mach numbers encountered. Incipient shock formation was shown to be unlikely using a worst-case analysis. Pressure waves were calculated to pass through the heat exchangers quickly compared to the cycle time.

A review of the literature has shown that immediate attention is needed in the following areas to assess the trade-offs between heat transfer and viscous dissipation in oscillating flow:

1. The process of transition must be understood more clearly. Work on this topic in tubular geometries will improve the understanding of heat transfer and pressure drop mechanisms in the heaters and coolers of Stirling engines.

2. The means by which turbulence structure is affected by flow oscillation must be better understood, possibly leading to ways of modifying standard turbulence models so that turbulent oscillating flows can be accurately predicted.

3. The effects of thermal and hydrodynamic entrance lengths on heat transfer and pressure drop in tubes and regenerator matrices must be better understood.

4. A test of the permeability model should be made. It may provide a more general characterization of regenerator matrices than the characterization by hydraulic radius and porosity currently used.

Once these topics have been addressed, non-sinusoidal oscillating flow should be studied experimentally to determine how general the results of 1-4 are. A computational program can then use the experimental data from 1-3 to calculate heat transfer in oscillating flow with compression and expansion of the working gas. Its results should be confirmed experimentally.

83

ACKNOWLEDGEMENTS

REFERENCES

Andersen, N. E. (1979): "Stirling Total Energy System (STES)." Thesis
for the Danish Licentiat Degree (Lich. Techn.) at the Laboratory for
Energetics, The Technical University of Denmark, Report #RE 79-8,
September 1979.

Beavers, G. S. and Sparrow, E. M.(1969): "Non-Darcy Flow through
Fibrous Porous Media." ASME Paper 69-APM-CC.

Beavers, G. S. and Sparrow, E. M. (1971): "Compressible gas flow
through a porous material." Int. Journal of Heat and Mass Transfer,
Vol. 14, pp. 1855-1859.

Beavers, G. S., Sparrow, E. M., and Rodenz, D. E. (1973): "Influence
of Bed Size on the Flow Characteristics and Porosity of Randomly Packed
Spheres." ASME Journal of Applied Mechanics, pp. 655-660, September.

Benson, R. S. and Baruah, P. C. (1965): "Non-Steady Flow in a Gauze in
a Duct." Journal of Mech. Engr. Science, Vol. 7, No. 4, pp. 449-459.

Berchowitz, D. (1985): Conversations in August and September.

Berger, S. A., Talbot, L. and Yao, L.-S. (1983): "Flow in Curved
Pipes." Annual Review of Fluid Mechanics, Vol. 15, pp. 461-512.

Cayzac, R., Fauchas, J. and Clarion, C. (1985): "Stability of Unsteady
Parallel Flows by the Method of Energy." In: Kozlov, V. V. (ed):
Laminar-Turbulent Transition. 2nd IUTAM Symposium on Laminar-Turbulent
Transition, Novosibirsk 1984. Berlin: Springer-Verlag.

Chan, K. W., and Baird, M. H. (1974): "Wall Friction in Oscillating
Liquid Columns." Chemical Engineering Science, Vol. 29, pp. 2093-2099.

Charreyron, P. O. (1984): "Convective Heat Transfer Enhancement in
Unsteady Channel Flow--A Review." In: Roethe, P. H. (ed): Forum on
Unsteady Flow, ASME FED-Vol. 15, presented at the Winter Annual Meeting
of the ASME, New Orleans, LA, December 9-13, 1984.

Chen, N. C. J. and Griffin, F. P. (1983): "Effects of Pressure-Drop
Correlations on Stirling Engine Predicted Performance." 18th
Intersociety Energy Conversion Engineering Conference. Proceedings
(IECEC paper 839114), pp. 708-713. New York: American Institute of
Chemical Engineers.

Davis, S. H. (1976): "The Stability of Time-Periodic Flows." In:
VanDyke, M., Vincenti, W. and Wehausen, J. V. (eds): Annual Review of
Fluid Mechanics, Vol. 8, p. 57-74.

Dijkstra, K. (1984): "Non-Stationary Heat Transfer in Heat
Exchangers." 19th Intersociety Energy Conversion Engineering
Conference. Proceedings (IECEC paper 849092), pp. 1886-1891.
LaGrange, IL: American Nuclear Society.

Disselhorst, J.H.M., and van Wijngaarden, L. (1980): "Flow in the Exit of Open Pipes during Acoustic Resonance." Journal of Fluid Mechanics, Vol. 99, Part 2, pp. 293-319.

Dochat, G. R. (1985): Letter to Authors. 5 November.

Drake, D. G. (1965): "On the Flow in a Channel Due to a Periodic Pressure Gradient." Quart. Journ. Mech. and Applied Math., Vol. 18, Part 1, pp. 1-10.

Dunn, P. D., Rice, G., Preston, C. C., Lipman, N., Stowley, J., Alexander, W. A., Rix, D. H., Burrough, W. E., Marshall, E. L., Reader, G. T., Clarke, M. A., Slee, R. H., and Parker, D. A. (1982): "20 kW UK Consortium Stirling Engine-Specification and Manufacture." In: Stirling Engines-Progress towards Reality. Proceedings of a Conference Held 25-26 March, 1982 at the University of Reading. I MechE Conference Publications 1982-2. London: The Institute of Mechanical Engineers.

Dybbs, A., Kar, K., Groeneweg, M., Ling, J. X. and Naraghi, M. (1984): "A New Interpretation of Internal Heat Transfer Coefficients Porous Media." ASME Paper 84-WA/HT-51.

Edwards, M. F. and Wilkinson, W. L. (1971): "Review of Potential Applications of Pulsating Flow in Pipes." Transactions of the Institute of Chemical Engineers, Vol. 49, No. 2, pp. 85-94.

Faulkner, H. B. and Smith, J. L., Jr.(1984): "The T-S Diagram as an Indicator of Instantaneous Wall-to-Gas Heat Transfer Driven by a Quasi-Static Periodic Gas Pressure." ASME Paper 84-WA/HT-45.

Finegold, J. G. and Sterrett, R. H. (1978): "Stirling Engine Regenerators Literature Review." Jet Propulsion Laboratory Report No. 5030-230, July 15, 1978. Pasadena: California Institute of Technology.

Galitseiskii, B. M. and Ushakov, A. N. (1981): "Heat Exchange in Porous Media." Journal of Engineering Physics, Vol. 41, No. 3, September 1981, pp. 351-356. Translation from: Inzhenerno-Fizicheskii Zhurmal, Vol. 41, No. 3, pp. 428-435, September.

Gedeon, D. (1986): "Mean-Parameter Modelling of Oscillating Flow." ASME Journal of Heat Transfer, Vol. 108, pp. 513-518, August.

Goldberg, P. (1958): "A Digital Computer Simulation for Laminar Flow Heat Transfer in Circular Tubes." MS Thesis, Department of Mechanical Engineering, MIT. Cambridge, MA.

Grassmann, P. and Tuma, M. (1979): "Kritische Reynolds-Zahlen bei Oszillierenden und Pulsierenden Rohrströmungen." Wärme-und Stoffübertragung, Vol. 12, p. 203.

Harness, J. B. and Neumann, P. E. L. (1979): "Digital Computer Simulation of Voidage in a Regenerator." In: Timmerhaus, K. D. (ed): Advances in Cryogenic Engineering. New York: Plenum Press.

Hino, M., Sawamoto, M. and Takasu, S. (1976): "Experiments on the Transition to Turbulence in an Oscillatory Pipe Flow." Journal of Fluid Mechanics, Vol. 75, Part 2, pp. 193-207.

Hwang, M. F. and Dybbs, A. (1980): "Oscillation Heat Transfer in a Small Tube." Report FTAS/TR-80-149, MS Thesis, Department of Mechanical and Aerospace Engineering, Cleveland: Case Western Reserve University, September.

Hwang, M. F. and Dybbs, A.(1983): "Heat Transfer in a Tube with Oscillatory Flow." ASME Paper 83-WA/HT-90.

Iguchi, M., Ohmi, M. and Maegawa, K. (1982): "Analysis of Free Oscillating Flow in a U-Shaped Tube." Nihon Kikaigakkai (Bulletin of the JSME), Vol. 25, No. 207, pp. 1398-1405, September.

Incropera, F. P., and DeWitt, D. P.(1981): Fundamentals of Heat Transfer. New York: John Wiley and Sons.

Iwabuchi, M. and Kanzaka, M. (1982): "Experimental Investigation into Heat Transfer under the Periodically Reversing Flow Condition in Heated Tube." In: Stirling Engines-Progress towards Reality. Conference on 25-26 March 1982 at the University of Reading (UK). I MechE Conference Publications 1982-2, paper #C24/82. London: I. Mech. Engineers.

Jimenez, J. (1973): "Nonlinear Gas Oscillations in Pipes. Part 1. Theory." Journal of Fluid Mechanics, Vol. 59, Part 1, pp. 23-46.

Jones, J. D. (1985): "Flow Losses in Stirling Engine Heat Exchangers." 20th Intersociety Energy Conversion Engineering Conference, Proceedings (IECEC Paper 859437), Vol. 3, pp. 366-371, Warrendale, PA, Society of Automotive Engineers.

Joseph, D. D., Nield, D. A. and Papanicalaou, G. (1982): "Nonlinear Equation Governing Flow in a Saturated Porous Medium." Water Resources Research, Vol. 18, No. 4, pp. 1049-1052, August.

Joshi, C. H., Kamm, R. D., Drazen, J. M. and Slutsky, A. S. (1983): "An Experimental Study of Gas Exchange in Laminar Oscillatory Flow." Journal of Fluid Mechanics, Vol. 133, pp. 245-254.

Kays, W. M. and London, A. L. (1964 and 1984): Compact Heat Exchangers. 2nd and 3rd edition. New York: Mc Graw-Hill.

Kerczek see Von Kerczek

Kim, J. C. (1970): "An Analytical and Experimental Study of Heat Transfer and Flow Friction Characteristics for Periodically Reversing Flow through the Porous Matrix of Thermal Regenerators." Ph.D. Thesis, Mechanical Engineering Department, Purdue University.

Kirmse, R. E. (1979): "Investigation of Pulsating Turbulent Pipe Flow." Transactions of the ASME, Journal of Fluids Engineering, Vol. 101, pp. 436-442.

Kita, Y., Adachi, Y. and Hirose, K. (1980): "Periodically Oscillating Turbulent Flow in a Pipe." Nihon Kikaigakkai (Bulletin of the JSME), Vol. 23, No. 179, pp. 656-664, May.

Kurzweg, U. H. (1985a): "Enhanced Heat Conduction in Fluids Subjected to Sinusoidal Oscillations." ASME Journal of Heat Transfer, Vol. 107, pp. 459-462, May.

Kurzweg, U. H. (1985b): "Enhanced Heat Conduction in Oscillating Viscous Flows within Parallel-Plate Channels." Journal of Fluid Mechanics, Vol. 156, pp. 291-300.

Martini, W. R. (1982): Stirling Engine Design Manual. Second Edition. Richland, WA: Martini Engineering.

Macdonald, I. F., El-Sayed, M. S., Mow, K. and Dullien, F. A. L. (1979): "Flow through Porous Media - the Ergun Equation Revisited." Ind. Eng. Chem. Fundam., Vol. 18, No. 3.

Merkli, P. and Thomann, H. (1975a): "Transition to Turbulence in Oscillating Pipe Flow." Journal of Fluid Mechanics, Vol. 68, Part 3, pp. 567-575.

Merkli, P. and Thomann, H. (1975b): "Thermoacoustic Effects in a Resonance Tube." Journal of Fluid Mechanics, Vol. 70, Part 1, pp. 161-177.

Miyabe, H., Takahashi, S. and Hamaguchi, K. (1982): "An Approach to the Design of Stirling Engine Regenerator Matrix Using Packs of Wire Gauzes." 17th Intersociety Energy Conversion Engineering Conference. Proceedings (IECEC Paper 829306), pp. 1839-1844. Piscataway, NJ: Institute of Electrical and Electronics Engineers.

Ohmi, M., Iguchi, M. and Urahata, I. (1982): "Flow Patterns and Frictional Losses in an Oscillating Pipe Flow." Nihon Kikaigakkai (Bulletin of the JSME), Vol. 25, No. 202, pp. 536-543, April.

Organ, A. J. (1975): "The Concept of 'Critical Length Ratio' in Heat Exchangers for Stirling Cycle Machines." 10th Intersociety Energy Conversion Engineering Conference. Proceedings (IECEC Paper 759151), pp. 1012-1019. Piscataway, NJ: Institute of Electrical and Electronics Engineers.

Organ, A. J. (1982a): "Dimensional Analysis of Pumping Losses in a Stirling Cycle Machine." 17th Intersociety Energy Conversion Engineering Conference. Proceedings (IECEC Paper 829280), pp. 1694-1698. Piscataway, NJ: Institute of Electrical and Electronics Engineers.

Organ, A. J. (1982b): "Gas Dynamics of the Temperature-Determined Stirling Cycle." Journal of Mech. Engr. Science, Vol. 23, No. 4, pp. 207-216.

Organ, A. J. (1984): "An Inquiry into the Mechanism of Pressure Drop in the Regenerator of the Stirling Cycle Machine." 19th Intersociety Energy Conversion Engineering Conference. Proceedings (IECEC Paper 849006), pp. 1776-1781. American Nuclear Society.

Park, J. and Baird, M. (1970): "Transition Phenomena in an Oscillating Manometer." Canadian Journal of Chemical Engineering, Vol. 48, pp. 491-495.

Peacock, J. A. and Stairmand, J. W. (1983): "Film Gauge Calibration in Oscillatory Pipe Flow." J. Phys. E: Sci. Instrum., Vol. 16, pp. 571-576.

Perry, R. H., Chilton, C. H. and Kirkpatrick, S. D. (1973): Chemical Engineers' Handbook. 4th Edition, New York: McGraw-Hill.

Petukhov, B. S., Polyakov, A. F. and Martynenko, O. G. (1982): "Buoancy Effect on Heat Transfer in Forced Channel Flow." In: Grigull, U. et al. (eds.): Heat Transfer 1982. Proceedings of the Seventh International Heat Transfer Conference, München FRG, 1982. Washington: Hempisphere Publishing Company.

Pinker, R. A. and Herbert, M. V. (1967): "Pressure Loss Associated with Compressible Flow through Square-Mesh Wire Gauzes." Journal of Mech. Engr. Science, Vol. 9, No. 1, pp. 11-23.

Rice, G., Jones, J. D., Dadd, M. W. and Thonger, J. (1983): "U.K. Consortium Stirling Engine Regenerator Effectiveness and Heater Performance." 18th Intersociety Energy Conversion Engineering Conference. Proceedings (IECEC Paper 839115), pp. 714-719. New York: American Institute of Chemical Engineers.

Rice, G., Thonger, J. C. T. and Dadd, M. W. (1985): "Regenerator Effectiveness Measurement." 20th Intersociety Energy Conversion Engineering Conference. Proceedings (IECEC Paper 859144), pp. 3.266-3.271. Warrendale, PA: Society of Automotive Engineers.

Richardson, E. G. and Tyler, E. (1929): "The Transverse Velocity Gradient near the Mouths of Pipes in which an Alternating or Continuous Flow of Air is Established." Proc. Phys. Soc. London, Vol. 42, Part 1.

Richey, A. (1986): Letter to Authors. 6 January.

Rix, D.H. (1984): "Some Observations on the Behaviour of a High-Performance Stirling Cycle Machine". 19th Intersociety Energy Conversion Engineering Conference. Proceedings (IECEC Paper 849008), pp.1782-1787. American Nuclear Society.

Schlichting, H. (1979): Boundary Layer Theory. 7th Edition, New York: McGraw-Hill.

Schreiber, J. (1983): "Testing and Performance Characteristics of a 1-kw Free-Piston Stirling Engine." NASA Technical Memorandum 82999. Cleveland, OH: NASA Lewis Research Center, April.

Sergeev, S. (1966): "Fluid Oscillations at Moderate Reynolds Numbers." Fluid Dynamics, Vol. 1, No. 1, pp. 121-122.

Seume, J.R., and Simon, T.W.(1986): Oscillating flow in Stirling Engine Heat Exchangers". 21st Intersociety Energy Conversion Engineering Conference. Proceedings (IECEC Paper 869118), pp. 533-538. Washington: American Chemical Society.

Sexl, T. (1930): "Über den von E. G. Richardson entdeckten 'Annulareffekt'." Zeitschrift für Physik, Vol. 61, pp. 349-362.

Shah, R. K. (1981): "Thermal Design Theory for Regenerators." In: Kakaç, S., Bergles, A. E. and Mayinger, F. (eds.): Heat Exchangers-Thermal-Hydraulic Fundamentals and Design. Washington: Hemisphere Publishing Company.

Shapiro, A. S. (1954): "Compressible Fluid Flow." Vol. 2. New York: The Ronald Press.

Shizgal, B., Goldsmith, H. L. and Mason, S. G. (1965): "The Flow of Suspensions through Tubes IV: Oscillatory Flow of Rigid Spheres." Canadian Journal of Chemical Engineering, Vol. 43, No. 3, pp. 97-101.

Sobey, I. J. (1985): "Observations of Waves during Oscillatory Channel Flow." Journal of Fluid Mechanics, Vol. 151, February.

Sudou, K., Sumida, M., Takami, T. and Yamane, R. (1985): "A Study of Oscillatory Flow in Curved Pipes." Nihon Kikaigakkai (Bulletin of the JSME), Vol. 28, No. 245, November.

Sumida, M. and Sudou, K. (1985): "Oscillatory Flow in Curved Pipes of Rectangular Cross-Section (1st Report, Numerical Analysis of Laminar Flow in Square-Sectioned Pipes)." Nihon Kikaigakkai (Bulletin of the JSME), Vol. 28, No. 243, pp. 1899-1905, September.

Takahachi, S., Hamaguchi, K., Miyabe, H. and Fujita, H. (1984): "On the Flow Friction and Heat Transfer of the Foamed Metals as the Regenerator Matrix." 2nd International Conference on Stirling Engines, Paper 3-4. Shanghai: The Chinese Society of Naval Architecture and Marine Engineering and the Chinese Society of Engineering Thermophysics.

Taylor, D. R. and Aghili, H. (1984): "An Investigation of Oscillating Flow in Tubes." 19th Intersociety Energy Conversion Engineering Conference. Proceedings (IECEC Paper 849176), pp. 2033-2036. American Nuclear Society.

Telionis, T. P. (1981): "Unsteady Viscous Flows." Springer Series in Computational Physics ISBN 3-540-10481-X, New York: Springer-Verlag.

Tew, R. C., Jr. (1983): "Computer Program for Stirling Engine Performance Calculations." DOE/NASA/51040-42, NASA TM-82960. Cleveland, OH: NASA Lewis Research Center, January.

Tew, R.C., Jr. (1986): Private Communication on IECEC Paper 869118. Letter of 4/24/86 to the authors.

Trikha, A. K. (1975): "An Efficient Method for Simulating Frequency-Dependent Friction in Transient Liquid Flow." ASME Journal of Fluids Engineering, pp. 97-105, March.

Uchida, S. (1956): "The Pulsating Viscous Flow Superposed on the Steady Laminar Motion of Incompressible Fluid in a Circular Pipe." Zeitschrift für Angewandte Mathematik und Physik, Vol. 7, pp. 403-422.

Urieli, I. and Berchowitz, D. M. (1984): Stirling Cycle Engine Analysis. Bristol (England): Adam Hilger.

Valensi, J. (1947): "Oscillations d'un liquide pesant et visqueux dans un tube en U de faible diamètre." Comptes Rendus de la Académie des Sciences de Paris, Vol. 224, pp. 446, 532, 893 and 1695.

Vasiliev, O. F. and Kvon, V. I. (1971): "Friction Forces of Unsteady Flows in Open Channels and Pipes." International Association for Hydraulic Research, Proceedings of the 14th Conference, Vol. 1, Subject B.

Von Kerczek, C. and Davis, S. H. (1972): "The Stability of Oscillatory Stokes Layers." Studies in Applied Mathematics, Vol. LI, No. 3.

Walker, G. (1962): "Regeneration in Stirling Engines. The Engineer, Vol. 214, pp.1097-1103, December.

Walker, G. (1963): "Pressure Drop across Regenerator of a Stirling Cycle Machine". The Engineer, Vol. 216, pp.1063-1066, December.

Walker, G. (1980): Stirling Engines. Oxford: Clarendon Press.

Walker, G. and Vasishta, V. (1971): "Heat-Transfer and Flow-Friction Characteristics of Dense-Mesh-Wire-Screen Stirling Cycle Regenerators." In: Timmerhaus, K. D. (ed): Advances in Cryogenic Engineering, Vol. 16, 1971, pp. 302-311, New York: Plenum Presss.

Watson, E. J. (1983): "Diffusion in Oscillatory Pipe Flow." Journal of Fluid Mechanics, Vol. 133, pp. 233-244.

West, C. D. (1983): Liquid Piston Stirling Engines. New York: Van Nostrand Reinhold.

White, F. M. (1974): <u>Viscous Fluid Flow</u>, p. 144. New York: McGraw-Hill.

Willmott, A. J. and Duggan, R. C. (1980): "Refined Closed Methods for the Contra-Flow Thermal Regenerator Problem." International Journal of Heat and Mass Transfer, Vol. 23, pp. 655-662.

Willmott, A. J. and Hinchcliffe, C. (1976): "The Effect of Gas Heat Storage upon the Performance of the Thermal Regenerator." International Journal of Heat and Mass Transfer, Vol. 19, pp. 821-826.

Womersley, J. R. (1955): "Method for the Calculation of Velocity, Rate of Flow and Viscous Drag in Arteries when the Pressure Gradient is Known." Journal for Physiology, Vol. 127, pp. 553-563.

Yamane, R., Oshima, S., Sudo, K., Sumida, M., Okamoto, N. and Kizaki, M. (1985): "Study of Oscillatory Flow in a Curved Channel." Nihon Kikaigakkai (Bulletin of the JSME), Vol. 28, No. 237, March.

Youssef, Sadek (1986): "Isothermal Analysis of a Rhombic Drive Stirling Engine and Comparison with Schmidt Analysis." Internal Report, Mechanical Engineering Department, University of Minnesota, Minneapolis.

Zielke, W. (1968): "Frequency-Dependent Friction in Transient Pipe Flow." Journal of Basic Engineering, Trans. ASME, Series D, Vol. 90, No. 1, pp. 109-115, March.

APPENDIX A: A SURVEY OF PRESSURE, REYNOLDS-NUMBER AND MACH NUMBER

   VARIATIONS

   Figures of the pressure, Reynolds number and some Mach number

variations are provided to give the reader the opportunity to assess the

quality of the data base discussed in Chapter 7.   Figures A1 and A2 show

results of the isothermal analysis of a GPU-3 (Youssef 1986).   Figures A3

through A14 were obtained by Schmidt analysis.

   - Flow is positive towards the cold end.

   - full line - hot end

   - dashed line - cold end
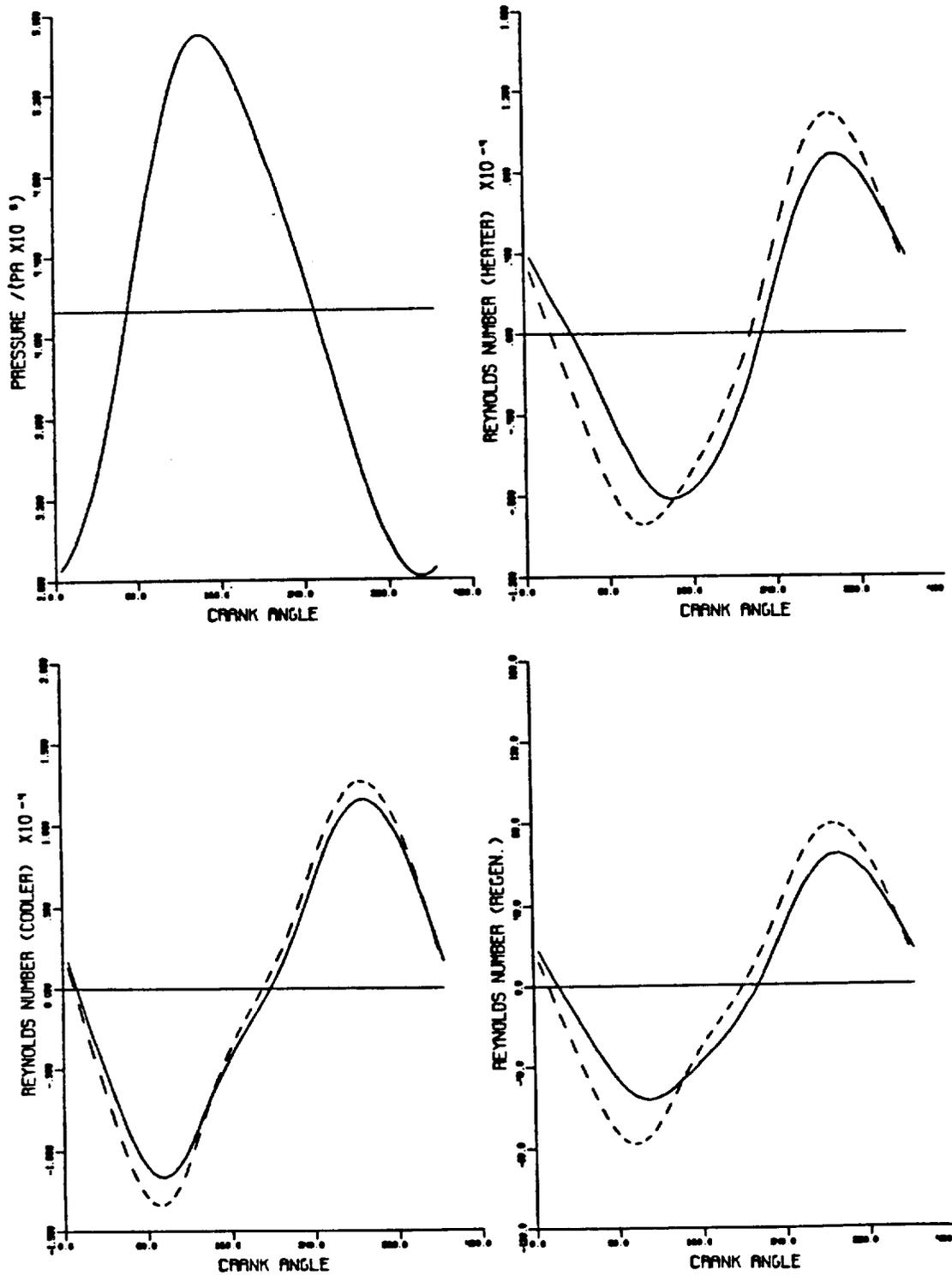
Figure A-1: Results of the isothermal analysis of a GPU 3:
pressure and Reynolds numbers
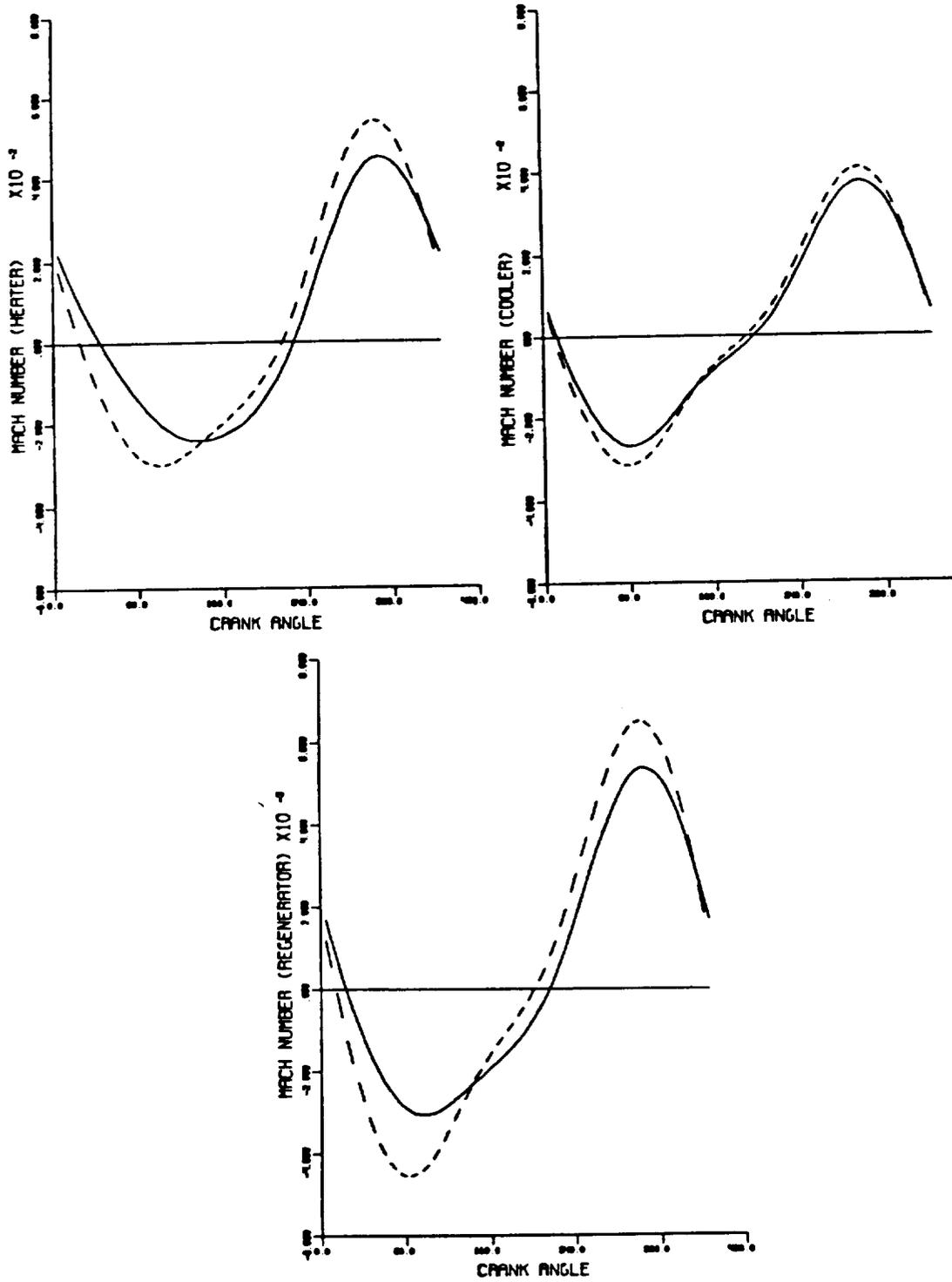
Figure A-2: Results of the isothermal analysis of a GPU 3: Mach numbers
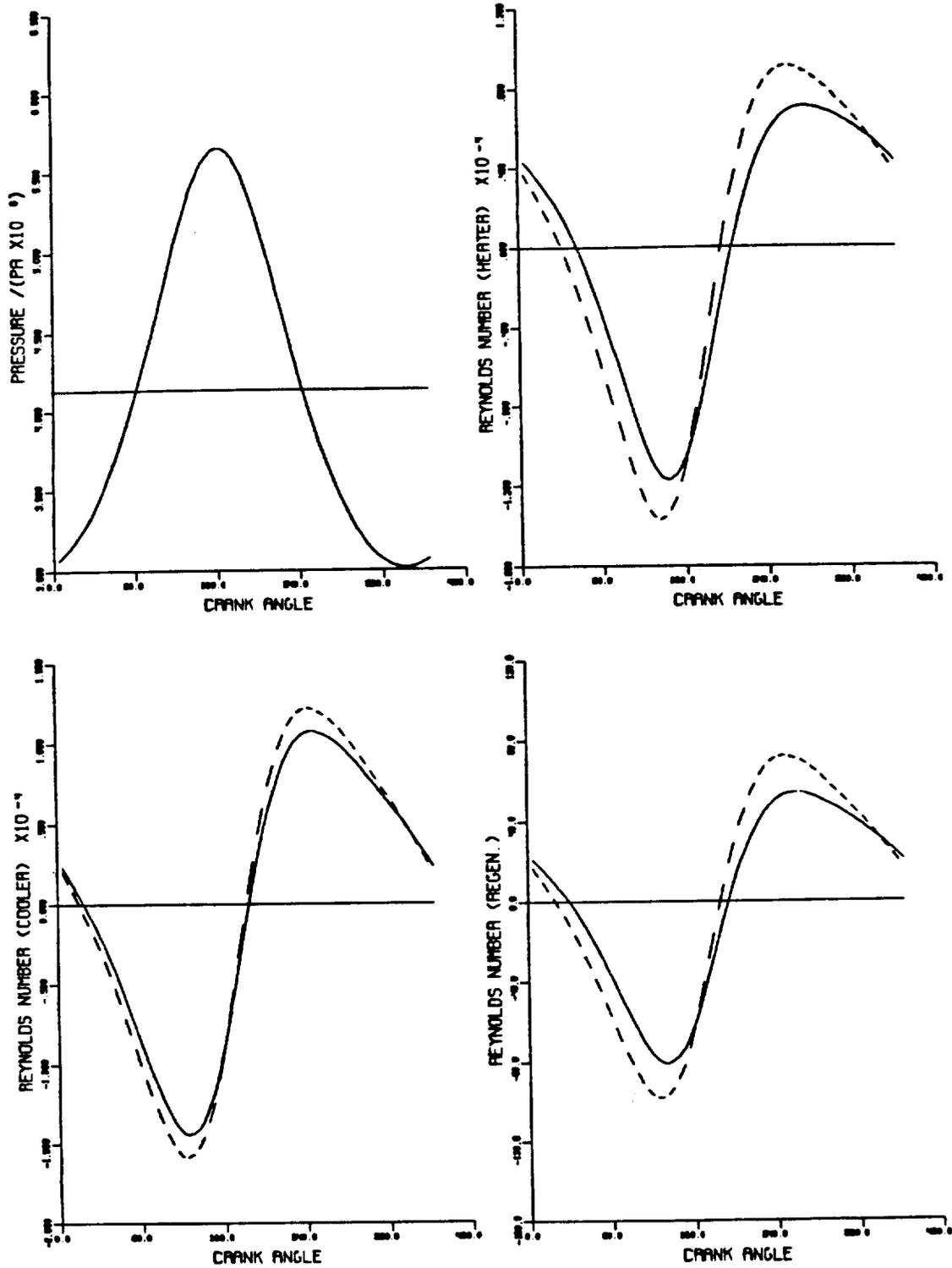
95

Figure A-3:   GPU 3

Figure A-4:   MODI

97

Figure A-5:   P40

98
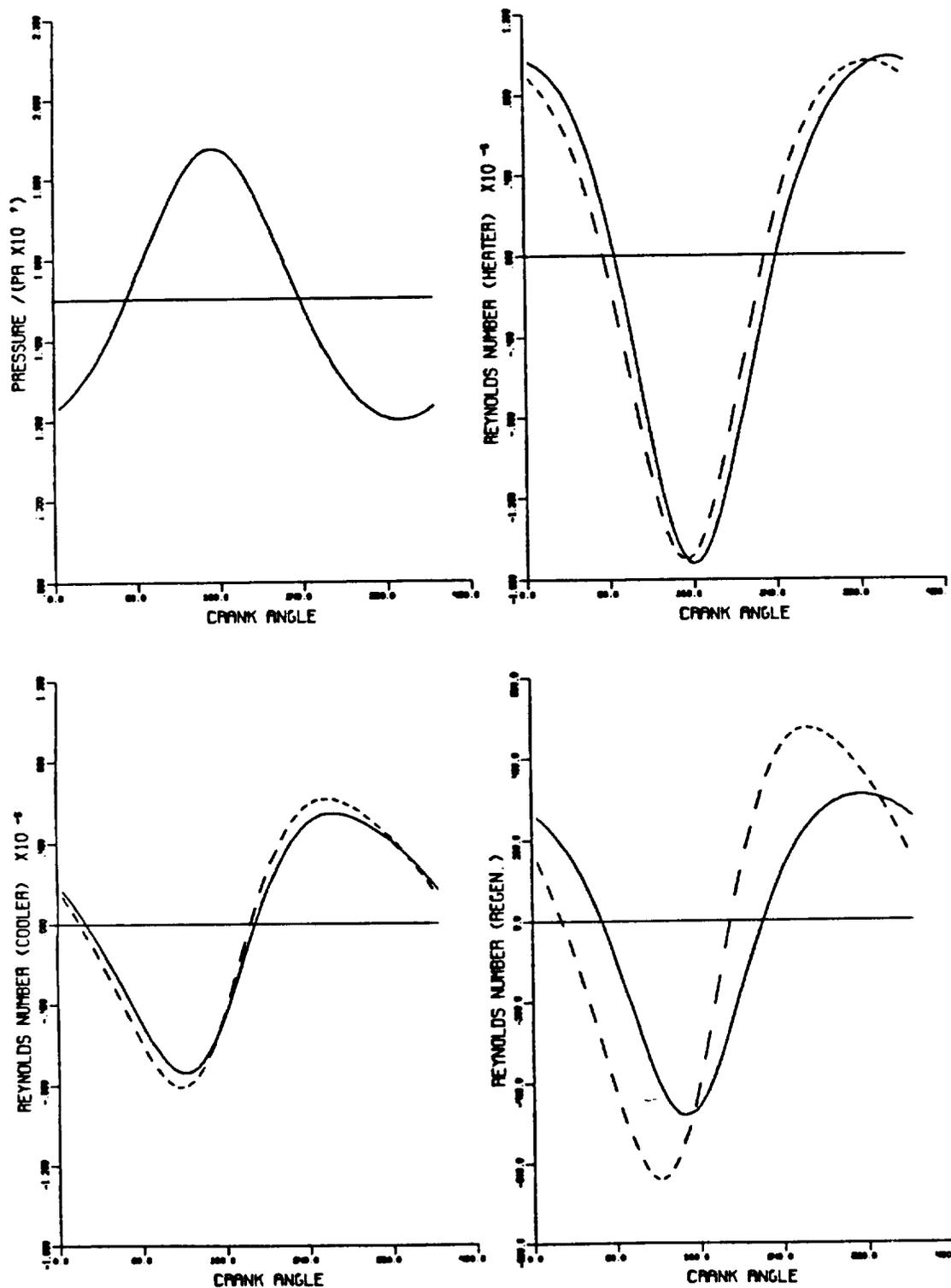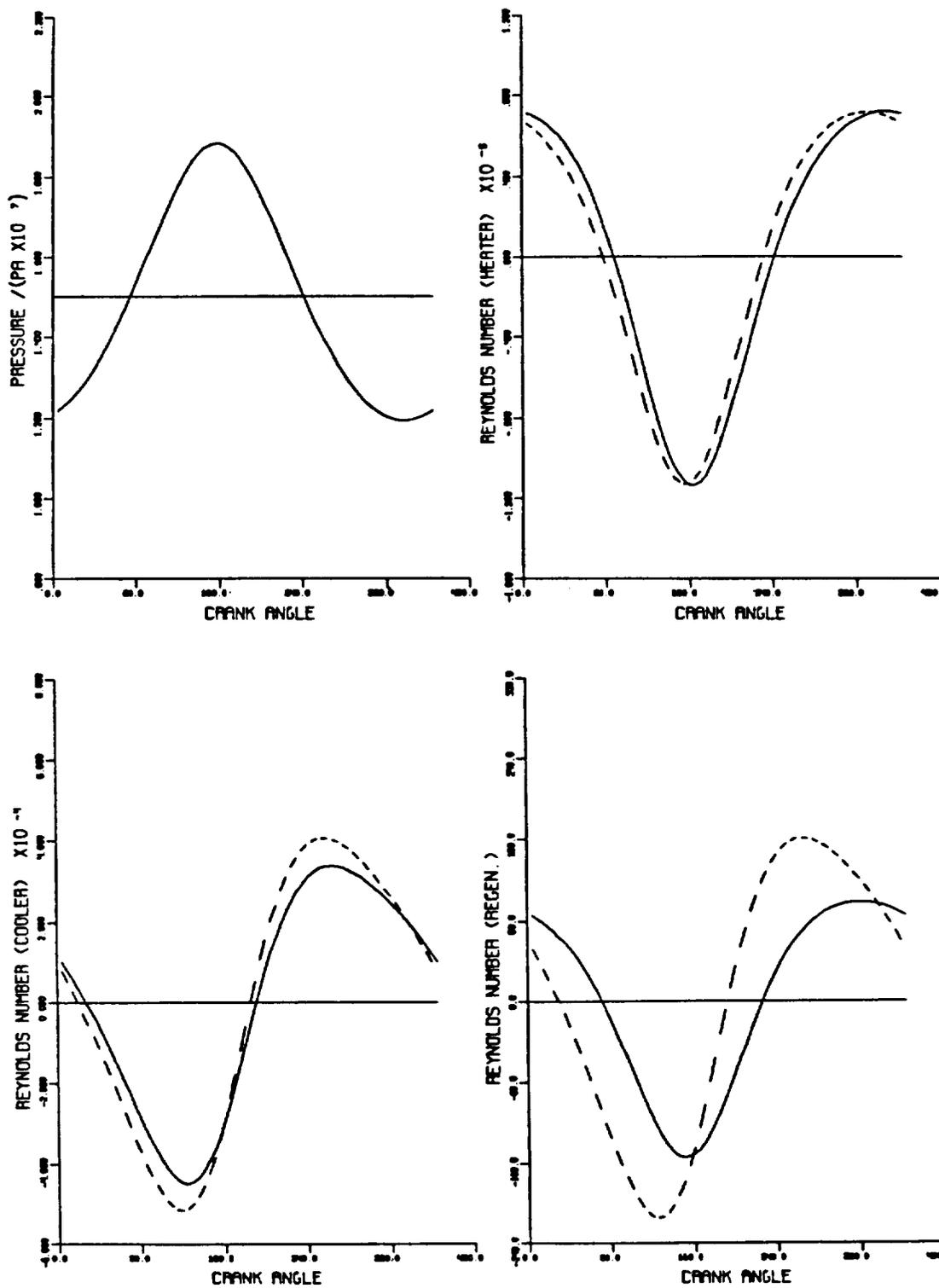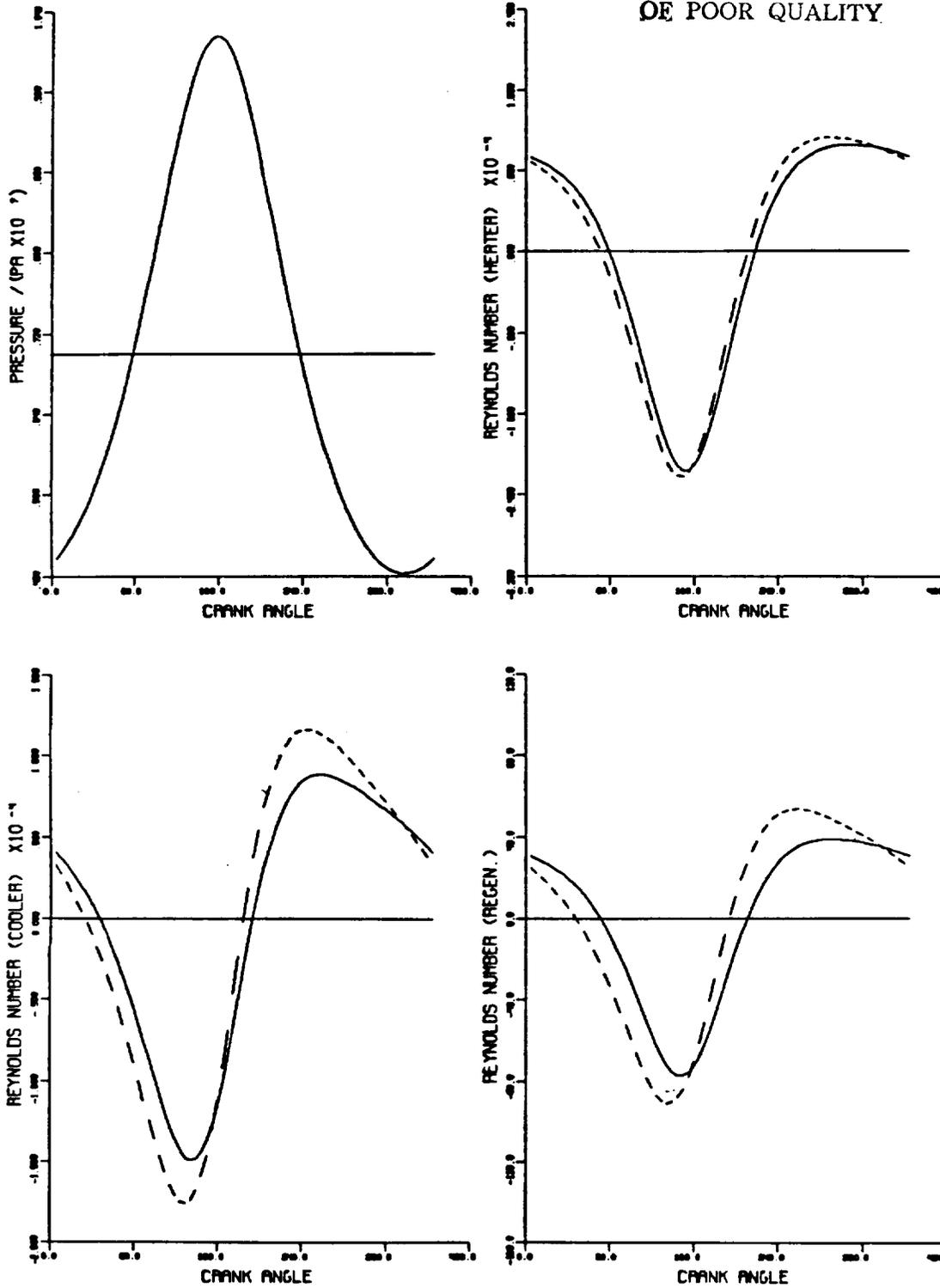
Figure A-6:   STES

Figure A-7:   UK

100

Figure A-8:   4-215

101

Figure A-9: 4L23

102

Figure A-10:   EM

103

Figure A-11:   Genset

104
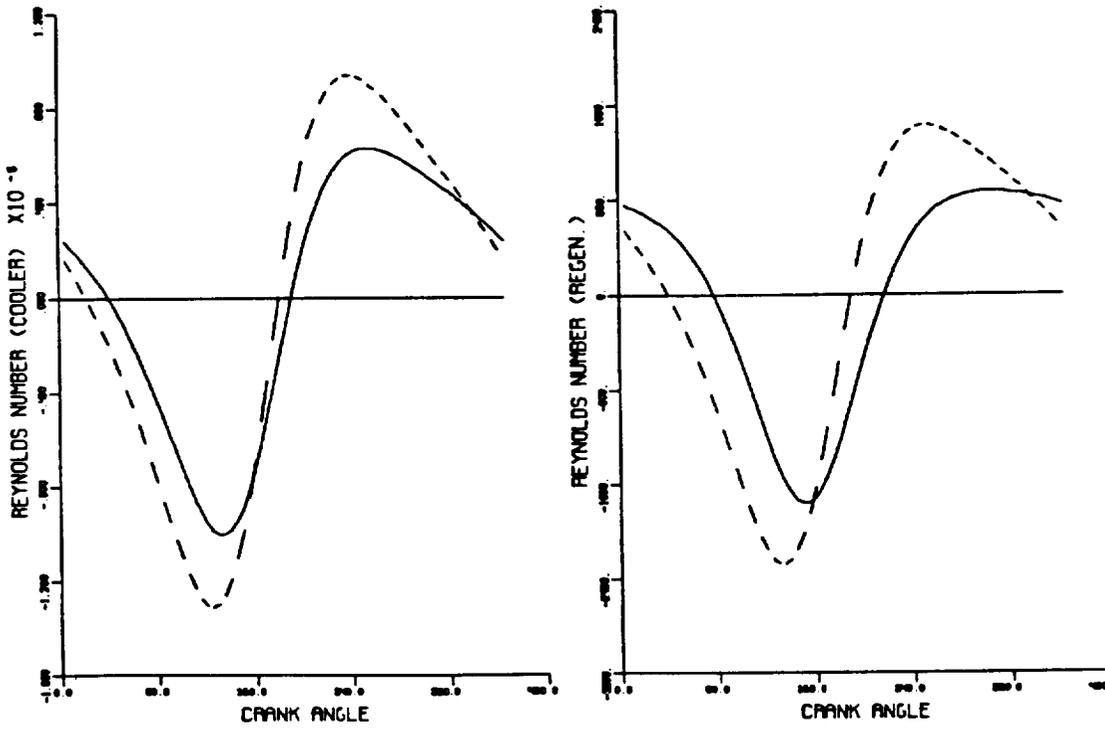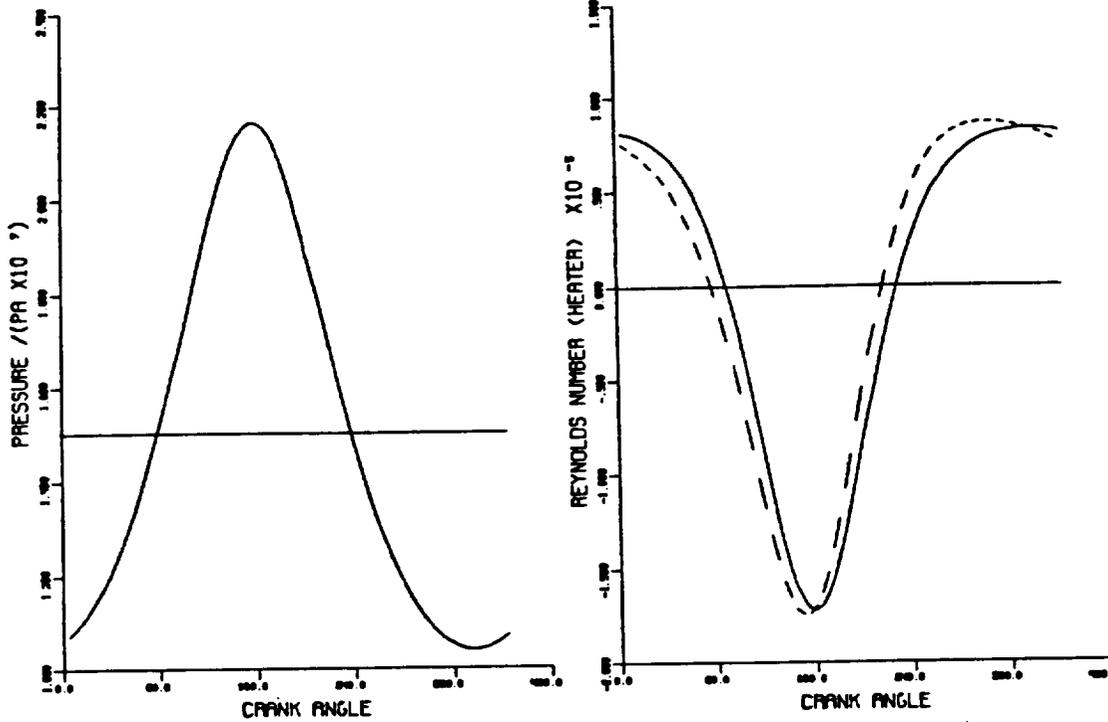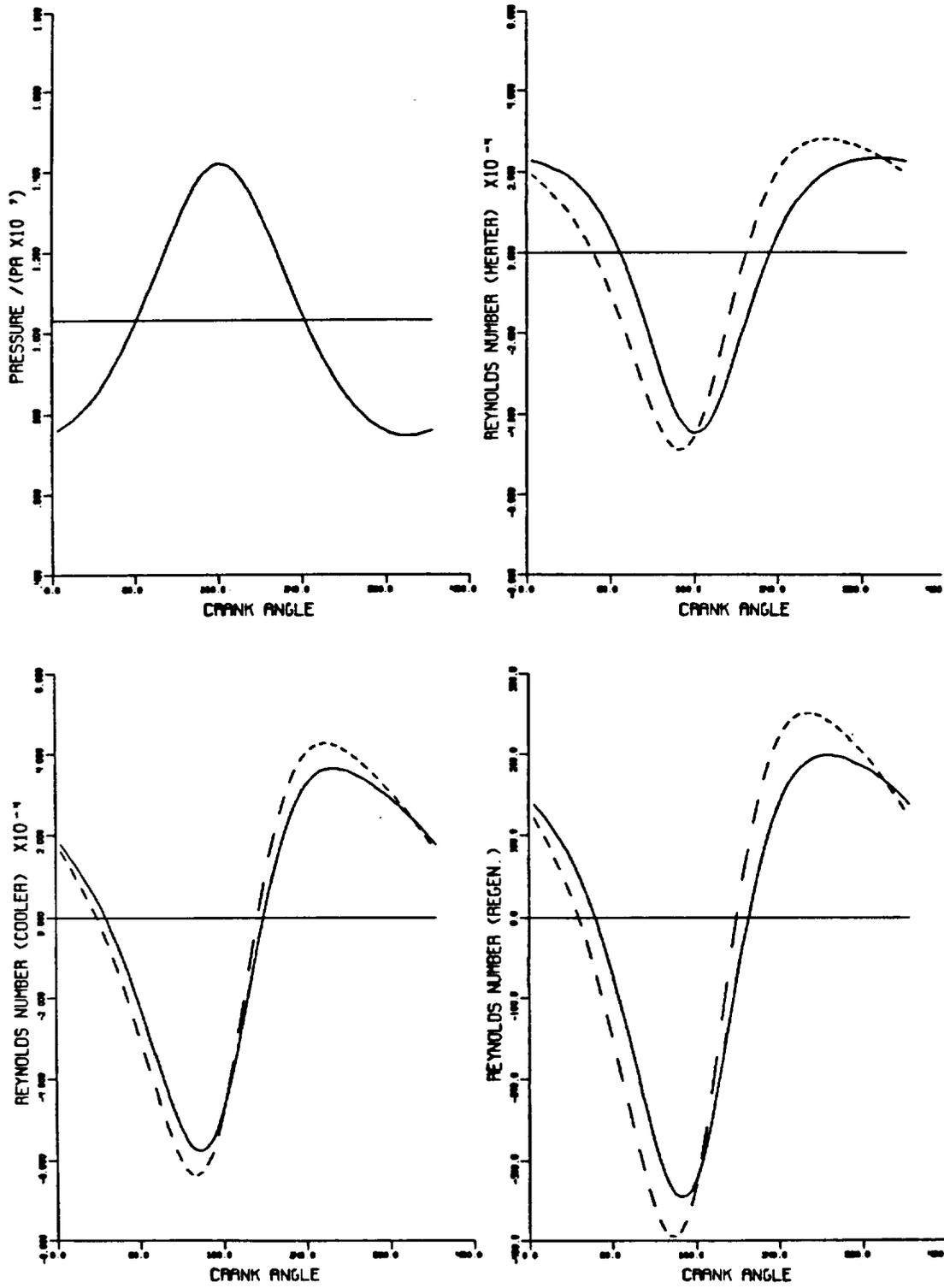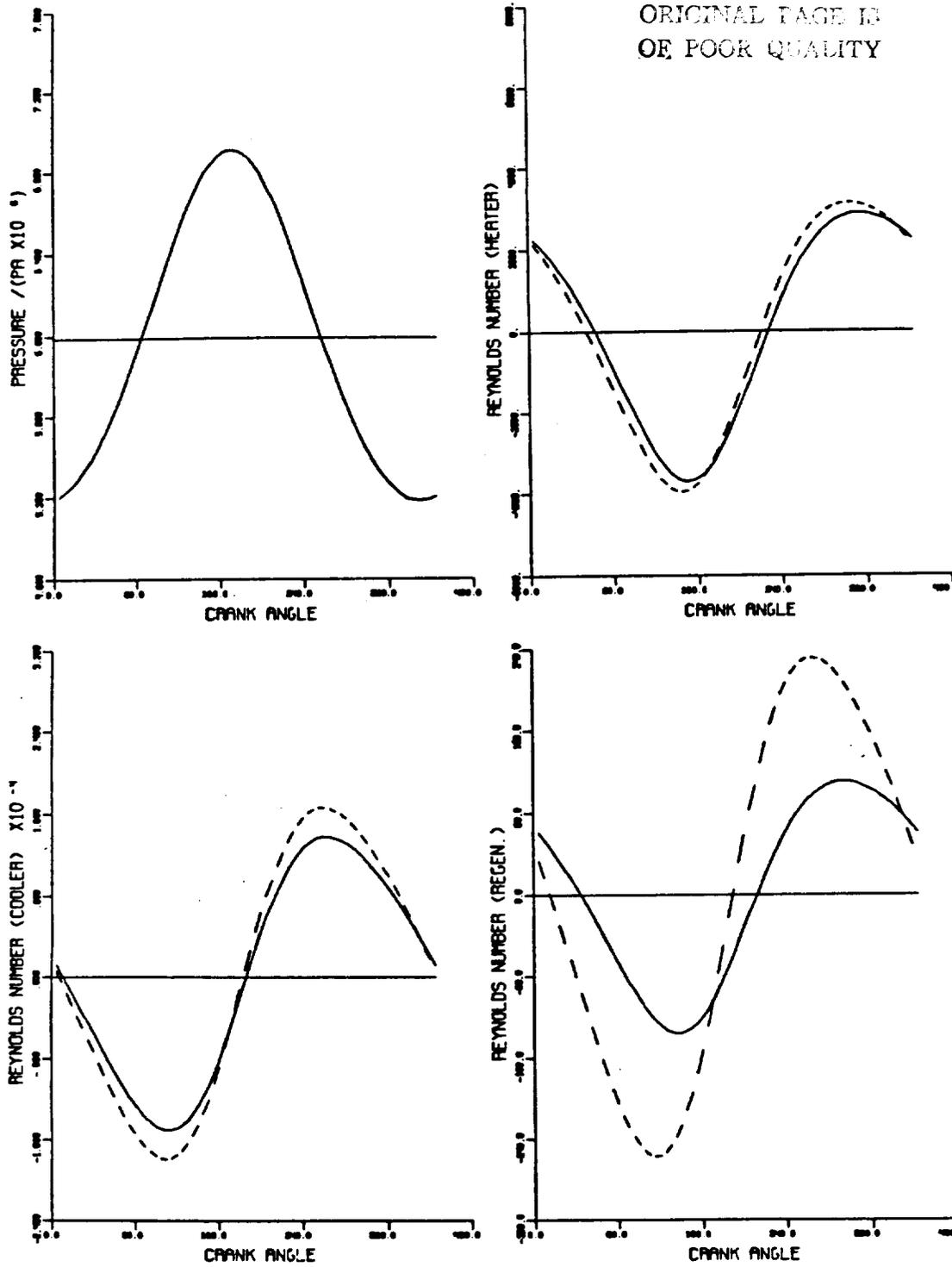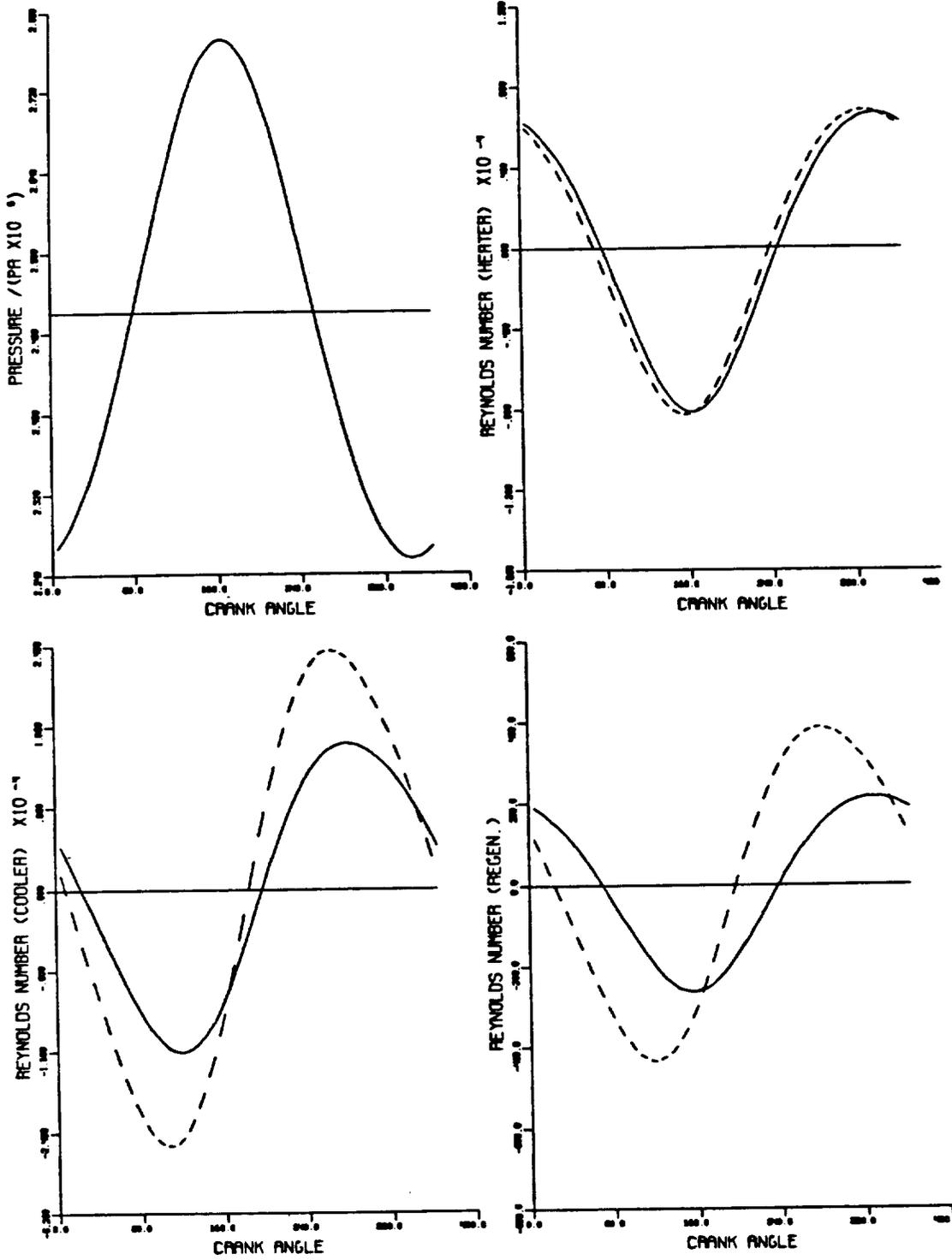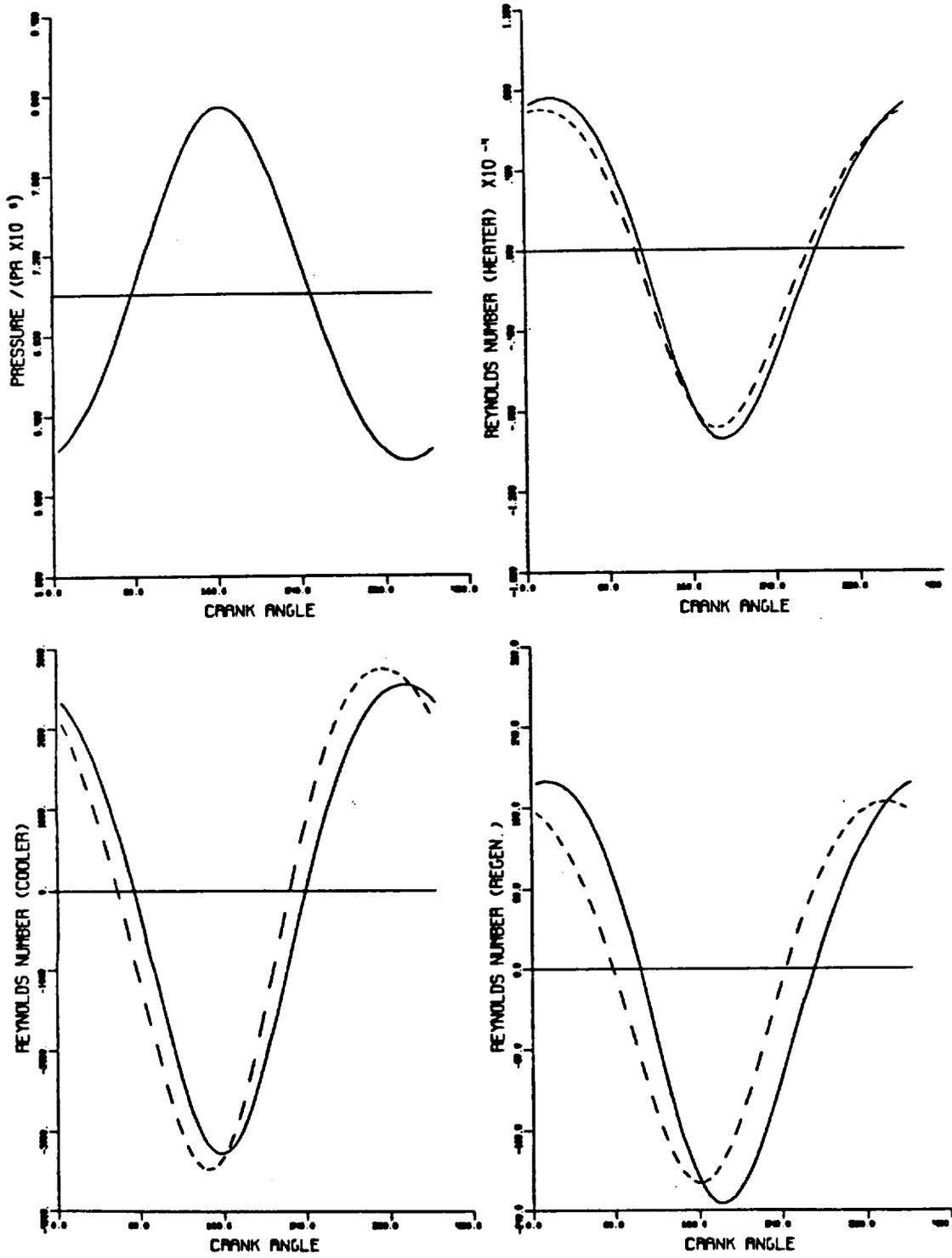
Figure A-12:   RE1000

Figure A-13:   SPDE-T

106

Figure A-14:   SPDE-D

107
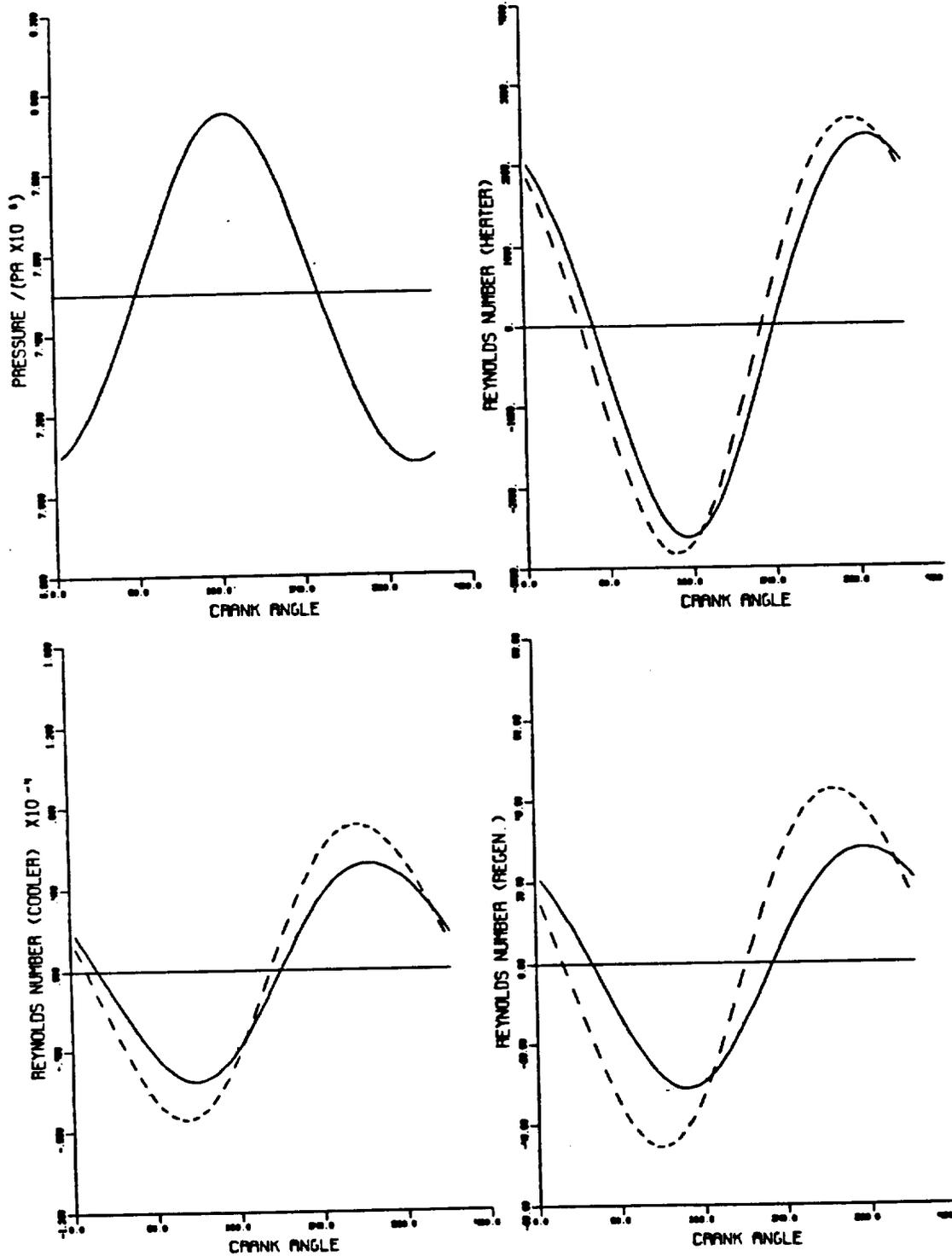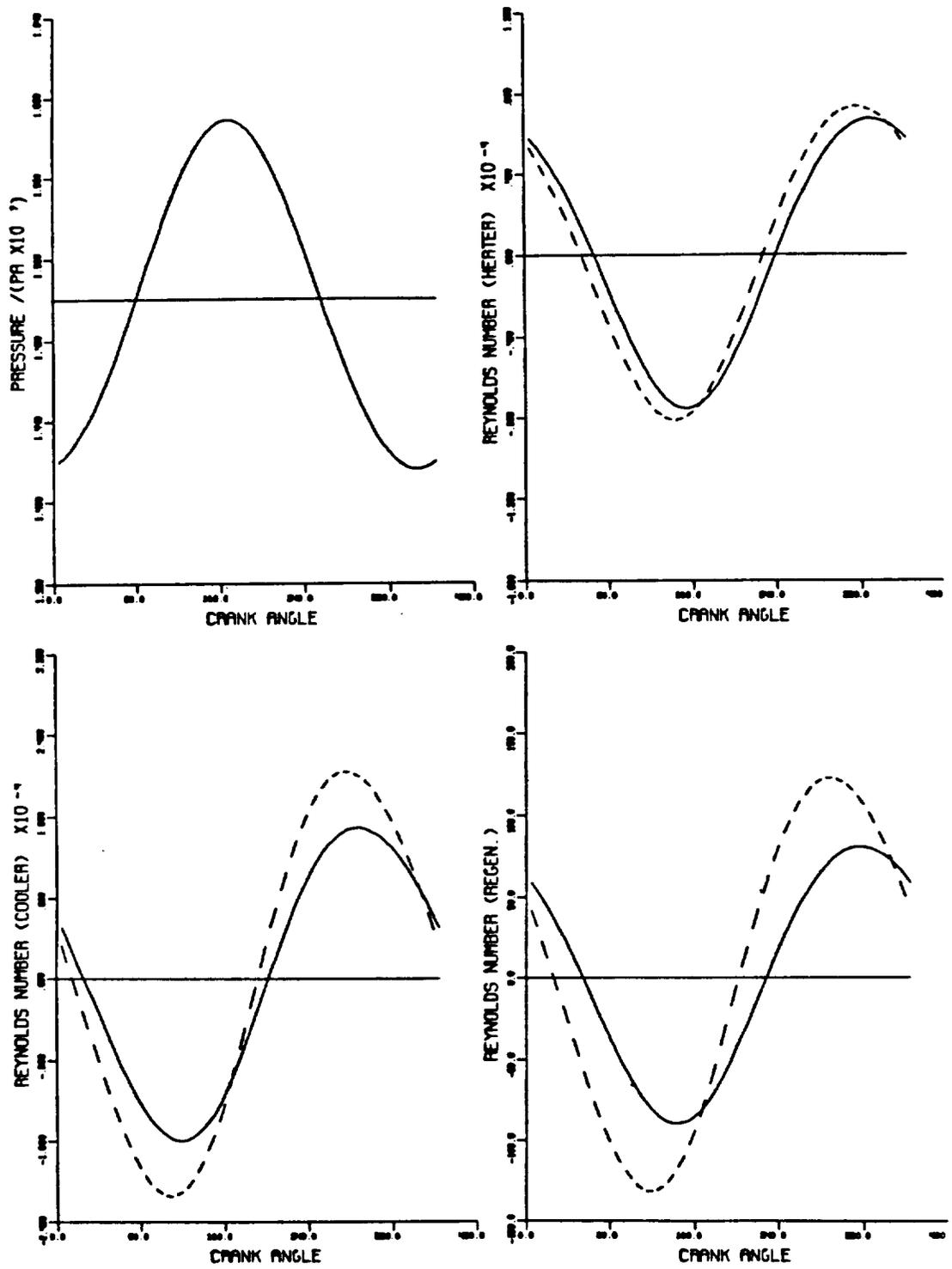
APPENDIX B: DERIVATION OF SIMILARITY PARAMETERS

Normalization of the momentum equations

To normalize the momentum equation, the following dimensionless variables are used:

$$\vec{x}^* = \frac{\vec{x}}{L}$$

$$p^* = \frac{p - p_0}{\rho\, U^2}$$

$$\vec{u}^* = \frac{\vec{u}}{U}$$

$$t^* = t/t_0$$

$$\nabla^* = L\nabla$$

$$\rho^* = \frac{\rho}{\rho_0}$$

$$\mu^* = \frac{\mu}{\mu_0}$$

$$\nu^* = \frac{\mu^*}{\rho^*}$$

Neglecting gravity, the momentum equation is:

$$\frac{\partial \vec{u}}{\partial t} + \vec{u}\cdot\nabla\vec{u} = -\frac{\nabla p}{\rho} + \frac{\mu}{\rho}\nabla^2\vec{u}$$

$$\frac{U}{t_0}\frac{\partial \vec{u}^*}{\partial t^*} + \frac{U^2}{L}\vec{u}^*\cdot\nabla^*\vec{u}^* = -\frac{U^2}{L}\frac{\nabla^* p^*}{\rho^*} + \frac{\mu_0}{\rho_0}\frac{U}{L^2}\frac{\mu^*}{\rho^*}\nabla^{*2}\vec{u}^*$$

$$\frac{L^2\rho_0}{t_0\mu_0}\frac{\partial \vec{u}^*}{\partial t^*} + \frac{UL\rho_0}{\mu_0}\vec{u}^*\cdot\nabla^*\vec{u}^* = -\frac{\rho_0 UL}{\mu_0}\frac{\nabla^* p^*}{\rho^*} + \nu^*\nabla^{*2}\vec{u}^*$$

For the oscillating pipe flow problem, the following scales are used:

length scale $\quad L = d/2 \quad$ pipe radius

velocity scale $\quad U = u_{m,max} \quad$ amplitude of the mean velocity

time scale $\quad t_o = 1/\omega \quad$ period of oscillation / 2π

$$\frac{\omega \, d^2}{4 \, \nu_o} \frac{\partial \vec{u}^*}{\partial t} + \frac{1}{2} \frac{u_{m,max} \, d}{\nu_o} \vec{u}^* \cdot \nabla^* \vec{u}^* = -\frac{1}{2} \frac{u_{max} \, d}{\nu_o} \frac{\nabla^* p^*}{\rho} + \nu^* \nabla^{*2} \vec{u}^*$$

$$Re_\omega \frac{\partial \vec{u}^*}{\partial t^*} + \frac{Re_{max}}{2} \vec{u}^* \cdot \nabla^* \vec{u}^* = -\frac{Re_{max}}{2} \frac{\nabla^* p^*}{\rho} + \nu^* \nabla^{*2} \vec{u}^*$$

where $\quad Re_{max} = \dfrac{u_{m,max} \, d}{\nu} \quad$ and $\quad Re_\omega = \dfrac{\omega \, d^2}{4\nu}$.

The dimensionless frequency Re_ω appears as a coefficient of the unsteady inertia term in the normalized Navier-Stokes equation and the amplitude Reynolds number Re_{max} appears as a coefficient of the steady inertia term. Dividing by the maximum Reynolds number, the following form is obtained:

$$\frac{\omega \, d}{2 \, u_{m,max}} \frac{\partial \vec{u}^*}{\partial t^*} + \vec{u}^* \cdot \nabla^* \vec{u}^* = -\frac{\nabla^* p^*}{\rho} + \frac{2 \, \nu_o}{u_{m,max} \, d} \nu^* \nabla^{*2} \vec{u}^*$$

$$\frac{Str}{2} \frac{\partial \vec{u}^*}{\partial t^*} + \vec{u}^* \cdot \nabla^* \vec{u}^* = -\frac{\nabla^* p^*}{\rho} + \frac{2}{Re_{max}} \nu^* \nabla^{*2} \vec{u}^*$$

In this form, the Strouhal number and the Reynolds number appear as the coefficients:

$$Re_{max} = \frac{u_{m,max} \, d}{\nu_o} \quad \text{and} \quad Str = \frac{\omega \, d}{u_{m,max}}$$

Normalization of the energy equation

The energy equation is:

$$\rho c_p \left(\frac{\partial T}{\partial t} + \vec{u}\cdot\nabla T\right) = \frac{\partial p}{\partial t} + \vec{u}\cdot\nabla p + \nabla\cdot(k\nabla T) + \phi$$

where ϕ is the dissipation function, using Stokes' hypothesis (e.g. Schlichting 1979, p.60):

$$\phi = \tau_{ij}\frac{\partial u_i}{\partial x_j} = \mu\left(\frac{\partial u_i}{\partial x_j}\right)^2$$

The normalized variables are chosen as:

$$t^* = \omega t$$

$$\vec{x}^* = \frac{\vec{x}}{d/2}$$

$$\vec{u}^* = \frac{\vec{u}}{u_{m,max}}$$

$$p^* = \frac{p - p_{mean}}{\rho_0\, u_{m,max}^2}$$

$$T^* = \frac{T - T_c}{T_h - T_c}$$

$$\nabla^* = d/2\ \nabla$$

$$\rho^* = \rho/\rho_0$$

$$k^* = k/k_0$$

$$\mu^* = \mu/\mu_0$$

$$c_p^* = c_p/c_{po}$$

$$\phi^* = \mu^*\left(\frac{\partial u_i^*}{\partial x_j^*}\right)^2$$

With these variables, the energy equation is:

110

$$\rho_0 \, c_{po} \, \rho^* \, c_p^* \, \left(\omega(T_h - T_c) \frac{\partial T^*}{\partial t^*} + \left(u_{m,max} \, \vec{u}^* \cdot \frac{\nabla^*}{d/2} T^* \right) (T_h - T_c) \right) =$$

$$\omega \, \rho_0 \, u_{m,max}^2 \, \frac{\partial p^*}{\partial t^*} + \left(u_{m,max} \, \vec{u}^* \cdot \frac{\nabla^*}{d/2} p^* \right) \rho_0 \, u_{m,max}^2$$

$$+ (T_h - T_c) \, k_0 \, \frac{\nabla^*}{d/2} \cdot \left(k^* \, \frac{\nabla^*}{d/2} T^* \right) + \mu_0 \, \left(\frac{u_{m,max}}{d/2} \right)^2 \, \phi^*$$

$$\rho^* \, c_p^* \, \left[\frac{\omega \, d/2}{u_{m,max}} \frac{\partial T^*}{\partial t^*} + \vec{u}^* \cdot \nabla^* T^* \right] = \frac{\omega \, u_{m,max} \, d/2}{c_{po}(T_h - T_c)} \frac{\partial p^*}{\partial t^*} + \frac{u_{m,max}^2}{c_{po}(T_h - T_c)} \vec{u}^* \cdot \nabla^* p^*$$

$$+ \frac{k_0}{\rho_0 c_p} \frac{1}{d/2 \, u_{m,max}} \nabla^* \cdot (k^* \nabla^* T^*) + \frac{\mu_0}{\rho_0 c_{po}} \frac{u_{m,max}}{d/2} \frac{\phi^*}{(T_h - T_c)}$$

$$\rho^* c_p^* \, \left[\frac{2 \, Re_\omega}{Re_{max}} \frac{\partial T^*}{\partial t^*} + \vec{u}^* \cdot \nabla^* T^* \right] = \frac{2 \, Re_\omega \, Ec}{Re_{max}} \frac{\partial p^*}{\partial t^*} + Ec \, \vec{u}^* \cdot \nabla^* p^*$$

$$+ \frac{1}{Pr \, Re_{max}} \nabla^* \cdot (h^* \nabla^* T^*) + \frac{Ec}{Re_{max}} \phi^*$$

Finally, the normalized energy equation is:

$$\rho^* c_p^* \, (2 \, Re_\omega \frac{\partial T^*}{\partial t^*} + Re_{max} \, \vec{u}^* \cdot \nabla^* T^*) = 2 \, Re_\omega \, Ec \, \frac{\partial p^*}{\partial t^*} + Ec \, Re_{max} \, \vec{u}^* \cdot \nabla^* p^*$$

$$+ \frac{\nabla^* \cdot (k^* \nabla^* T^*)}{Pr} + Ec \, \phi^*$$

where $Ec = \frac{u_{m,max}^2}{c_p \, (T_H - T_L)}$ is the Eckert number.

Similarity parameters ℓ/d and A_R

The similarity parameters are obtained from the normalization of the streamwise component (x,u) of the momentum equation. Geometric similarity ensures similarity in the other components (y and z), e.g., the ℓ/d - ratio in pipe flow ensures that the boundary layer growth in the hydrodynamic developing length is similar.

The set of parameters relevant for heat transfer in oscillating flow then consists of: ℓ/d, Re_{max}, Re_ω, Pr, Ec and A_R. This set contains two parameters more than in steady flow. One of these parameters, however, is redundant for sinusoidal flow; if the velocity is

$$u_m = u_{m,max} \sin (\omega t)$$

then the maximum displacement of an average fluid element is calculated by integration over half the cycle

$$2 \, x_{m,max} = {_0}{\int}^{T/2} u_{m,max} \sin(\omega t) \, dt = 2 \, \frac{u_{m,max}}{\omega}$$

By the definition of A_R

$$A_R = \frac{2 \, x_{m,max}}{\ell} = \frac{2 \, u_{m,max}}{\omega \ell}$$

but

$$\frac{Re_{max}}{Re_\omega} = \frac{u_{m,max}}{\omega} \frac{d \, 4}{d^2} = \frac{4 \, u_{m,max}}{\omega \, d}$$

therefore

$$A_R = \frac{1}{2} \frac{d}{\ell} \frac{Re_{max}}{Re_\omega}$$

For other, non-sinusoidal fluid motion, the integration will yield a different proportionality factor than 1/2. In any case, A_R is a function of ℓ/d, Re_{max} and Re_ω. Therefore, the set of similarity parameters for heat transfer is reduced by one to

$$A_R \text{ or } (\ell/d), \quad Re_{max}, \quad Re_\omega, \quad Ec \quad \text{and} \quad Pr.$$

Experimental data will show whether A_R or ℓ/d is more appropriate in correlating heat transfer results.

Calculation of the Reynolds number for regenerator matrices

The hydraulic diameter for regenerator matrices in the Stirling engine data base is calculated based on the definition used by Kays and London (1984, p. 8):

$$d_h/\ell = \phi \, A_c/A_h$$

where A_c = flow cross-sectional area

A_h = total heat transfer area

ℓ = heat exchanger length

d_h = ϕ x void volume/heat transfer area

ϕ = porosity

Figure B-1 shows a cross-section of two layers of a woven-screen regenerator, where s is the wire spacing (i.e., the inverse of the screen pitch) and d_w is the wire diameter.

CROSS-SECTION   FRONT VIEW (INFLOW DIRECTION)
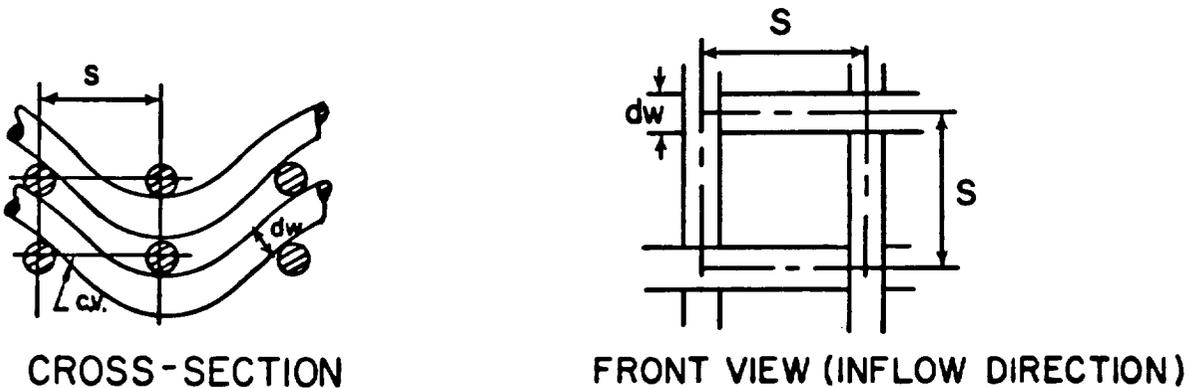
Figure B-1:   Schematic of a wire mesh regenerator screen.

To a first approximation, the control volume (c.v.) contains a solid volume

$$V_s = \frac{\pi}{4} \, d_w^2 s$$

113

The porosity is defined as the ratio of void volume V_v to total volume V_t.

$$\phi = \frac{V_v}{V_t} = \frac{V_t - V_v}{V_t}$$

The heat transfer area in the control volume is

$$A_h = \pi d_w s$$

Then the hydraulic diameter is (Kays and London 1984, p. 8)

$$d_h = \phi \frac{V_v}{A_h} = \phi \frac{\phi V_t}{A_h} = \frac{\phi}{\phi - 1} \frac{V_s}{A_h} = d_w \frac{\phi}{\phi - 1}$$

This is the expression commonly used for the hydraulic diameter.

The <u>characteristic velocity</u> in the Reynolds number is calculated as the average velocity in a cross-section with effective flow area

$$A_c = \phi s^2$$

Then the characteristic velocity is

$$u_m = \frac{V}{\phi}$$

where V is the superficial mean velocity, i.e., the mean velocity of the flow just before entering or after leaving the matrix.

$$u_m A_c = V A_f$$

where A_f is the total regenerator frontal area, i.e., the cross-sectional flow area when the matrix is removed.

APPENDIX C: VELOCITY PROFILES IN LAMINAR FLOW

The plots below show velocity profiles for laminar, incompressible, fully developed, oscillating flow for eight dimensionless frequencies. The velocity profiles were calculated from the equations given by Uchida (1956) for pulsatile flow by taking the limit as the mean velocity goes to zero.
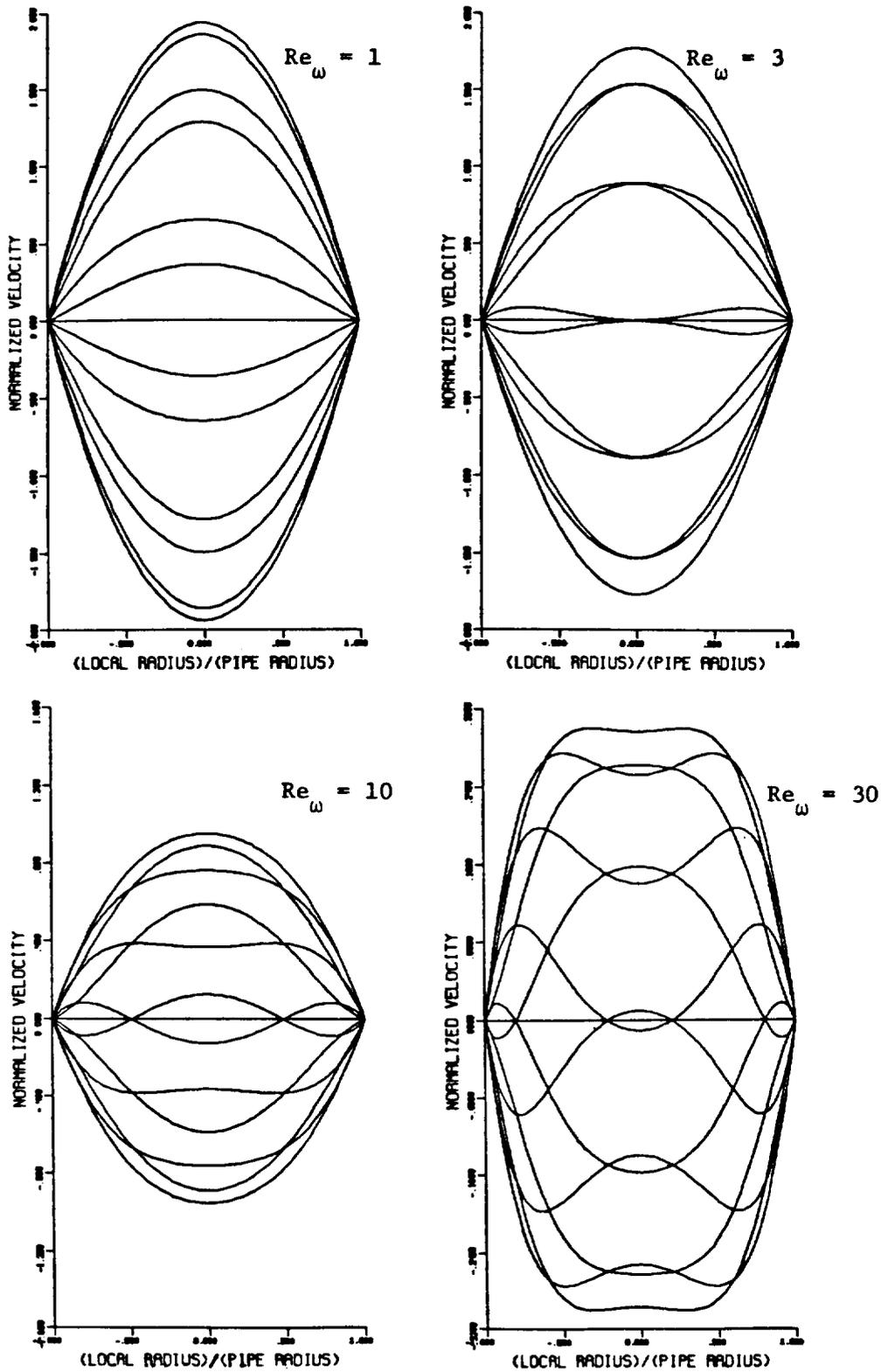
Figure C-1:   Velocity profiles in laminar flow
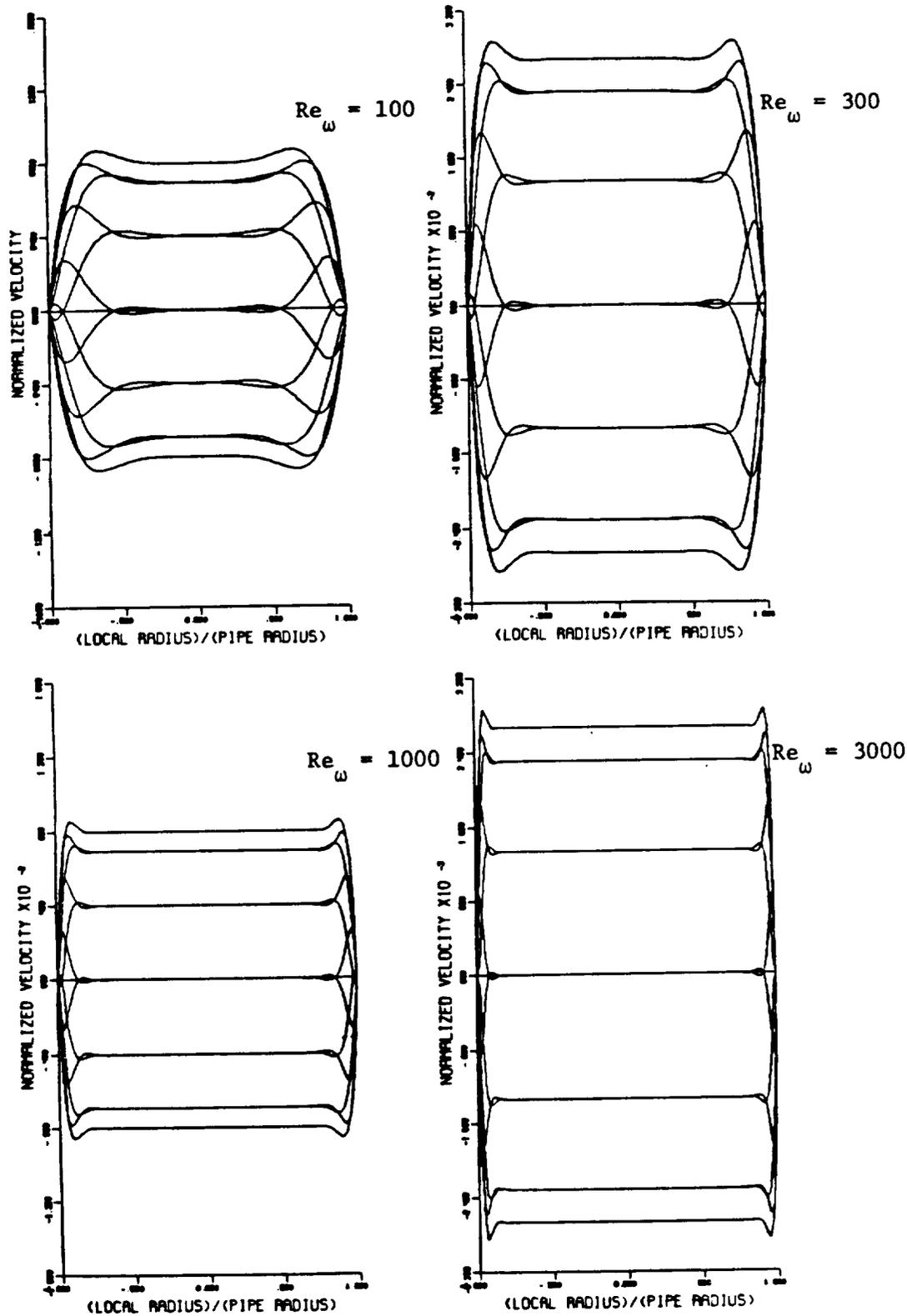
Figure C-1: Velocity profiles in laminar flow
(continued)

117

APPENDIX D: EQUATIONS OF OBSERVATIONS OF TRANSITION

This appendix provides the equations describing the lines in Figure 3-8. The ranges of applicability are based on the range over which the original references provide experimental data to support these equations.

Reference	Equation	Range
Grassmann and Tuma (1979)	$Re_{max} = 141\ Re_\omega^{0.75}$	$42 \leq Re_\omega \leq 520$
	$Re_{max} = 15300$	$520 < Re_\omega \leq 943$
Iguchi et al. (1982) laminar → transitional	$Re_{max} = 400\sqrt{Re_\omega}$	$100 < Re_\omega < 800$
transitional → turbulent	$Re_{max} = 800\sqrt{Re_\omega}$	$100 < Re_\omega < 800$
Ohmi et al. (1982)	$Re_{max} = 800\sqrt{Re_\omega}$	$18.4 \leq Re_\omega \leq 546$
Park and Baird (1970)	$Re_{max} = 188\ Re_\omega^{2/3}$	$35 \leq Re_\omega \leq 1000$
Sergeev (1966)	$Re_{max} = 700\sqrt{Re_\omega}$	$16 \leq Re_\omega \leq 1600$

APPENDIX E: EFFECTS OF PRESSURE PROPAGATION

Resonance

A necessary condition for resonance in Stirling engines is that the flow length between pistons is greater than half the wavelength (λ) of pressure propagation.

$$\lambda = \frac{a}{f}$$

where a = speed of sound

f = engine frequency

The smallest λ is obtained for small a (low temperature) and large f. For the only air-charged engine in the data base (Genset), the smallest λ is:

$$\lambda = \frac{\sqrt{YRT}}{f} = \frac{\sqrt{1.41 \times 286.7 \times 367 \text{ m/sec}}}{60 \text{ sec}^{-1}} = 6.42\text{m}$$

For He and H_2-charged engines the worst case would be the He-charged SPDE-D, the smallest λ is:

$$\lambda = \frac{\sqrt{YRT}}{f} = \frac{\sqrt{1.66 \times 2079 \times 350 \text{ m/sec}}}{105 \text{ sec}^{-1}} = 10.5\text{m}$$

The flow length between pistons may be found in the literature for the 4L23 (Martini 1982, p. 32) as 1.4m. It can be estimated for the GPU3 from Urieli and Berchowitz (1984, p. 36-37) as ~ 0.4m and for the UK engine from Dunn et al. (1982, p. 68) as > 0.78m. For all other engines in the data base it is expected to be less than 3m, estimated from the exterior dimensions of the engines.

The half-wavelengths, $\lambda/2$, for both cases exceed the flow length between pistons, therefore, resonance is not expected.

Shock incipience

A shock forms when pressure waves interfere constructively. This may be predicted by the method of characteristics. Consider a piston that oscillates sinusoidally in a tube (Fig. E-1).
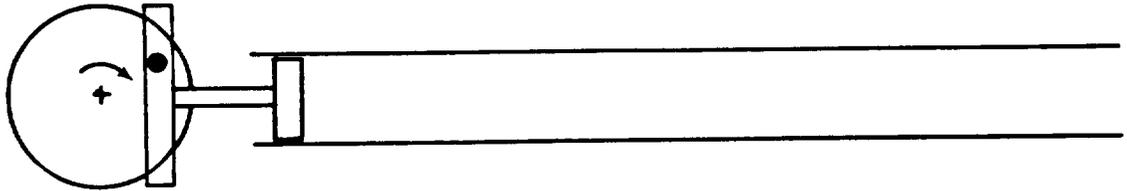

Figure E-1:   Oscillating piston in a tube

As the piston moves to the right, it continuously sends pressure waves to the open end. These can be represented in the t-x-plane as shown in Fig. E-2. Two pressure waves that were emitted by the piston at different times may interfere if the one emitted later travels faster (smaller slope of the t vs. x line).
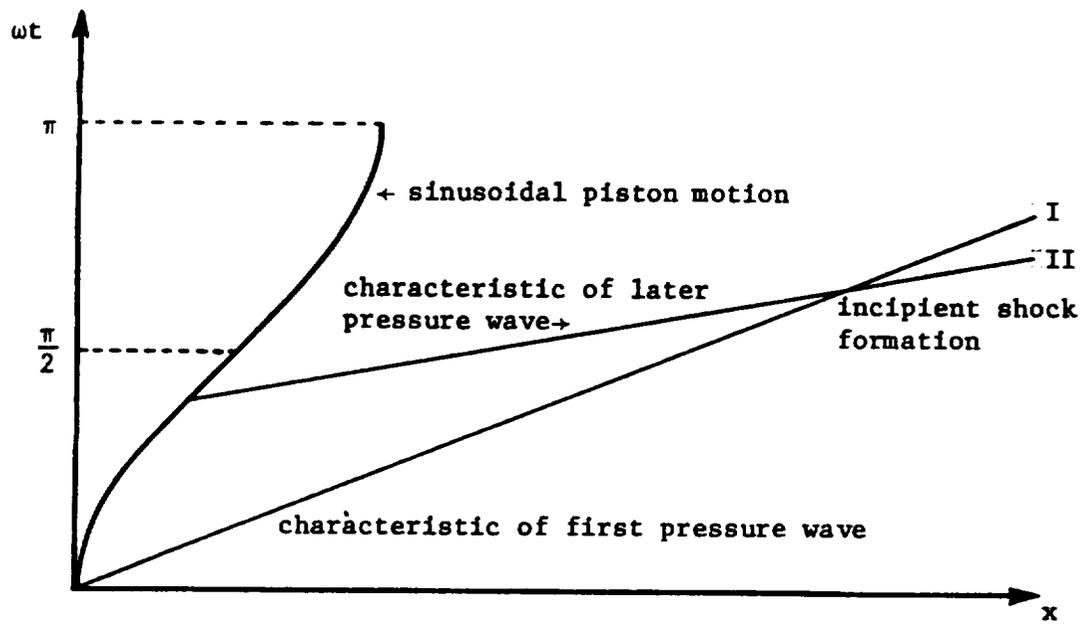
Figure E-2:   Method of characteristics

The lines describing the pressure wave propagation are characteristics. If the piston velocity is small compared to the velocity of sound, the slopes of both lines will be nearly equal:

$$(\frac{dt}{dx})_I = \frac{1}{a}$$

$$(\frac{dt}{dx})_{II} = \frac{1}{u_p + a}$$

If $a \gg u_p$, then $(\frac{dt}{dx})_I = (\frac{dt}{dx})_{II}$

Then the two lines will intersect far from the piston.

In an engine, the maximum piston velocity is smaller than the fluid velocity in the heat exchangers because the flow area is less than the piston area. Therefore, a worst case is obtained if the piston velocity is set to the highest fluid velocity found in the data base. The characteristics in Fig. E-2 are most likely to intersect if the period of the sinusoidal piston motion is small, i.e., the worst case should have the highest frequency. Due to the temperature gradient in an engine, the speed of sound varies. For the present simplistic analysis, the temperature is assumed to vary linearly with x.

The analysis is one-dimensional and ignores contractions, expansions, bends and regenerator matrices in the flow path. A fictitious worst case is composed of all the most favorable conditions for shock incipience encountered in the data base:

piston velocity amplitude	$M_{max} = 0.15$	UK-heater
frequency of oscillation	$\omega = 105 \ H_z$	SPDE-D
engine flow length	$L = 1.5m$	
	$L > 1.39m$	4L23

122

The temperature was assumed to vary linearly with x from 300K to 1050K. Consequently, the speed of sound varies as:

$$a(x) = \sqrt{\gamma R T(x)}$$

$$= \sqrt{\gamma R / L \left[(T_h - T_c)x + T_c \right]}$$

Then the two characteristics are described by

$$t^{\#}_I = \sqrt{\frac{L}{\gamma R}} \frac{2}{T_h - T_c} \left[\sqrt{(T_h - T_c)x^{\#} + T_c L} - \sqrt{T_c L} \right]$$

$$t^{\#}_{II} - t_o = \sqrt{\frac{L}{\gamma R}} \frac{2}{T_h - T_c} \left[\sqrt{(T_h - T_c)x + T_c L} \right.$$

$$\left. + u_{po}\sqrt{\frac{L}{\gamma R}} \left\{ 1 - \ln\left(\sqrt{(T_h - T_c)x + T_c L} + \sqrt{\frac{L}{\gamma R}} u_{po} \right) \right\} \right]^{x^{\#}}_{x_o}$$

where u_{po} is the piston velocity at t_o, when the pressure wave leaves the piston and $\#$ denotes shock incipience due to interference of pressure waves.

Test cases for air, hydrogen and helium were calculated for different values of t_o but shock incipience was not observed in any of these test cases (e.g., Fig. E-3).

123
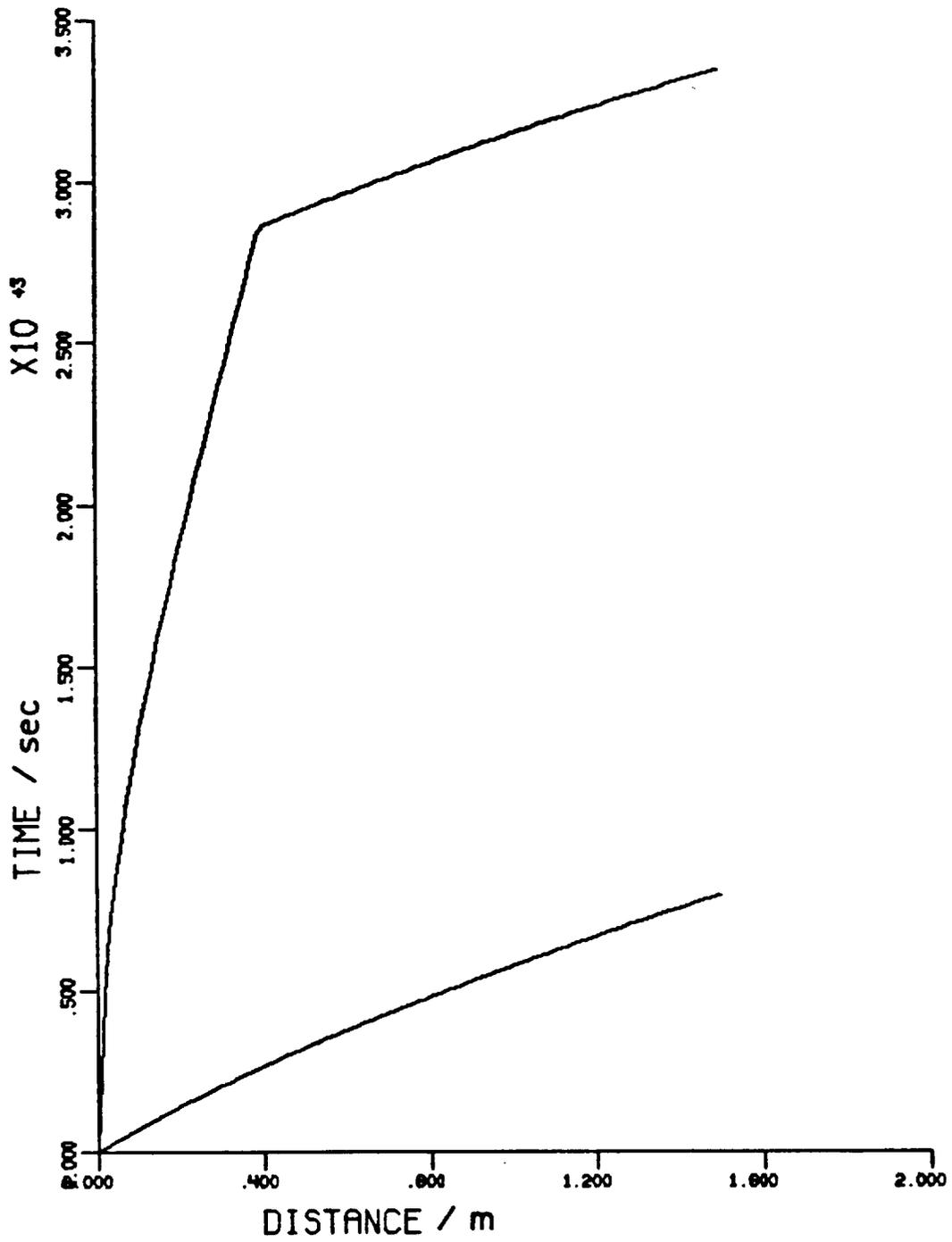
Figure E-3:   Characteristics for a test case with hydrogen

APPENDIX F: AUGMENTATION OF AXIAL TRANSPORT

From Watson (1983, p. 241), the augmentation coeffficient is

$$Au = \Psi (Wo, Pr) V_T^2 \qquad Wo = \sqrt{Re_\omega}$$

with

$$\Psi = \frac{1 - \dfrac{B_2(Wo)}{B_2(Wo \sqrt{Pr})}}{8\pi^2(1 - Pr^{1/2}) B_3(Wo)}$$

where

$$B_2(Wo) = \frac{Wo\, B''(Wo) + B'(Wo)}{B'(Wo)}$$

and

$$B_3(Wo) = \frac{Wo^3 B(Wo) + B'(Wo) - WoB''(Wo) - Wo^2 B'''(Wo)}{Wo^3 B'(Wo)}$$

$$B^n = \frac{d^n}{dWo^n} (ber^2(Wo) + bei^2(Wo))$$

Ber and bei are the Kelvin functions. A series solution for B and its derivations is provided by Watson (1983, p. 241).

Based on this series solution, the plot of the augmentation function Ψ shown below was generated (Figure F1). The axial heat transfer can be found as discussed in section 4.2 if an axial temperature gradient is assumed. Sample calculations are not included here because they involve proprietary geometry data.

125
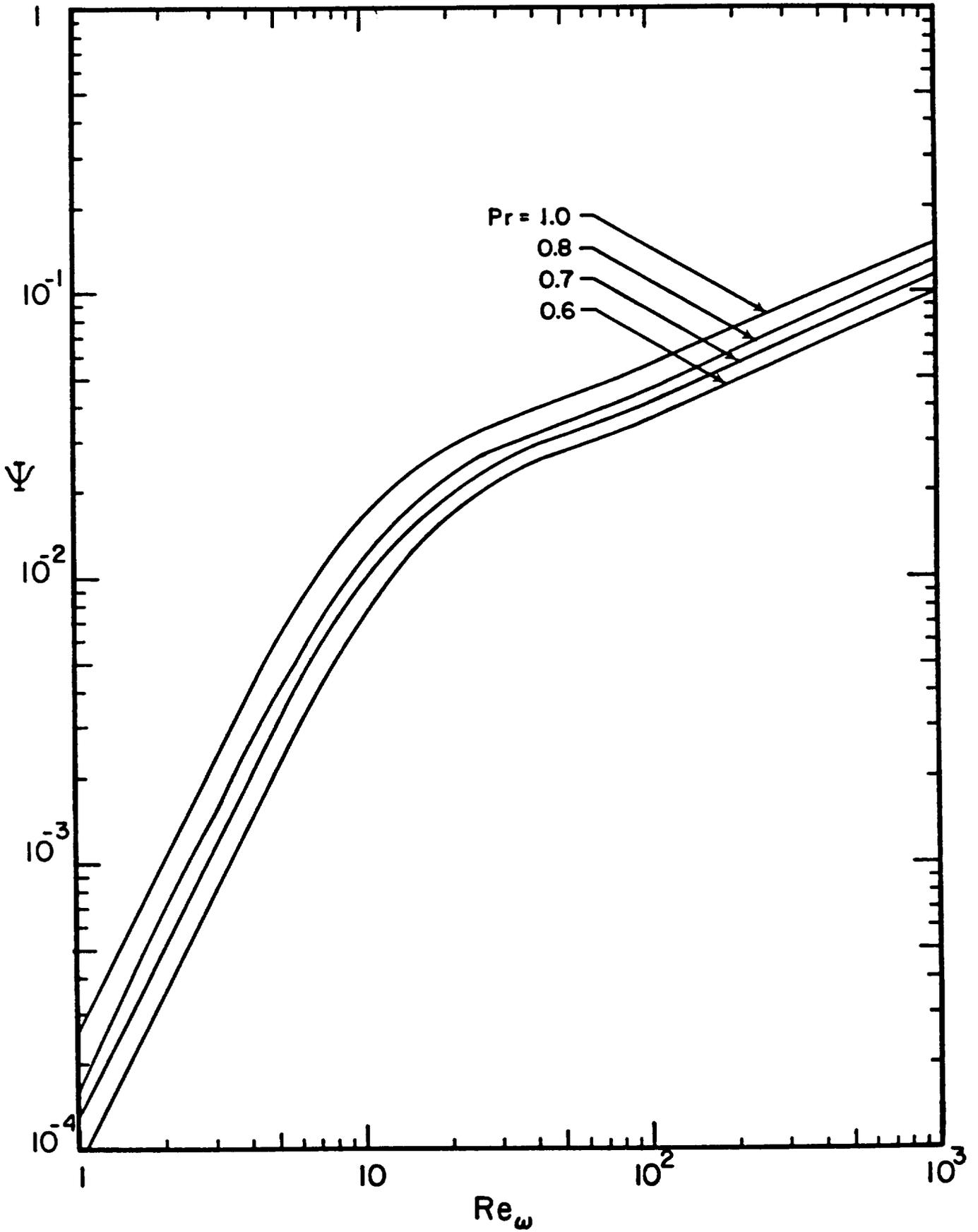
Figure F-1:   Augmentation function for axial heat transfer

Report Documentation Page

1. Report No. NASA CR-182108	2. Government Accession No.	3. Recipient's Catalog No.

4. Title and Subtitle	5. Report Date
A Survey of Oscillating Flow in Stirling Engine Heat Exchangers	March 1988
	6. Performing Organization Code

7. Author(s)	8. Performing Organization Report No.
Terrence W. Simon and Jorge R. Seume	None
	10. Work Unit No. 586-01-11

9. Performing Organization Name and Address	11. Contract or Grant No.
University of Minnesota School of Mechanical and Aerospace Engineering 111 Church Street S.E. Minneapolis, Minnesota 55455	NAG 3-598
	13. Type of Report and Period Covered

12. Sponsoring Agency Name and Address	Contractor Report Annual
National Aeronautics and Space Administration Lewis Research Center Cleveland, Ohio 44135-3191	14. Sponsoring Agency Code

15. Supplementary Notes

Project Manager, James E. Dudenhoefer, Power Technology Division, NASA Lewis Research Center.

16. Abstract

Similarity parameters for characterizing the effect of flow oscillation on wall shear stress, viscous dissipation, pressure drop and heat-transfer rates are proposed. They are based on physical arguments and are derived by normalizing the governing equations. The literature on oscillating duct flows, regenerator and porous media flows is surveyed. The operating characteristics of the heat exchangers of eleven Stirling engines are described in terms of the similarity parameters. Previous experimental and analytical results are discussed in terms of these parameters and used to estimate the nature of the oscillating flow under engine operating conditions. The operating points for many of the modern Stirling engines are in or near the laminar-to-turbulent transition region. In several engines, working fluid does not pass entirely through heat exchangers during a cycle. Questions that need to be addressed by further research are identified.

17. Key Words (Suggested by Author(s))	18. Distribution Statement
Stirling Oscillating flow Flow Heat exchangers	Unclassified - Unlimited Subject Category 34

19. Security Classif. (of this report)	20. Security Classif. (of this page)	21. No of pages	22. Price*
Unclassified	Unclassified	132	A07